Novel Single-unit Membrane Filtration System for Concentration and Buffer Exchange of Protein Solutions using Continuous Ultrafiltration/Diafiltration

Zur Erlangung des akademischen Grades eines
DOKTORS DER INGENIEURWISSENSCHAFTEN (DR.-ING.)

von der KIT-Fakultät für Chemieingenieurwesen und Verfahrenstechnik des
Karlsruher Instituts für Technologie (KIT)
genehmigte

DISSERTATION

von
M. Sc. Ruijie Tan
aus Chongqing, China

Erstgutachter/-in: Prof. Dr.-Ing. Matthias Franzreb
Zweitgutachter/-in: Prof. Dr.-Ing. Jürgen Hubbuch
Tag der mündlichen Prüfung: 27.05.2021

For my family

Acknowledgments

This dissertation would not have been possible without the help and support from many people that I have met along the way.

My deepest gratitude certainly goes to my Ph.D. supervisor Prof. Dr.- Ing. Matthias Franzreb. I would like to thank him to provide me the wonderful chance to be his Ph.D. student. During my Ph.D. period, he firmly supported me with his invaluable knowledge, patient guidance, and professional advice. His mentorship has immeasurably influenced my personal and academic development, which surely will help me in my future career. Thanks for guiding me through the difficulties and challenges and always being so understanding and kind.

I would like to acknowledge Prof. Dr.-Ing. Jürgen Hubbuch for generously spending his time reviewing this dissertation and helping me improve this work. Special thanks also to Fabian Hezel who actively contributed to this work during his thesis.

I would like to thank the Karlsruhe House of Young Scientists (KHYS) for financial support during my stay abroad at the University College London (UCL), and special thanks to Prof. Daniel Bracewell at UCL for his support and inspiration on my research work.

I would like to sincerely thank all members in the group of Prof. Franzreb, it has been an enjoyable experience to work with you. Special thanks to my lovely office colleagues Huyen-Tram Tran, Juliane Diehm, and Sefkan Kendir for all of their suggestions to my research work and boundless support in my daily life. I also would like to express my gratitude to André Tschöpe and Frank Kirschhöfer for experimental troubleshooting, to Benedikt Sapotta and Laura Kuger for improving the dissertation writing, to Marvin Klaiber, Dr. Raphael Greifenstein, Carsten-Rene Arlt, Robin Wagner, Magdalene Lenz for their kind helps constantly. My special gratitude to my former colleagues Elisabeth Schmalbach, Benedikt Ketterer, Jonas Hübner, and Moritz Ebeler for their assistance and support when I arrived in Germany first year.

I would also like to sincerely thank Mike Füssler, Jonas Wohlgemuth for helping construct the experiment setup, Dr. Manuel Tsotsalas, Dr. Qi An and Dr. Salma Begum for the guidance in synthesizing membranes, Dr. Matthias Schwotzer, Jonas Kaltenbach, Stefan Heißler, and Dr. Zhihua Fu for training and assisting me in the membrane characterization.

I also want to express my appreciation to the China Scholarship Council (CSC) foundation which sponsored my Ph.D. fellowship.

I am truly blessed to have a wonderful family and group of friends who have always been there for me. My special gratitude goes to Minghao Kong for always being here

to support me. Finally, I must thank my parents and siblings for all their love, encouragement, and support throughout the years.

Abstract

Biopharmaceutical products (such as recombinant proteins and vaccines) play a central role in modern medicine. The manufacturing process of such large biomolecules includes multiple upstream and downstream processing steps. The raw material is being transformed into crude intermediate products by upstream processing, and the final products are gained by several sequential downstream processing steps, such as isolation and concentration of the target biomolecules, intermediate purification, and polishing. Especially because of their ease of operation and flexibility, membrane-based unit operations are widely used in these downstream processing schemes. However, despite the basically simple underlying physical principles, membrane-based technologies encounter diverse challenges and obstacles when applied to biological feed solutions. In the case of ultrafiltration, concentration polarization (CP) and fouling phenomena of accumulated proteins at membrane surfaces are a major hurdle for system performance. A common way to reduce the degree of accumulation is so-called tangential flow filtration (TFF) in which the retentate is pumped at high velocities parallel to the membrane surface. However, the resulting short residence times within the membrane module require that the retentate is guided in a loop and passes the pump and membrane several times, resulting in a batchwise process. As an alternative to the traditional batchwise operation, continuous processing gets more and more attention over the past years due to its distinguished advantages, such as the reduction of the equipment footprint and a constant and improved product quality.

In case of ultra- and diafiltration, continuous processing is achieved by so-called single pass tangential flow filtration (SPTFF) and single pass diafiltration (SPDF). However, because of the limited concentration factors achieved within conventional SPTFF units, the formulation of highly concentrated protein solutions requires cascades including several of these filter units as well as the respective pumps, reservoir tanks, valves and tubings. In consequence, current systems for continuous UF/DF are characterized by increased complexity, high capital costs, and the demand for sophisticated measurement and control technology.

In this work, a novel single-unit membrane filtration system for continuous UF/DF is presented. The 3D-printed prototype of the filtration module is composed of two lateral compartments and one central middle part, clamping two commercial UF membranes between the lateral and the central parts. All three parts contain a hollow-grid structure creating flow channels and mechanically supporting the membranes. The combination of three channels and two membranes allows to withdraw permeate

and simultaneously deliver fresh diafiltration buffer into the central retentate channel. In order to have full control over the different feed and effluent streams of the module, the system is operated in constant flow mode with transient pressures. This is achieved by connecting the module with three high performance piston pumps and multi-port valves provided by a commercial ÄKTA Explorer FPLC system. Although these systems are originally intended for applications in chromatography, they also allow a convenient online monitoring of UV and conductivity signals in case of diafiltration experiments. In addition, the integrated multiport valves and the programmable control software enable new operation modes of filtration module, such as a cyclically alternating for direction of diafiltration buffer through the membranes.

In the beginning the filtration module was characterized by the determination of the water flux through the membranes under different transmembrane pressures applied, and of the duration needed to reach quasi-stationary operation for both tasks, concentrating of a protein feed and buffer exchange of the original feed solution. In the first small prototype having a flow path length of only 47 mm, concentration factors of five could be achieved, however, the obtained buffer exchange efficiency was only 46%. Thus, a second prototype module with increased flow path length and optimized hydrodynamics was designed and fabricated.

In subsequent experiments, pure diafiltration with alternating flow direction of the diafiltration buffer was investigated by applying the same flow rate in the feed and retentate stream. The influence of various parameters, including the duration of the switching intervals between the DF flow direction, the flow mode between the feed solution and DF buffer (co-current and counter-current), the number of diavolumes applied, and the volumetric flowrate of the feed solution, on the DF efficiency was investigated comprehensively. The results show, that the DF efficiency could be increased from the initial 46% in the small prototype up to 99.3% at 7.2 diavolumes and a switching interval of 3 min. Those findings approve that the switching events of the flow direction of DF buffer through the membranes works like a cyclic inherent backflush and reduces concentration polarization and the corresponding pressure build-up strongly.

To understand the complex hydrodynamics and mass transport phenomena in the designed novel membrane module, a 2D finite element (FEM) model has been developed using COMSOL Multiphysics. Considering the porous grid-structure present in each flow channel of the module, a dynamic version of the Brinkman equation was used for the simulation of the hydrodynamics, including time varying local pressures and velocities. The modeling of the transport of dissolved species was achieved by common mass balances including convective flux tangential and perpendicular to the

membrane, back diffusion into the bulk solution and eddy dispersion caused by the flow through the coarse grid. The simulated results are in good agreement with the experimental data. Seeking optimal parameter settings for higher diafiltration efficiencies, key factors such as pressures, velocities, and local concentrations of protein and salt within the module were predicted using the developed model. In a parameter study it showed, that compared to the method applying switching events, the unidirectional operation manner results in better diafiltration efficiency. However, in this operation mode there exists a comparably low, maximum allowable feed load to guarantee that the maximum pressure within the module will not exceed the pressure limit of the system. When a higher feed load is required, the method of alternating DF buffer flow can be applied to reduce the pressure built-up, but at the expensive of intensified mixing effects in the module and correspondingly a reduced diafiltration performance.

In summary, this thesis presents a thorough experimental and theoretical study of a novel type of continuously operated, single pass tangential flow filtration system. The designed module is able to achieve up to 99.9% diafiltration efficiency (99.3% at 7.2 diavolumes) within a single filtration unit. By this its performance is comparable to more complex three-stage counter-current SPTFF systems, described so far in literature for continuous diafiltration.

Zusammenfassung

Biopharmazeutische Produkte (wie rekombinante Proteine und Impfstoffe) spielen eine zentrale Rolle in der modernen Medizin. Der Herstellungsprozess solch großer Biomoleküle umfasst mehrere vor- und nachgelagerte Verarbeitungsschritte. Das Rohmaterial wird durch sogenannte Upstream-Prozesse in Zwischenprodukte umgewandelt und die Endprodukte werden durch mehrere sequenzielle Downstream-Prozessschritte, wie z. B. Isolierung und Konzentration der Ziel-Biomoleküle, gewonnen. Vor allem aufgrund ihrer einfachen Bedienung und Flexibilität sind membranbasierte Verfahren in diesen Downstream-Prozess-Schemata weit verbreitet. Trotz der im Grunde einfachen physikalischen Zusammenhänge stoßen membranbasierte Technologien jedoch auf eine Reihe von Herausforderungen und Hindernisse, wenn sie auf biologische Ausgangs-Lösungen angewendet werden. Im Falle der Ultrafiltration sind Konzentrationspolarisation (CP) und Fouling-Phänomene von akkumulierten Proteinen an der Membranoberfläche eine große Hürde für die Systemleistung. Eine gängige Methode, die Akkumulation von Proteinen zu reduzieren, ist die sogenannte Tangentialflussfiltration (TFF), bei der das Retentat mit hohen Geschwindigkeiten parallel zur Membranoberfläche gepumpt wird. Die daraus resultierenden kurzen Verweilzeiten innerhalb des Membranmoduls erfordern jedoch, dass das Retentat in einem Kreislauf geführt wird und Pumpe und Membran mehrfach passiert, was zu einem chargenweisen Prozess führt. Als Alternative zum traditionellen chargenweisen Betrieb finden Prozesse mit kontinuierlicher Betriebsweise aufgrund ihrer Vorteile, wie z. B. der Reduzierung der Anlagengröße und einer konstanten und verbesserten Produktqualität, n den letzten Jahren immer mehr Beachtung.

Im Falle der Ultra- und Diafiltration wird eine kontinuierlicher Betriebsweise durch die sogenannte Single-Pass-Tangential-Flow-Filtration (SPTFF) und Single-Pass-Diafiltration (SPDF) erreicht. Aufgrund der begrenzten Konzentrationsfaktoren, die in konventionellen SPTFF-Einheiten erreicht werden, erfordert die Herstellung von hochkonzentrierten Proteinlösungen jedoch ein Kaskadensystem, das mehrere dieser Filtereinheiten sowie die entsprechenden Pumpen, Vorratstanks, Ventile und Schläuche umfasst. Aktuelle Systeme zur kontinuierlichen UF/DF sind daher durch erhöhte Komplexität, hohe Investitionskosten und den Bedarf an anspruchsvoller Mess- und Regeltechnik gekennzeichnet.

In dieser Arbeit wird ein neuartiges Single-Unit-Membranfiltrationssystem für kontinuierliche UF/DF vorgestellt. Der 3D-gedruckte Prototyp des Filtrationsmoduls besteht aus zwei Seitenteilen und einem zentralen Mittelteil, wobei zwei kommerzielle UF-Membranen zwischen den seitlichen und dem zentralen Teil eingespannt sind. Alle

drei Teile enthalten eine Hohlgitterstruktur, die Strömungskanäle schafft und die Membranen mechanisch stützt. Die Kombination aus drei Kanälen und zwei Membranen ermöglicht es, Permeat abzuziehen und gleichzeitig frischen Diafiltrationspuffer in den zentralen Retentatkanal zu liefern. Um die volle Kontrolle über die verschiedenen Zu- und Ablaufströme des Moduls zu erhalten, wird das System im mit konstanten Volumenströmen aber transienten Drücken betrieben. Dies wird durch die Verbindung des Moduls mit drei Hochleistungskolbenpumpen und Mehrwegeventilen erreicht, die von einem kommerziellen ÄKTA Explorer FPLC-System bereitgestellt werden. Obwohl diese Systeme ursprünglich für Anwendungen in der Chromatographie vorgesehen sind, ermöglichen sie auch eine komfortable Online-Überwachung von UV- und Leitfähigkeitssignalen bei Diafiltrationsversuchen. Darüber hinaus ermöglichen die integrierten Multiport-Ventile und die programmierbare Steuerungssoftware neue Betriebsmodi des Filtrationsmoduls, wie z.B. ein zyklischer Wechsel der Flussrichtung des Diafiltrationspuffers durch die Membranen.

Zu Beginn wurde das Filtrationsmodul durch die Bestimmung des Wasserflusses durch die Membranen bei verschiedenen anliegenden Transmembrandrücken und durch die Dauer, die zum Erreichen eines quasistationären Betriebs für beide Aufgaben, Aufkonzentrierung eines Proteinlösung und Pufferaustausch, benötigt wird, charakterisiert. Im ersten, kleinen Prototyp mit einer Strömungspfadlänge von nur 47 mm konnten Konzentrationsfaktoren von fünf erreicht werden, die erzielte Pufferaustausch-Effizienz betrug jedoch nur 46%. Daher wurde ein zweites Prototypmodul mit vergrößerter Strömungspfadlänge und optimierter Hydrodynamik entworfen und hergestellt.

In anschließenden Experimenten wurde die reine Diafiltration mit wechselnder Flussrichtung des Diafiltrationspuffers bei gleicher Flussrate des Feed- und Retentatstroms untersucht. Der Einfluss verschiedener Parameter, darunter die Dauer der Umschaltintervalle zwischen den DF-Strömungsrichtungen, der Strömungsmodus zwischen Feed-Lösung und DF-Puffer (Gleichstrom und Gegenstrom), die Anzahl der aufgegebenen Diavolumina und der Volumenstrom der Feed-Lösung, auf die Diafiltrationseffizienz wurde umfassend untersucht. Die Ergebnisse zeigen, dass die Diafiltrationseffizienz von anfänglichen 46% im kleinen Prototyp auf 99,3% bei 7,2 Diavolumina und einem Schaltintervall von 3 min gesteigert werden konnte. Diese Ergebnisse bestätigen, dass die Schaltvorgänge der Flussrichtung des DF-Puffers durch die Membranen wie eine zyklische inhärente Rückspülung wirken und die Konzentrationspolarisation und den entsprechenden Druckaufbau stark reduzieren.

Um die komplexen Hydrodynamik- und Stofftransportphänomene in dem neuartigen Membranmodul zu verstehen, wurde ein 2D-Finite-Elemente-Modell (FEM) mit COMSOL Multiphysics entwickelt. Unter Berücksichtigung der porösen Gitterstruktur, die in jedem Strömungskanal des Moduls vorhanden ist, wurde eine dynamische Version der Brinkman-Gleichung für die Simulation der Hydrodynamik verwendet, einschließlich zeitlich variierender lokaler Drücke und Geschwindigkeiten. Die Modellierung des Transports der gelösten Spezies wurde durch übliche Massenbilanzen erreicht, die den konvektiven Fluss tangential und senkrecht zur Membran, die Rückdiffusion in die Bulk-Lösung und die durch die Strömung durch das grobe Gitter verursachte Dispersion beinhalten. Die simulierten Ergebnisse sind in guter Übereinstimmung mit den experimentellen Daten. Auf der Suche nach optimalen Parametereinstellungen für höhere Diafiltrationseffizienzen wurden mit dem entwickelten Modell Schlüsselfaktoren wie Drücke, Geschwindigkeiten und lokale Konzentrationen von Protein und Salz innerhalb des Moduls vorhergesagt. In einer Parameterstudie zeigte sich, dass die unidirektionale Betriebsweise im Vergleich zur Methode mit einem Wechsel der Strömungsrichtung des DF-Puffers zu einer besseren Diafiltrationseffizienz führt. Allerdings ist in dieser Betriebsart nur eine vergleichsweise geringe, maximal zulässige Flächenbelastung (spezifischer Filtratfluss) zu erreichen, da der maximale Druck im Modul das Drucklimit des Systems nicht überschreiten darf. Wenn eine höhere Flächenbelastung erforderlich ist, kann die Methode der alternierenden Strömungsrichtung des DF-Puffers angewendet werden, um den Druckaufbau zu reduzieren. Dies geschieht allerdings zu dem Preis verstärkter Mischeffekte im Modul und einer entsprechend reduzierten Diafiltrationsleistung.

Zusammenfassend wird in dieser Arbeit eine gründliche experimentelle und theoretische Untersuchung eines neuartigen, kontinuierlich betriebenen, Tangentialfluss Filtrationssystems vorgestellt. Das entworfene Modul ist in der Lage eine Diafiltrationseffizienz von bis zu 99,9% (99,3% bei 7,2 Diavolumen) in einer einzigen Filtrationseinheit zu erreichen. Damit ist seine Leistung vergleichbar mit komplexeren dreistufigen Gegenstrom-SPTFF-Systemen, die bisher in der Literatur für die kontinuierliche Diafiltration beschrieben wurden.

Table of Contents

List of Figures

List of Tables

1 Introduction

1.1 Background

The biotechnology industry is dedicated to the production of various biomaterials and biomolecules for applications in food, chemistry, and biopharma. Especially due to the broad application in therapeutics or diagnostics, the demand for biological products including vaccines or recombinant proteins is steadily increasing during the last decades [1–3]. A generic biopharmaceutical processes is commonly divided into upstream and downstream processes to reach the desired final products. During the upstream processing, the target microbes and/or cells are grown from starting materials to the crude product mixture in the appropriate culture broth. This processing involves all steps related to the initial acquisition of tissue, primary cell isolation, cell culture and harvest of cells [4]. The subsequent downstream processing is designed to achieve the desired quality of the fill-finish products, containing the concentrated bioingredients with minimum impurities and the formulated buffer for safe storage and delivery. All necessary remaining steps such as product capture, virus clearance, purification, polishing, and formulation are accomplished in downstream processing [3,5,6]. Within this scope, a complete bioprocess for the manufacturing of biological products generally consist of five stages in sequential orders: isolation, expansion, differentiation, separation/purification, and preservation [4]. In practice, the production procedures need to be adjusted to the corresponding products. For instance, the procedures mentioned above are complete for the production of secreted products like monoclonal antibodies (mAbs); while for the production of bacterial products via continuous processing, the process operations of cell lysis and, in many cases, protein re-folding have to be added [3,6,7]. Various unit operations have been applied in downstream processing to recover the desired products from its crude biomass. It embraces a wide range of fractionation and purification methods including filtration, chromatography, extraction, centrifugation, and precipitation [1,8–11]. From an economic point of view, the simplest and cheapest separation units should be carried out earlier than the expensive and complex ones in the process [12].

Membrane processes were originally developed for applications in the fields of food, dairy and water industry [13,14]. However, over the past decades they have been broadly employed also bioprocessing. Common applications in this field are microfiltration for the clarification of crude biomass, membrane-adsorber for purification and polishing steps, as well as ultrafiltration (UF) and/or diafiltration (DF) for the concentration and formulation of biotechnological products (typically proteins or DNA) [3,15,16]. Compared to alternative separation units like chromatography,

membrane systems have several advantages including flexible operating to scale-up, high throughput, and almost identical residence time for all molecules during the course of the filtration process [17–19]. Much research efforts have been devoted to the development of membrane materials, modules, and optimized processes [20].

In downstream processing, ultrafiltration is used primarily for concentrating the macromolecules retained by the membrane, while diafiltration is designed to exchange or dilute the buffer in which the macromolecule is dissolved. In industry, UF/DF is widely done batchwise, using filtration modules in combination with recycle loops, hold-up tanks, and a stepwise or continuous addition of diafiltration buffer [21,22]. Comparing to batchwise, continuous processes have the potential to significantly reduce the cost of goods and footprints of equipment, increase manufacturing flexibility, as well as enhance the product quality [5,9,23,24]. In order to change batchwise to continuous processing, single pass tangential flow filtration (SPTFF) gets increasing attention in this decade, because it avoids the necessity of hold-up tanks and recycles loops. In a SPTFF unit, the feed flow passes the filtration system only once. By this, unwanted temperature rise and high shear-stress resulting from multiple passes through the pump and the loop can be reduced drastically, facilitating to provide a beneficial process conditions for the fragile biomolecules. In 2011, Casey et al. [25] proposed a continuous cascade SPTFF system to concentrate bovine Immunoglobulin G (IgG) from 3 to 25-fold when applying different feed concentrations ranging from 5 to 45 g/L. This configuration is proved to be applicable to high value biomolecules which are sensitive to shear-stress or high temperature. Arunkumar et al. [26] firstly utilized an SPTFF system for the in-process cell culture harvest of six different biological assets simultaneously. By adding a high capacity adsorptive filter during primary recovery to reduce the process-related particulates and soluble impurities, they maintained stable hydraulic conditions. The robustness of the system was demonstrated by the small variance of the performance from cell culture lot-to-lot deployment. In another study, Rucker-Pezzini et al. [27] presented a sequential diafiltration setup including three SPTFF units to remove small impurities during continuous monoclonal antibody purification. The specified exchange efficiency of 99.75% was obtained with only six diavolumes of diafiltration buffer applied. They also emphasized the significance of the trade-off between the reduction of fresh buffer consumption and the increasing system complexity when increasing the number of stages. More recently, the group of Zydney constructed multi-stage countercurrent single pass DF systems and reused the permeate from one stage as the diafiltration buffer in the previous stage. By this they obtained a slightly reduced diafiltration performance but a strong reduction of buffer consumption [27–29]. Although the

reported use of co- and counter-current cascades of SPTFF systems improves the efficiency of continuous UF and DF applications clearly, the resulting systems and their control are complex and result in increased costs for this unit operation. In addition, because of the reduced flow rates within the retentate channels, conventional SPTFF are more prone to the problems of concentration polarization (CP) and related phenomena such as membrane fouling [30–35]. Especially due to the increasing importance of continuous process control also in the biopharmaceutical industry, there is therefore a need for novel continuous membrane filtration modules that combine a simple design with high efficiency.

1.2 Research Objectives

This dissertation is aimed to design and realize truly continuous UF/DF processes by developing a novel single unit membrane module for the concentration of macromolecules and their formulation by buffer exchange. Besides the design, fabrication and experimental testing of the UF/DF module, extensive computational modeling should be used in order to optimize the module and to find optimum process conditions using a minimum amount of experiments. The model should be able to predict local concentration and pressure profiles under various operation modes providing different flow patterns, and to extract key figures of the process such as, concentration factors, diafiltration efficiencies, and dynamic pressure build-up. In details, the following objectives had to be accomplished in this work:

(1) Conceptualization of a novel single unit membrane module, capable of conducting continuous ultra- and diafiltration. Fabrication of prototypes of this module by the help of additive manufacturing in combination with commercial membrane sheets.

(2) Characterization of the designed system and experimental demonstration of its capability to achieve continuous concentration of a model protein while simultaneously changing the buffer.

(3) Scale-up of the prototype module and characterization of its diafiltration performances for different flow configurations (unidirectional, co-current, and counter-current).

(4) Model development and simulation of the designed system to thoroughly understand the underlying transport processes of dissolved species within the module, thus determining optimal operation settings for different demands.

2 Fundamentals

2.1 Membrane filtration for downstream processing

Membranes are generally characterized by the pore size or nominal molecular weight cutoff (MWCO), which is typically considered as the molecular weight of the solute that has a rejection coefficient of 90% [14]. For pressure-driven membrane processes, the primary separation mechanism is on the basis of molecules size compared to the membrane pore size. At the membrane-solution interface, the larger biomolecules are retained by the membrane while the smaller molecules can penetrate the membrane freely. Proteins are composed by a linear sequence of 20 natural-occurring amino acids and thus have a complex three-dimensional geometry structure [36]. The hard sphere model is widely used to obtain a representative radius of the protein [22]:

$$r = 0.88 \cdot \mathrm{MW}^{\frac{1}{3}} \tag{2.1}$$

where r is the protein radius in nm and MW its molecular weight in kilo Daltons (kDa). Notably, due to the diffuse ion cloud around charged proteins, the effective radius of proteins employed in a membrane process may be significantly larger than this simplified theoretical prediction [37].

In addition to its characteristic pore size, the structure and charge of the membrane also influence the separation performance [15]. However, in the practical designing of membrane processes, membrane selectivity, the volumetric permeate flux and the membrane system capacity are determining factors for the separation efficiency [14]. The membrane selectivity is decided by the distribution of pores, membrane composition and the membrane surface properties [38,39]. The system capacity is estimated as the volume of feedstock solution that can be processed per unit membrane area in the allowance of the existing system limitations, e.g. regarding maximum pressures [14]. For example, using a hydrophobic polysulfone membrane may cause the adsorption of some biomolecules at the pore entrance and thus change the effective MWCO as well as solvent flux and sieving coefficient, defined as the concentration ratio of molecules in the filtrate and feed flow [40]. The volumetric permeate flux of a membrane is defined as J ($\frac{L}{m^2 \cdot h}$):

$$J = L_P \cdot TMP \tag{2.2}$$

and

$$L_P = \frac{\mathrm{Q}}{A \cdot TMP} \tag{2.3}$$

where L_P is hydraulic permeability (volumetric flow rate per unit membrane area per unit pressure, $L/(m^2 \cdot h \cdot bar)$) and TMP is transmembrane pressure. Because of the concentration polarization and membrane fouling phenomena, the actual permeate flux detected is generally lower than the theoretical value of the clean membrane [22]. Concentration polarization is reversible and always observed at the upstream membrane surface, while fouling is irreversible and occurs on or within the pores of the surface and underneath. In addition, extremely concentrated solutes may deposit on the external surface of the membrane as gel layer [41].

Based on the pore size of the membrane, pressure-driven membrane processes can be classified into microfiltration (MF), ultrafiltration (UF), nanofiltration (NF) and reverse osmosis (RO), as shown in Fig. 2.1. The range of the pore sizes used in these processes is commonly defined as 0.02-10 µm for MF [14,40,42], 10-100 nm for UF [42,43], 1-10 nm for NF, and < 1nm for RO [43,44], respectively.

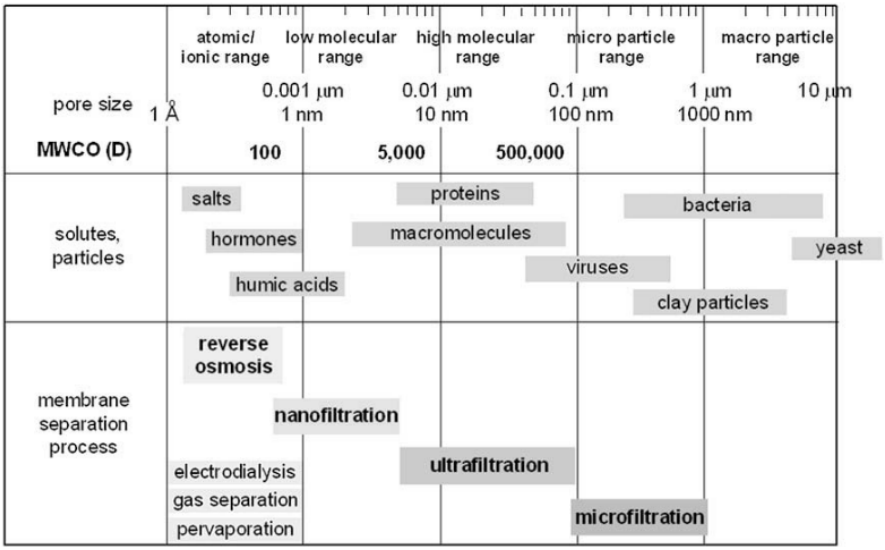

Fig. 2.1 Membrane pore sizes in various filtration processes and the corresponding examples of typical solutes and particles [44].

Microfiltration membranes enable to reject intact cells, bacterial and cell debris but allow the proteins and smaller solutes (like salts, viruses) to pass simultaneously. Ultrafiltration membranes are usually utilized to separate proteins and other macromolecules from smaller solutes like amino acids. Therefore, ultrafiltration membranes are advantageous to concentrate proteins in the frame of downstream processes for protein purification. The degree of concentration obtainable during a single pass of the membrane system is determined by the flow rate ratio between the feed and retentate streams. Nanofiltration membranes are often used to separate e.g. amino acids or antibiotics from small salts and water. Reverse osmosis membranes

are broadly explored to produce high quality water by removing practically all dissolved substances, including sugars and salts. In addition to those mentioned pressure-driven membrane processes used in biotechnological industry, there also are concentration-driven filtration process like dialysis and temperature-driven separation like membrane distillation. Dialysis is mainly based on the diffusion effect caused by the solute concentration gradient near the membrane, especially hemodialysis has been commonly developed for the treatment of kidney failure in biomedicine.

According to the flow direction of feed relative to the membrane position, filtration manners are classified mainly as normal flow filtration (also named dead-end filtration) and tangential flow filtration (TFF), as illustrated in Fig. 2.2 [45]. In normal flow filtration mode, the feed flow direction is perpendicular to the membrane surface and all components transport towards the membrane. The retained macromolecules deposit gradually on the membrane which may result in a severe flux decay over time. Therefore, dead-end filtration is mostly selected for processing of feedstocks with a very low concentration of retainable particles or molecules. In the manner of tangential flow filtration, the feed flow is directed parallel to the membrane, which means the concentrated proteins on the membrane can be swept away due to the shear stress of the flow, thus maintaining the permeate flux at an acceptable level.

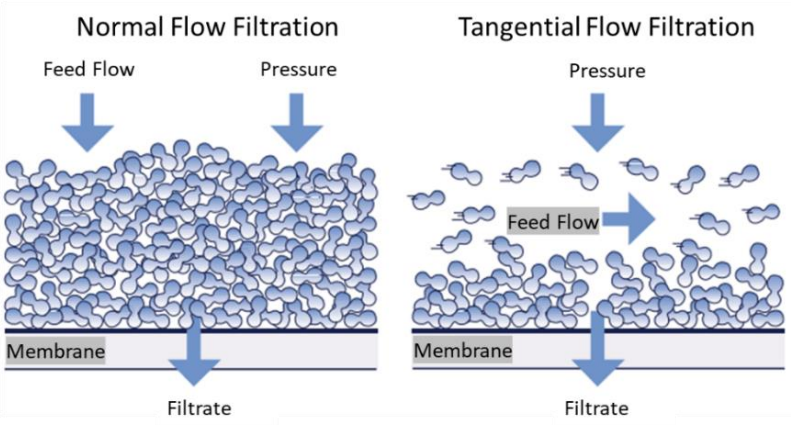

Fig. 2.2 Typical modes of normal flow (Dead-end) filtration and tangential flow filtration [45].

2.2 Membrane fouling during ultrafiltration

Ultrafiltration has been widely used in concentrating biological targets such as proteins and the membrane process performance is mainly determined by the permeate flux. Therefore, the deposition of molecules on the membrane surface or within the membrane pore structure is a serious limitation to the process efficiency because it has a negative influence on this key figure, increasing capital and

operational costs [46]. The phenomenon of accumulation of the rejected component at the membrane surface is commonly known as concentration polarization. Early in 1972, Mark C. Porter presented the concentration polarization phenomenon in ultrafiltration firstly [34]. In those early stages, concentration polarization was recognized as one of the reasons for membrane fouling, resulting in a severe decrease of the transmembrane flux [34,47]. Later some studies extended the theory of fast initial concentration polarization by the fouling phenomena of cake or gel formation and pore plugging, being long-term effects during the filtration process when the solute concentration over the membrane exceeds its solubility [31,33,48,49].

Membrane fouling and the related phenomena including concentration polarization, cake or gel formation, and pore plugging lower the permeability and selectivity of membranes inevitably. The flux decay across the membrane is undergoing three phases. Howell and Velicangil [50] claimed that the first phase accomplishes in a few seconds, reaching a quasi-steady-state concentration distribution at the membrane surface. The initial reduction of permeate flux is attributed to this concentration polarization, providing a rapid buildup of a proteinaceous film over the membrane surface. Such a film is obviously increasing the resistance to permeate flow in addition to the intrinsic resistance of the membrane [51]. In the following around ten minutes, the adsorption of macromolecules onto the membrane surface and pores result in a further gradual decline of permeation rates. Finally, the long-term decay of permeate flux is attributed to the third stage of membrane fouling. In this stage, the highly concentrated retained solutes start to form a gel or cake layer between the polarization layer and the membrane surface. The porous cake layer is corresponding to the packing capacity of the retained solutes, which is the predominant factor to decline the flux at a slower rate continuously [31,50,52–54]. The pressure drops across the membrane itself will maintain at a relatively constant level. However, applying excess transmembrane pressure will not increase the hydraulic permeate flux because the applied additional pressure will mainly be absorbed by a compression of thicker cake layer increasing its resistance [31,34].

2.2.1 Theory of concentration polarization and membrane fouling

Concentration polarization (CP) and membrane fouling are major limiting factors in the ultrafiltration process due to the subsequent reduction in permeate flux. Therefore, considerable studies have been explored in this area to thoroughly understand these phenomena. The main theories utilized to describe these phenomena are the mass balance of solutes (convective-diffusive transport) determined by the hydrodynamic conditions in ultrafiltration and the osmotic pressures associated with the

thermodynamic properties of solutes in different layers, such as the pure polarization layer adjacent to the membrane, and gel or cake layer between the membrane surface and the polarization.

In the pressure-driven membrane filtration process, CP or fouling level is determined by the difference in solute molecules transported towards the membrane surface and resuspending back to the bulk solution. The polarization layer starts to form when the convective transport towards the membrane is greater than the back-diffusive flow to the bulk solution. Fig. 2.3 illustrates the schematic of steady state of concentration polarization at the membrane surface in typical cross-flow filtration [30].

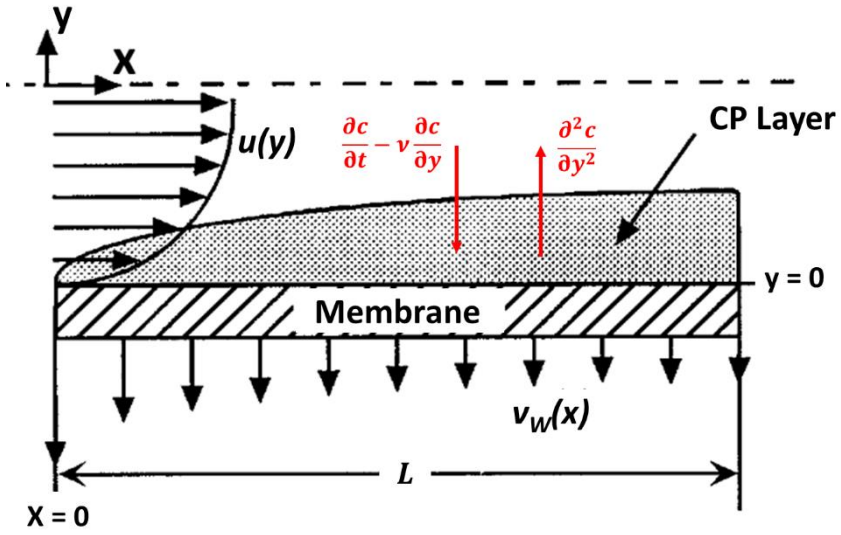

Fig. 2.3 Scheme of the concentration polarization in typical cross-flow filtration. The axial velocity u declines with the decreasing distance from the membrane surface, and the local permeate flux v_w has a reverse proportionality to the thickness of the local CP layer. The thickness of the CP layer is determined by the convection-diffusion transport near the membrane surface.

The spatial distribution of the solute can be described by a two-dimensional convective-diffusion equation is employed to describe the system with the assumption of constant density and diffusivity of solutes [49]:

$$\frac{\partial c}{\partial t} + u\frac{\partial c}{\partial x} + v\frac{\partial c}{\partial y} = D\,\frac{\partial^2 c}{\partial y^2} \tag{2.4}$$

where c is the concentration of solutes, v is the flow velocity orthogonal to the membrane surface, u is the velocity parallel to the membrane, and D is the diffusion coefficient of the retained molecules. In Eq. (2.4), the terms on the left side indicate the accumulation and the pressure-driven convective transport of solutes and the right side describes the diffusion behavior of species based on Fick's law. The models

based on this equation are well-known, including but not limited to the film model, gel-polarization model, gel- or cake-layer model, which will be illustrated in section 2.3.2 in detail.

2.2.2 Fouling reduction

The accumulation of retained solutes on the membrane is an inevitable, complex phenomenon and hard to counteract once established. Such deposition behavior of molecules is generally described as reversible concentration polarization and/or irreversible membrane fouling [33,55,56]. In the case of concentration polarization, the aggregated solutes on the membrane can resuspend to the bulk when the applied pressure across the membrane diminishes; while membrane fouling related phenomena - a gel or cake layer, pore blocking, or plugging - are normally irreversible and difficult to combat once the foulant block or plug into the pores. A myriad of practical approaches against the flux decay caused by the above-mentioned phenomena have been pursued, including but not limited to pretreat the feedstock [47,57], surface modification of the membrane and selection of suitable membrane materials [58–60], optimization of the hydrodynamics in the feed flow module [61,62], and good fluid management techniques [2,63].

When planning a membrane process, it is of significance to choose the suitable membrane type according to the properties of the target biomolecular solution. For example, Kwon and Zydney et al. [64] found for the formulation of the same model PEGylated protein, the fully retentive regenerated cellulose membranes have an enhanced filtration performance than the partially retentive polyethersulfone membranes because of the different dominating deposition behavior. The main reason for the flux decay in the case of cellulose membranes is concentration polarization; while when using the polyethersulfone membrane, membrane fouling was observed. Those foulants were composed of aggregated PEGylated proteins which have the properties of increased size, greater hydrophobicity, and lower electrostatic interactions. Kelly and Zydney [65] demonstrated that the fouling phenomenon is also impacted by the physicochemical characteristics of proteins. The proteins containing a free thiol group are more easily to form protein aggregates through the intermolecular thiol-disulfide bonds.

Besides, a large number of researches have clearly demonstrated the critical role of membrane chemistry [56,58,59,66,67], protein properties like shape and charge, solution conditions such as pH, salt concentration (ionic strength) [68–70], and addition of antifoam to decrease the viscosity of the solution, on the rate and degree of fouling phenomena. A well investigated example is ultrafiltration of bovine serum albumin

(BSA) [68,70,71]. The isoelectric point (IEP) of this globular protein is at pH = 4.8, where it has a minimum solubility. As a consequence, the agglomerating tendency of proteins is maximized when the pH environment of the solution in the system is close to 4.8.

Various flow systems have also been constructed to minimize the concentration polarization by an increased back transport of aggregates from the polarization layer into the bulk solution. The most straightforward way is to reduce the thickness of the polarization layer by increasing turbulent mixing at the membrane surface [72]. Using a magnetically driven stirrer to slow down the deposition speed during the course of the filtration process is a simple and direct way in the laboratory [34]. In comparison, effective fluid management by novel designs of membrane modules, such as flat-plate, open-tube, hollow fiber, and spiral-wound is popular in the industry [47]. Those modules can provide either turbulent or high-shear stress laminar flow by allowing the feed stream to flow tangentially over the membrane surface. In another study, Watanabe et. al [46] reduced concentration polarization and controlled membrane fouling of humic substances during NF and MF processes by vibrating the membrane to increase the shear rate at the edge of the membrane, which can increase the mass transfer rate for back diffusion and thus decrease the concentration on the membrane. They verified the different mechanisms of back diffusion of large and small molecular substances. The shear-induced diffusion is the major factor for humic substances with a molecular weight of more than 6 kDa; while for substances with lower MW, both the shear-induced diffusion and Brownian diffusion are helpful to maintain the level of permeate flux.

2.3 Modeling of ultrafiltration processes

2.3.1 Fluid mechanics and mass transfer

For the hydrodynamics of aqueous solvents in a pressure-driven membrane process, the permeate flux can be predicted by Darcy's law in Eq. (2.5), which states the flux J is proportional to the applied pressure difference as driving force.

$$J = -\frac{K_M}{\mu} \nabla P \tag{2.5}$$

with μ being the dynamic viscosity of the fluid, ∇P is the pressure gradient in the flow direction, and K_M is the intrinsic permeability of a porous membrane, having the dimension of (length)². The intrinsic permeability is independent of the properties of fluid but related to the membrane properties. An integral of Eq. (2.5) yields:

$$Q = \frac{K_M A}{\mu \delta} \Delta P \tag{2.6}$$

where Q is the flow rate through the membrane, A is the effective membrane area, and δ is the thickness of the membrane. From Eq. (2.6), the pressure gradient can be expressed as:

$$\nabla P = \frac{\Delta P}{\delta} = \frac{TMP}{\delta} \tag{2.7}$$

A comparison with Eq. (2.3) reveals the relation between the intrinsic and the volumetric permeability of a membrane as:

$$K_M = L_P \cdot \mu \cdot \delta \tag{2.8}$$

When the solution contains macromolecules, which are too large to pass the membrane, the phenomena of concentration polarization or/and fouling occurs, limiting the process performance consequently. Therefore, prediction of those phenomena is crucial to understand the underlying transport of the solutes, to optimize the processing design, and to predict the system performance. Membrane fouling is dependent on various factors such as the hydrodynamics in the system and the properties of the solute and membrane [34,73], resulting in a complex system that is hard to predict by simple mass transfer models. Hence, the coupling of convective-diffusion equation for mass transfer balance, Navier-stokes equations for motion balance and the corresponding boundary conditions are solved to simulate the flow field containing the target solutes in the membrane modules. A generic flow chart for the mass transfer analysis is illustrated in Fig. 2.4 [52].

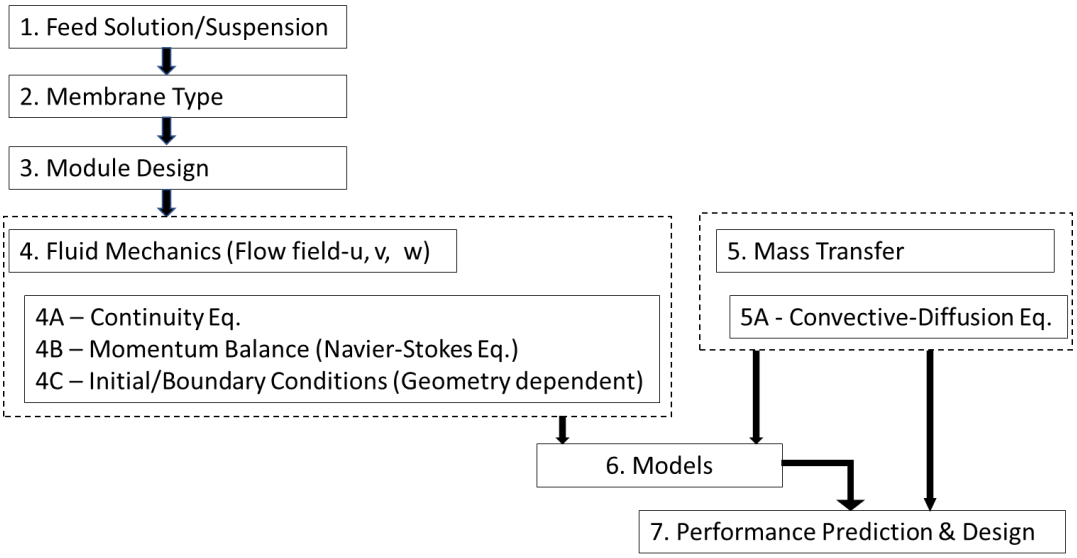

Fig. 2.4 Generic procedure for mass-transfer analyses. Adapted from Reference [52].

Solute transport from bulk solution to the membrane surface is governed by convective flow dragging the solute along with it [63]. The convective flux vector $\vec{J}$ is described as the product of solute concentration and the velocity vector, $\vec{J} = c\vec{v}$. For an incompressible fluid neglecting the body fields (e.g., gravity), the velocity vector must satisfy both the conservation of overall steady-state mass balance (continuity equation) and the steady-state momentum balance in each of the three dimensions (Navier-Stokes equations). The expression of the continuity and Navier-Stokes equations needed to be solved are

$$\vec{\nabla} \cdot \vec{v} = 0 \tag{2.9}$$

$$\vec{\nabla} \cdot \rho\vec{v}\vec{v} + \vec{\nabla}P + \vec{\nabla} \cdot \mu\vec{v} = \vec{0} \tag{2.10}$$

where ρ is the mass density of the solute, $\vec{\nabla}$ is the gradient vector operator, P is the scalar pressure field, and $\vec{v}\vec{v}$ is a dyadic product. The boundary conditions for the momentum balance are $\vec{v} = 0$ at the impermeable wall, $\vec{v} = v_W$ for a permeable wall and $\vec{v} = v_B$ for the fluid far away from the membrane surface. For a specific solute at steady state, without considering any chemical reactions among the solutes, the concentration profile is resulting by conservation of solute mass as:

$$\vec{\nabla} \cdot c\vec{v} + \vec{\nabla} \cdot D\vec{\nabla}c = 0 \tag{2.11}$$

where c is the concentration of the solute. In this partial differential equation, the second term on the left side represents the back-diffusion transport described by Brownian diffusion. The corresponding boundary conditions are $c = c_M$ at the membrane surface and $c = c_B$ for the fluid far away from the wall in free solution.

To describe the complex transport problem involving velocity flow and solute concentration accurately, it requires to simultaneously solve the set of five coupled non-linear partial differential equations (conservation of overall mass convection-diffusion equation, velocity fields in each of three dimensions Navier-Stokes equations, and solute concentration profile continuity equation) with boundary conditions [63,74,75].

Numerical modelling is a powerful tool to investigate the mechanisms of membrane fouling. Computational fluid dynamics (CFD) modelling, using numerical methods, has been performed widely to solve the complete set of aforementioned equations and predict the concentration profiles and flux distribution in membrane filtration [76–82]. These equations are solved by dividing the geometry of interest into finite elements or finite volumes and coupling discretization methods like finite difference and finite volume discretization with numerical methods [83]. Compared to the analytical mass and momentum transport models, the main advantage of CFD methods lies in their

ability to provide a rigorous analysis of the spatial and transient distribution of parameters such as solute concentration, flow, and pressure with a reduced number of assumptions [84,85].

2.3.2 Classical models for membrane fouling

Based on the mass balance of solutes and momentum balance of fluid during the filtration processes, there are various models describing and analyzing the phenomena of concentration polarization and membrane fouling. The boundary layer model (also named film theory-based model [77]) and the resistance-in-series model are commonly employed. In addition, considering the thermodynamic properties of the solution, the osmotic pressure model is also applied for the prediction of the performance of ultrafiltration processes.

Boundary layer model

Broadly speaking, the boundary layer model describes two phases of the deposition of large molecules at the membrane surface, including the stagnant film layer and the gel layer formation (also named cake-enhanced concentration polarization [86]). In this model, a thin layer of unmixed fluid with thickness δ is assumed to exist between the well-mixed feed solution and the membrane surface, as shown in Fig. 2.5 [72].

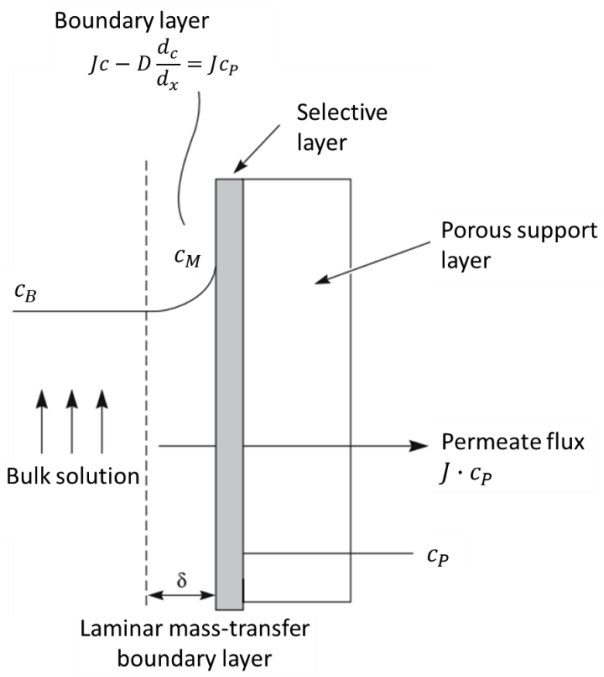

Fig. 2.5 Schematic description of the concentration polarization phenomenon at the membrane surface. Adapted from reference [72].

The concentration gradient, as the key controlling factor for the thickness of the polarization layer, is the driving force to diffuse concentrated solutes back into the bulk according to Fick's law. The solute concentration decreases from the maximum value at the membrane surface to the minimum concentration in the bulk [86]. In this hydrodynamic approach, in addition to an assumed constant diffusion coefficient of retained solutes and constant densities of solvent and solute, the concentration gradient parallel to the membrane surface is neglected compared to the concentration gradient in the direction perpendicular to the membrane [42].

When the system reaches steady state, a simple mass balance provides that the rate of solute flux passing through the membrane equals the convective transport rate of solutes towards the membrane minus the rate of back diffusion away from the membrane surface.

$$Jc_P = Jc - D\frac{d_c}{d_x} \tag{2.12}$$

where J is the transmembrane flux (m/s), c_P and c are solute concentrations in the permeate and boundary layer, respectively, D is the diffusion coefficient of the macromolecules (m²/s), and x is the distance to the membrane surface (m). For 100% solute retention, a good approximation for most proteins in ultrafiltration, c_P = 0. Thus [34,46],

$$Jc = D\frac{d_c}{d_x} \tag{2.13}$$

with a maximum concentration in the boundary layer, namely the concentration at the membrane surface c_M, an integration of Eq. (2.13) is obtained with the boundary conditions of $c(x = \delta) = c_B$ and $c(y = 0) = c_M$ [87],

$$J = \frac{D}{\delta}\ln\frac{c_M}{c_B} \tag{2.14}$$

where c_B is the solute concentration in the bulk solution. This shows that the permeate flux through the membrane is only influenced by the boundary thickness δ and the solute properties (D and the maximum concentration in the boundary layer c_M). Therefore, the method to enhance permeate flux is either to reduce the thickness of the boundary layer or to increase the overall mass-transfer coefficient k_{ov}.

$$k_{ov} = \frac{D}{\delta} \tag{2.15}$$

inserting Eq. (2.15) into (2.14), the permeate flux is defined as

$$J = k_{ov}\ln\frac{c_M}{c_B} \tag{2.16}$$

The mass-transfer coefficient k_{ov} varies in different flow regimes and also depends on the membrane configuration. It can be described by Leveque and Dittus-Bolter correlations for laminar flow and turbulent flow, respectively [71].
laminar flow:

$$Sh = k_L \frac{d_h}{D} = 1.62\ (Re\ Sc \frac{d_h}{\mathrm{L}})^{0.33} \tag{2.17}$$

turbulent flow:

$$Sh = k_t \frac{d_h}{D} = 0.023\ Re^{0.8}\ Sc^{1/3} \tag{2.18}$$

where Sh is the Sherwood number, k_L is the mass transfer coefficient in laminar flow, d_h is the equivalent hydraulic diameter, D is the diffusivity of the solute, Re is the Reynold number, Sc is the Schmidt number, and L is the length of the feed flow channel. Substitution of Re and Sc in Eq. (2.17) and (2.18) yields,

$$k_L = 1.62(\frac{uD^2}{d_h L})^{0.33} \tag{2.19}$$

$$k_t = 0.023 \frac{(u^{0.8} D^{0.67})}{(d_h{}^{0.2} \nu^{0.47})} \tag{2.20}$$

respectively. With u being the average fluid velocity through the channel and ν is the kinematic viscosity ($\nu = \mu/\rho$, being the ratio of viscosity and density of the fluid). One approach to increase the mass transfer coefficient is to increase the velocity through the regime according to Eq. (2.19) and (2.20), which consequently results in a higher shear stress. For a Newtonian fluid, the wall shear stress τ_W is defined by

$$\tau_W = \mu\gamma \tag{2.21}$$

where γ is the shear rate at the wall. For different module configurations, the shear rate is calculated by

$$\gamma = 6u/h \quad \text{for rectangle channels} \tag{2.22}$$

$$\gamma = 8u/d \quad \text{for tubes} \tag{2.23}$$

where h is the channel height and d is the tube diameter. Thus, a higher mass transfer coefficient can be obtained by increasing the shear stress as a result of increasing the flow velocity.

Several studies found that the oversimplified film model of Eq. (2.16) is insufficient to explain the flux trend versus the applied transmembrane pressure in long-term ultrafiltration for macromolecular feed solution and colloidal dispersion experiments. In these experiments, stable permeate flux through the membrane was observed when applying a series of increasing pressures at steady state. Michaels [87] and Blatt et al. [88] forwarded a hypothesis that the permeate flux is proportional to the applied

pressures when the concentration in the boundary layer is lower than the solute solubility. However, when the increasing concentration reaches the so-called 'gel concentration' c_G, retained solutes precipitate on the surface to form solid or thioxotropic gels. This hypothesis has been proved by Porter in 1972. He demonstrated in colloidal dispersions the post-formed polarization layer can grow into a close-packed gel layer and becomes thicker [34]. In this case, increased transmembrane pressure only temporarily produces a high flux, which brings more solutes towards the membrane and thus increases the hydraulic resistance to the flow by the thicker gel layer. As a result, the permeate flux subsequently reduces back to the stable level. In this case, c_M in Eq. (2.16) can be replaced by the maximum gel concentration c_G (or cake concentration for particle suspensions) and thus,

$$J_{lim} = k \ln \frac{c_G}{c_B} \tag{2.24}$$

with J_{lim} being the limiting flux. It is logarithmically related to bulk concentration c_B and approaches 0 when the limiting concentration in bulk $c_{B,lim}$ equals the gel concentration c_G. In addition to the classical boundary layer model, according to the hydrodynamics, thermodynamics and fundamental relationship of energy balance of particle suspensions, Song and Elimelech [31] proposed a novel dimensionless filtration factor N_F to completely describe the concentration polarization in cross-flow filtration. In their model, they also divided the deposition of particles on the membrane surface into two phases. One is the pure polarization layer, in which the flux through the membrane is proportional to the applied pressure. Furthermore, an additional cake layer forms between the membrane surface and the polarization layer when more solutes flow towards the membrane surface, as presented in Fig. 2.6.

Similar to the assumption in the boundary layer model, for the mathematical derivation of their theory, particles are treated as 'hard' spherical particles and thus no interaction between particles is considered. The expression of the dimensionless filtration number N_F is

$$N_F = \frac{4\pi {d_P}^3 (\Delta P)}{3kT} \tag{2.25}$$

where d_P is the effective particle radius, ΔP is the pressure drop across the accumulated layer, k is the Boltzman constant (1.38×10^{-23} J/K), and T is the absolute temperature. This number describes the ratio of the energy required to resuspend a particle from the accumulated layer into the bulk solution and the thermal (dissipative) energy. Comparing the filtration number to a critical value N_{Fc}, which is varied by the given particles and the filtration types (see Table 2.1), the polarization layer with its concentration-gradient is observed in the vicinity of the membrane surface only when

$N_F < N_{Fc}$. An additional cake layer will form between the membrane surface and the CP layer when $N_F > N_{Fc}$. This modified model based on the boundary layer film model is available for both porous and non-porous membrane, but limited to describe the concentration polarization phenomenon in processing for multi-components.

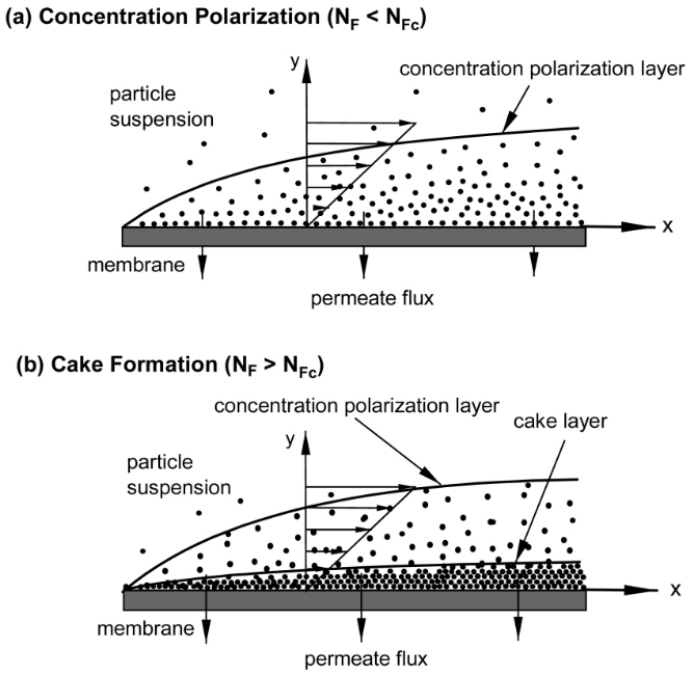

Fig. 2.6 Schematic description of concentration polarization and cake formation phenomena at the membrane surface. (a) Lower than the critical filtration number N_{Fc}, a pure concentration polarization layer forms. (b) Higher than the critical filtration number N_{Fc}, particles accumulate and form a cake layer [89].

Table 2.1 Ranges of the filtration number (N_F) for different cross-flow filtration systems

Filtration system	Pressure (kPa)	Particle size (m)	Filtration number (N_F)
Reverse osmosis	$10^3 – 4 \times 10^3$	3.6×10^{-10}	0.049 – 0.20
Ultrafiltration	$10^2 – 10^3$	$10^{-9} – 10^{-7}$	$0.10 – 10^6$
Microfiltration	< 30	$5 \times 10^{-8} – 10^{-5}$	$5 \times 10^3 – 5 \times 10^{10}$

Several studies have investigated the fouling phenomena based on the coupling of this analytical model and the associated numerical mathematic methods. Ahmad et al. [90] used a commercial CFD package to predict the concentration profile, mass transport and wall stress in the narrow channel. Using the film theory which links the hydrodynamics and mass transfer, they evaluated the thickness of the boundary layer from the simulated solute concentration at the membrane surface. Subramani et al. [77] compared the prediction of salt concentration polarization in cross-flow filtration

using a finite element method based numerical model and the classical film layer analytical model. They highlighted, in the case of a small lab-scale short membrane filtration channel with low cross-flow and low flux, that the results obtained with both approaches compared well with each other. While for the case of high cross-flow and high permeate flux in most full-scale modules, the film theory-based model overestimated the degree of concentration polarization (especially at the end section of channel), because it assumes a fully developed flow at the channel entrance and neglects the boundary thickness-dependent permeation. Later, Monfared et al. [91] simulated the influence of baffles arrangement to increase permeate flux during the gelatin-water ultrafiltration. Considering the interaction between the gelatin and the polysulfone membrane used, an appropriate interaction energy term coupling the amount of accumulated gelatin in the film layer at steady-state and the transient deposited gelatin concentration was included in the gelatin transport equation.

Resistance-in-series model

Ultrafiltration performance also can be explained by the resistance-in-series model, which is originally used for heat transfer problems. In this model, there is no need to evaluate the thickness of various layers in the vicinity of the membrane or the transport mechanism occurring [72]. The assumption made in this approach is that concentration polarization only occurs on the feed side of the membrane. The solute flux J crossing the membrane and the adjacent layers are described as

$$J = k_{ov}(c_B - c_P) \tag{2.26}$$

with k_{ov} being the overall mass transfer coefficient, c_B and c_P are solute concentrations in the feed bulk and permeate solution, respectively. Similarly, both the flux crossing the feed-side boundary layer and across the membrane are also J

$$J = k_{bl}(c_B - c_M) \tag{2.27}$$

$$J = k_M(c_M - c_P) \tag{2.28}$$

where k_{bl} and k_M are the mass transfer coefficients of the fluid boundary layer and the membrane, respectively, and c_M is the solute concentration at the membrane surface. From Eq. (2.26) - (2.28), a simple expression of the resistance-in-series model is derived as

$$\frac{1}{k_{ov}} = \frac{1}{k_M} + \frac{1}{k_{bl}} \tag{2.29}$$

The total mass transfer coefficient is predominantly impacted by the membrane intrinsic mass transfer coefficient k_M when the fluid boundary layer contributes in a large value k_{bl}, corresponding to a small resistance $1/k_{bl}$; when k_{bl} is small, the

resistance $1/k_{bl}$ turns to be the critical fraction of the total resistance to flow. k_{bl} is dependent on serval system parameters, resulting in empirical correlation of the type:

$$k_{bl} = constant\ u^{\alpha} h^{\beta} D^{\gamma} T^{\delta} \tag{2.30}$$

where u is the fluid velocity through the membrane module, h is the feed channel height. One limitation of this model is that those empirical correlations for the mass transfer coefficients require a large body of experimental data [34,92,93]. Thus this model is not suitable to evaluate new membrane processes or module designs.

An alternative expression for a resistance-in-series model is to take the total resistance of the membrane and the adjacent layers into consideration.

$$J = \frac{|\Delta P|}{\mu\,(R_M + R_S)} \tag{2.31}$$

where R_M is the intrinsic membrane resistance, which is calculated by

$$R_M = \frac{\Delta P}{J_w} \tag{2.32}$$

with J_w being the flux with pure water. R_S is the resistance caused by various layers such as the polarization, gel and filter cake layer. Therefore, it is possible to express the boundary layer model in terms of resistances according to the practical layers near the membrane, see Table 2.2.

Using this resistance-in-series model and with the help of the finite element method to solve the set of differential equations describing the mass transfer and hydrodynamics profiles, the fouling mechanism in the filtration process has been studied more and more comprehensively. In 2009, Marcos et al. [79] developed CFD models using the commercial software COMSOL to illustrate the transient flow and concentration profiles in a hollow fiber ultrafiltration system for concentrating soy protein extracts. A resistance model considering a global resistance, comprising of the resistances of the clean membrane, the polarization layer, the cake layer and the blocked pores was used to link the major parameters, such as the protein concentration, pressure and the permeate velocity through the membrane. In a separate study, Macedo et al. [96] used the resistance-in-series model to demonstrate the mass transfer mechanism in ultrafiltration using three different membranes for the concentration of pretreated ovine cheese whey. As the MWCO of membranes used in their study are 10 kDa and 20 kDa, and the molecular weights of the target whey proteins are 36.6 KDa and 14.2 KDa, respectively, the phenomena of both concentration polarization and membrane fouling (external and internal) were assessed. With the modeling results, they found the major contributor in the flux reduction varied with the used membrane material.

Table 2.2 Examples of the expressions of the boundary layer model in terms of various resistance layers

Expressions	Filtration system	Reference
$J = \frac{\lvert\Delta P\rvert}{\mu (R_M + R_S)}$	universal	
$J = \frac{\lvert\Delta P\rvert}{\mu (R_M + R_{bl} + R_G)}$	-	Fane [94]
$J = \frac{\lvert\Delta P\rvert}{\mu (R_M + R_{SD} - R_{SR})}$	stirred or cross-flow UF	Chudacek et al. [95]
$J = \frac{\Delta P}{\mu R_g}$, $R_g = R_M + R_{Pol} + R_{Cake} + R_{Block}$	constant TMP UF	Marcos et al. [79]
$J = \frac{\Delta P}{\mu (R_M + R_{CP} + R_F)}$	UF	Macedo et al. [96]
$J = \frac{\Delta P}{\mu (R_M + R_{AD})}$	unstirred dead-end UF	Luca et al. [97]

Note:

R_M, the membrane resistance

R_S, the polarized solutes resistance

R_{bl}, the boundary layers resistance

R_G, the gel-layer resistance (colloids)

R_{SD}, the deposited solutes resistance (=R_S)

R_{Block}, the blocked pore resistance

R_{SR}, the resistance removed by stirring

R_F, the fouling resistance

R_{Pol}, R_{CP}, the pure CP layer resistance

R_g, the global resistance

R_{Cake}, the cake-layer resistance (particles)

R_{AD}, the additional resistance

Luca et al. [97] used a multi-scale model integrating macroscopic and microscopic methods to simulate the UF performance for BSA aqueous solutions. They proposed one factor named the additional resistance R_{ad}, which can be derived from computations on the basis of BSA properties like the average surface charge, the effective diameter and contact molecular surface instead of empirical or semi-empirical correlations exploited from a set of experiments. By applying this factor to estimate the specific cake resistance, they observed a compact deposited BSA layer was adjacent to the membrane, and a reversible loose structure of concentration polarization layer was formed further away from the surface.

Osmotic pressure model

For a pure solvent feed flowing through a tortuous membrane channel under laminar flow conditions, the permeate flux can be described by:

$$J = \frac{|\Delta P|}{\mu R_M} \tag{2.33}$$

where J is the transmembrane flux (volumetric rate per unit membrane area), ΔP is the transmembrane pressure, μ is the viscosity of the solvent, and R_M is the intrinsic membrane resistance which can be expressed by the Carman-Kozeny equation [42]

$$R_M = \frac{180\,\delta\,(1-\varepsilon)^2}{d^2\,\varepsilon^3} = \frac{\delta}{\mathrm{K}_M} \tag{2.34}$$

where δ and K_M are the thickness and intrinsic permeability of the membrane, respectively. For the presence of solutes in ultrafiltration, the flux is generally calculated by:

$$J = \frac{|\Delta P| - |\Delta \pi|}{\mu\,(R_M + R_S)} \tag{2.35}$$

where ΔP is the pressure difference across the membrane, $\Delta \pi$ is the osmotic pressure difference, corresponding to $\pi(c_M) - \pi(c_P)$ with the concentration at membrane surface and in the permeate, respectively.

Compared to the solute concentration in reverse osmosis, the typical feed concentrations of macromolecules processed in ultrafiltration have a much smaller osmotic pressure. The osmotic pressure of dilute solutions is influenced by the solution pH, ionic strength and excluded volume. However, the concentration in the polarization layer can be one to two orders of magnitude higher than that in the bulk solution. In this case, even in ultrafiltration the resulting osmotic pressure can reach significant levels, as illustrated in Table 2.3. Consequently, the osmotic effect should be considered as long as the boundary layer remains Newtonian and no gel layer or precipitation occurs [42,94]. Although the osmotic pressure model has been proved equally useful to describe membrane filtration processes as the boundary layer resistance model [98], the osmotic effects are frequently ignored and the osmotic-pressure model is rarely employed for ultrafiltration systems but for forward osmosis system [80,99].

As mentioned above, the osmotic-pressure model is not frequently used for the analysis and prediction of concentration polarization and fouling phenomena in the UF process, but there are still a few published works integrating this model with others. In 2006, Bacchin [78] used finite volume CFD modelling to solve the momentum and mass transfer equations in cross-flow colloidal dispersion filtration of colloidal suspensions and to predict the relationship between the colloidal osmotic pressure and the volume fraction of the colloids. They state that the transition of deposition mechanism from the dispersed phase (a loose layer with a low fractal dimension) to the condensed phase (a compact ordered deposit) is determined by the critical flux

dividing the filtration conditions into the reversible concentration polarization (lower than the critical flux) and irreversible deposit or gel layer (higher than the critical flux).

Table 2.3 Osmotic pressure of model macromolecular solutions [49,98,100]

Conc. (g/L)	Osmotic pressure (kPa)				
	BSA (pH 5.4)	Whey proteins	Dextran		
			T10	T70	T500
100	7	63	72	21	13
200	25	126	216	97	84
300	60	298	595	284	267
400	134	685	1300	-	-

Instead of using the osmotic-pressure model independently, Fernández-Sempere et al. [101] proposed a mathematical model combing the convection-diffusion mechanism with the osmotic pressure model and the resistance-in-series model to predict the concentration and permeate flux profiles in dead-end UF of PEG-10000 solutions, the simulation results show reasonable agreement with the experimental data.

2.4 3D printing technology in bioengineering

The technology used for printing physical three-dimensional objects from digital models is called 3D printing (also known as ‘additive manufacturing’ or ‘rapid prototyping’). The principle of this technology is to form the desired item by laying down successive layers of material in different shapes. In 1984, Charles W. Hull firstly developed this technology and named it Stereo lithography [102]. A 3D image of an object is designed using computer-aided design (CAD) software, then the printer receives the structure information to print the object by depositing the materials layer-upon-layer. 3D printers are typically classified into four types according to their printing technology: stereo lithography (SLA), selective laser sintering (SLS), fused deposition modeling (FDM) and PolyJet photopolymerization [103–106]. Fig. 2.7 shows the schematic illustration of working principles of each type of 3D printer. The SLA printer is primarily composed of a vat to contain a photosensitive resin (photopolymer) and a laser source to provide the UV light. The vat can move freely in the vertical direction and the laser source can move horizontally. Since the photopolymer is photosensitive

to the laser beam, the material is solidified when expose to the UV light. This process is repeat for each layer until the item is fabricated completely.

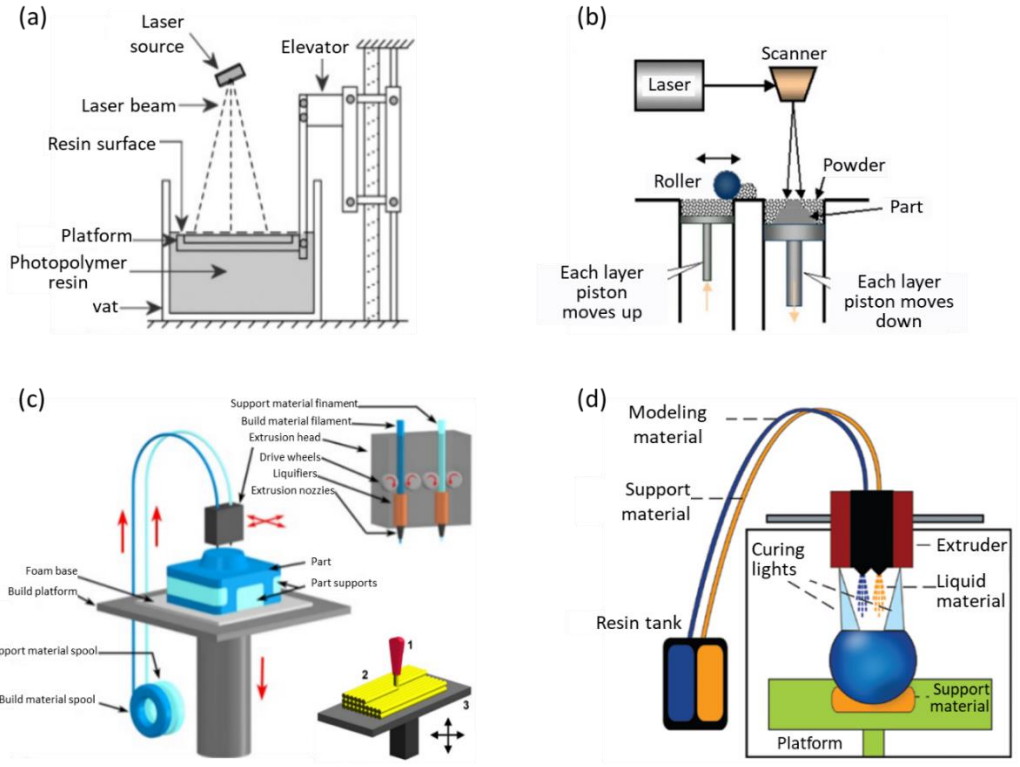

Fig. 2.7 Schematic illustration of working principles of typical 3D printers [107–109]. (a) SAL printer. (b) SLS printer. (c) FDM printer. (d) PolyJet printer.

In the SLS printer, the vat that contains the liquid photopolymers is replaced by a powder-bed. Each layer of the material is placed to the desired place by the controlling of a leveler or roller on the tray. The thickness of each layer is around 0.001 to 0.1 inches and it is controlled by the strength of the laser beam and material types [110]. A wide range of materials have been used for 3D printing including plastic, resin, metal, rubber, concrete, glass, ceramic or composite materials [111]. Compared to the laser strength used in SLA printer, much stronger laser strength (e.g. a carbon dioxide laser) is applied in SLS to fuse the small powder materials into a mass of desired 3D shape. In contrast to the SLA and SLS printers, the FDM printers have extrusion nozzles to melt the thermoplastic materials which are in the form of continuous filament. Each time, a small stream of plastic squeezed out from the nozzle will be formed into the designed shape on the flat build platform surface. PolyJet (also known as MultiJet) printer uses material jetting (MJ) 3D printing technology. It is composed of a build platform, a material container, and a carriage on which ultraviolet lights and jetting print heads are mounted. Before starting the print, photopolymer resin needs to be heated

appropriately to obtain the desired viscosity. When the carriage reaches the designated position, the printer heads selectively jet the liquid resin onto the build platform in the form of droplets, and immediately the UV lights cure them into an ever-growing solid. Then the build platform moves vertically to accommodate the next layer until the objects are finished [108]. Due to the multiple printing heads, PolyJet printers enable printing different materials simultaneously. In addition to fabricating the target objects during the printing process, support materials are also used to support the overhangs and thin features. The support materials are removed either mechanically (cutting, drilling), dissolved chemically (sodium hydroxide, etc.), or by heating the modules if paraffin wax is used as support material [107].

Due to the profound advantage in high reproducibility and resolution, facile and flexible manufacturing, the emerging additive manufacturing technology has been widely explored to build devices according to requirements, such as plastic molds in a microscale electrodialysis platform for desanilation [112], a fluidized bed reactor for intensification of electrochemical reactions [113], 3D printed multipumping system for the detection of lead [114] and 3D printed two-piece modular devices integrated with disk-based solid phase extraction (SPE) for the water analytics [115].

With the notable transition of the application from the industrial design, construction, and biomedical applications to the recent bioseparation and chromatography, more printable materials have been developed such as cellulose hydrogels and agarose [116–119]. In 2014, Fee et al. [120] firstly used 3D printing technology to fabricate a monolithic chromatography columns, in which not only the uniform particle size distribution but also the location and orientation of each bead can be controlled precisely in the porous bed with the help of replicate CAD models. They demonstrated their novel approach is not limited to chromatography application and has the potential to design various geometry elements for the packed bed according to the demands of any application (e.g. filtration and catalytic reaction) requiring fluid-solid contacting. More recently, Moleirinho et al. [121] proposed the application of 3D printing in the purification of viral particles of downstream processing using 3D printed porous chromatographic stationary phases. By functionazing two different ligands (hydroxyapatite and DEAE) on the cellulose columns, they achieved a comparable recovery yield and dynamic binding capacity with other conventional/traditional techniques for viral purification, such as density gradient ultracentrifugation and anion exchange chromatography using membrane adsorbers. In their study, they proved that the use of 3D printing technology in the field of bioseparation is more flexible and can both meet the specific purification requirements with customized columns and avoid complicated packaging procedures. All in all, 3D printing technology opens new

avenues for the production paradigm and manufacturing possibilities because of the merit and easy share between different laboratories.

3 Design of a novel module for continuous UF/DF system

3.1 Design and fabrication of the membrane module

There are several types of modeling software tools to create 3D printable objects. For instance, the easy-to-use options such as Tinkercad for beginners, Blender for amateurs and advanced users, Autodesk Inventor for advanced users and professionals. In this study, Inventor was used for the designing of the novel membrane module. The designed module mainly exists of two 3D-printed lateral parts to contain either fresh diafiltration buffers or permeates, and one 3D-printed middle part form the feed-retentate channel. The channels of all three parts are filled with a hollow grid-structure mechanically supporting the two UF membranes which are placed between the middle part and the upper and lower lateral parts (Fig. 3.1 (a)). A 3D printer PolyJet system EDEN 260 (Stratasys, Eden Prairie, USA.) was used to print the modules with high resolution. It has the nominal resolution in x-, y-direction of around 40 µm and in z-direction of 17 µm, providing the ability to print sufficiently fine structures. In addition, it offers the ability to print smooth surfaces, an important feature to avoid leakage when assembling the membrane between the parts. Fig. 3.1 shows an exploded view of the first prototype of the designed module and a photograph of the 3D printed parts. The material used for the 3D printed parts is either VeroWhite or VeroClear, both are composed of a UV curable polyacrylate polymer with good chemical resistance.

The grid-structure of the middle part is preliminarily designed as a hollow-carved cubes arrangement, providing no obstacle for the flow in y-direction (perpendicular to the membrane surface) while guiding and diverting the flow in x-direction (parallel to the membrane surface). In the system, species transport in the feed-retentate channel is influenced by the convective flux towards the membrane, back diffusion away from the surface and eddy dispersion effects based on the flow through the grid structure. In order to investigate the influence of the flow path in the grid, in addition to the grid structure shown above, four other grid structures of the middle part were designed, leading to different degrees of eddy dispersion effects (Fig. 3.2). With the pillar-support grid-structure (Fig. 3.2 (a)), the membrane area covered by the grid is minimum, thus providing the maximum effective membrane area.

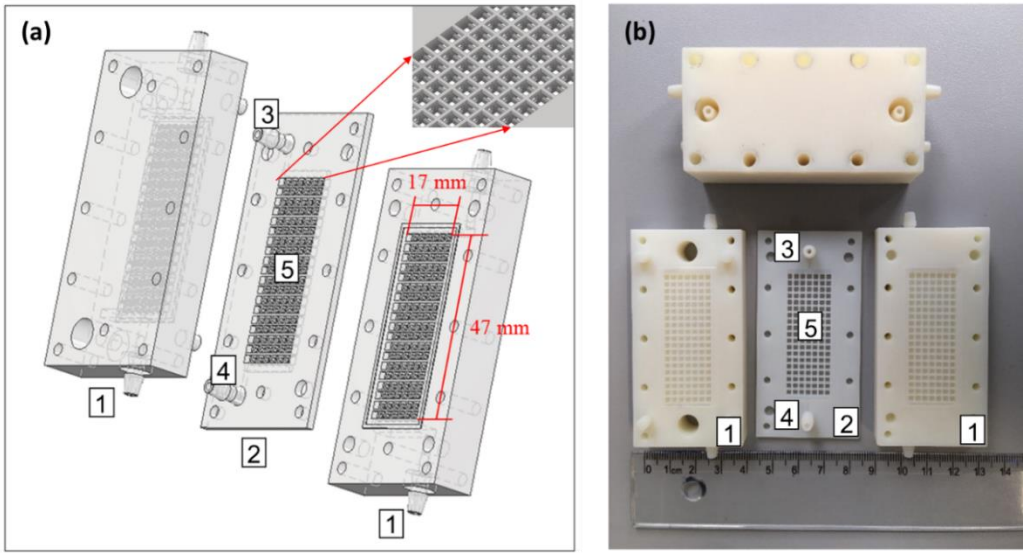

Fig. *3.1 Exploded view and photograph of the first prototype of the novel membrane module for continuous UF/DF. (a) 3D printable models designed in Autodesk Inventor, (b) 3D printed modules produced using a PolyJet system EDEN 260. 1. lateral part to transport either diafiltration buffer or permeate solution; 2. middle part forming the feed-retentate channel and the mechanical support of the membranes; 3. inlet of the feed flow; 4. outlet of the retentate flow; 5. hollow-carved grid structure to allow tangential flow along the membrane surface.*

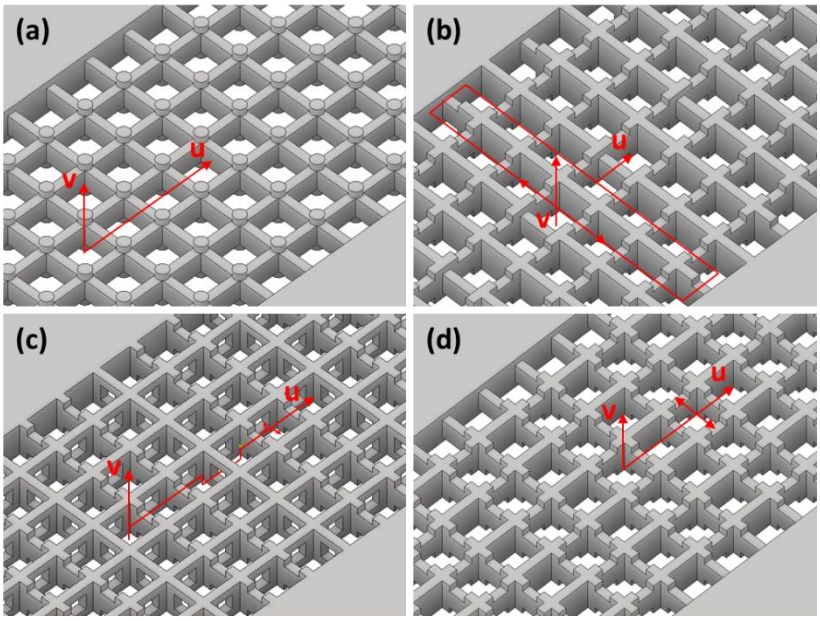

Fig. 3.2 Different designs of the grid-structure of the middle part of the membrane module. (a) Pillar-support grid-structure, (b) Grid-structure with maximized flow path length, (c) Grid-structure with highly anisotropic flow path, (d) Grid-structure with minimized flow path length.

However, in case of this minimized support area, the mechanical load onto different parts of the pressurized membrane must be considered to prevent membrane damage. The grid-structures of the middle part in Fig. 3.2 (b) and (d) have similar characteristic of the flow perpendicular to the membrane, however, they differ in the way the flow is guided with the plain of the grid. Structure (b) enforces a meandering flow guiding the fluid towards the sides of the channel and back into the middle. By this, the length of the flow path is increased, and because the volumetric flow rate is kept constant, the flow velocity in the cubes is increased. In contrast, the grid-structure in (d) provides multiple flows path along the grid, reducing the flow velocity in the single cubes. The highly anisotropic flow path grid-structure in (c) offers strong eddy dispersion effects due to the strongly varying directions of the streamlines along both, short and long, membrane sides.

For the purpose of increasing the buffer exchange efficiency using the novel module design, an advanced version was developed to provide longer residence time of the feed solution by increasing the length of the flow path.

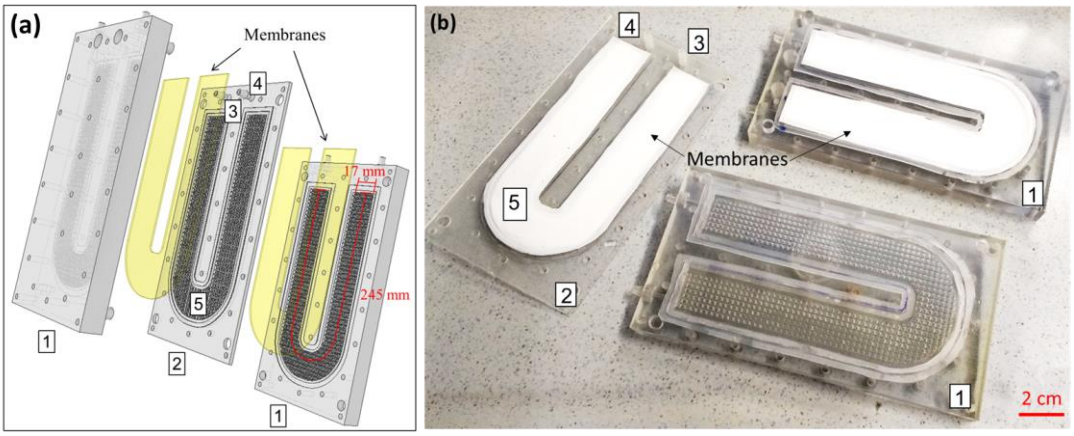

Fig. 3.3 Scaled-up membrane module for continuous DF. (a) 3D printable models designed in Autodesk Inventor, (b) 3D printed parts fabricated by the PolyJet system EDEN 260. 1. lateral part to transport either the diafiltration buffer or the permeate solution; 2. middle part forming the feed-retentate channel and mechanically support two membranes located next to it; 3. inlet of the feed flow; 4. outlet of the retentate flow; 5. hollow-carved grid structure to allow the tangential flow along the membrane surface.

As shown in Fig. 3.3, the main features of the scaled-up module are the same as the prototype one, only the length of the channel guiding feed, retentate, diafiltration buffer, and permeate was increased almost 5-fold.

3.2 Experimental set-up

The overview of the experimental set-up used in this study is shown in Fig. 3.4. The system in (a) is for the continuous concentration of proteins and simultaneous buffer exchange. A commercial cross-flow system (SARTOFLOW® Smart, Sartorius) was applied in this case. With the exception of replacing the original filter cartridge with the prototype membrane module and the addition of a syringe pump for the supply of the feed solution, the system was not altered. In our case, the SARTOFLOW system was used to pump fresh diafiltration buffer in a loop through the upper lateral part and to record the weights of the storage tank of fresh diafiltration buffer and the storage vessel of the retentate stream in-real time. In addition, the pressures in the feed, retentate and the inlet of the diafiltration buffer were recorded A syringe pump (Pump 11, Harvard Apparatus) was used for pumping the feed solution into the middle part of the module at a constant flow rate, independent of the pressures in the system.

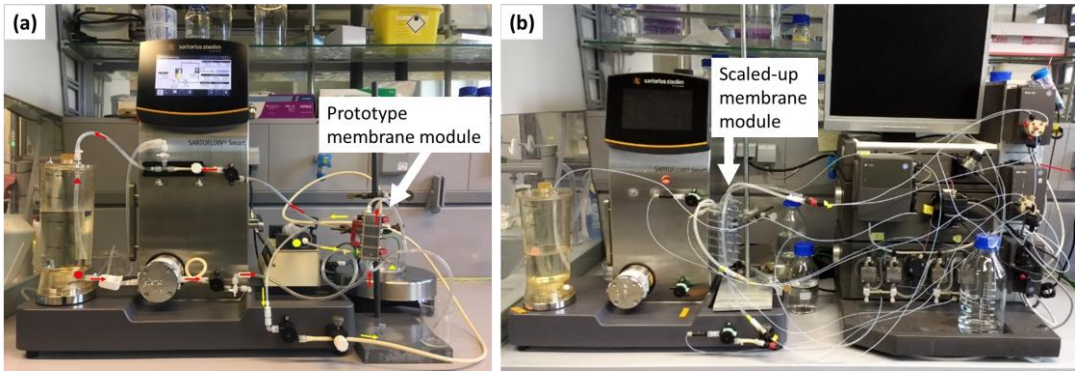

Fig. 3.4 Overview of the system used for UF/DF. (a) System coupled with the prototype membrane module for continuous UF/DF simultaneously, (b) System coupled with the scaled-up memembrane module for high efficiency buffer exchange using continuous DF.

For the characterization and testing of the scaled-up prototype of the membrane module a second, sophisticated test setup was established, allowing various new operation modes such as counter-current flow directions of retentate and DF buffer. The test setup consisted of an ÄKTA FPLC system and the SARTOFLOW cross-flow filtration system (see Fig 3.4b). The Äkta was used to convey the volume flows and to measure the protein concentration and the buffer conductivity. In addition, the flow direction of the diafiltration buffer was controlled by means of the multiport valves and the control software of the FPLC system Unicore. Conductivity and UV signal were monitored in real time. Pressures and weight changes of the storage tanks of diafiltration buffer and permeate were recorded using the SARTOFLOW. Pump A of the ÄKTA system was used to pump the feed. Pump B was used to control the flow of

the retentate. The use of the high-pressure piston pumps of the FPLC system ensures a precise control of the volume flows of feed and retentate, independent of dynamic pressure build-up in the membrane module. For reliable operation of the piston pump B controlling the retentate flow, a counterpressure exceeding the one at the retentate outlet has to be generated downstream of pump B. This can easily be accomplished by connecting a thin capillary of appropriate length to the pressure side of the pump B. Besides the capillary, the retentate passed the UV measuring cell and the conductivity cell of the FPLC system. Since only two scales were available for real-time data tracking, the weights of the respective containers, before and after the experiment, were noted for feed and retentate and converted into a volume flow rate by dividing the experiment duration. The optional sample pump of the ÄKTA system was used to deliver the diafiltration buffer, pumping the buffer from the tank on the online scale of the SARTOFLOW system into the membrane module via the pressure sensor. The permeate was transferred at ambient pressure via a tubing from the module to the permeate tank placed on the second on-line balance. All volume flows were calculated based on the change in weight, assuming a density of 1 g/cm^3.

Process control was thus carried out at constant volume flows and variable pressures. To keep the hold-up volume of the periphery as low as possible, ÄKTA capillaries were used for the majority of the tubing. This ensured a faster response of the system to volume flow changes. Since the module and the pressure sensors are equipped with luer-lock connectors, appropriate adapters are needed to connect them with the ÄKTA capillaries. The pressures for the calculation of the transmembrane pressure were measured at the diafiltration side between the sample pump and the module. Because of the short flow path in the module and the comparably low feed flow rates, the pressure drop in the retentate channel is neglected and the same pressure on the feed and the retentate connectors of the module is assumed. This simplification had to be made due to the design and location of the pumps, sensors and valves.

4 Publications and Manuscripts

Continuous Ultrafiltration/Diafiltration using a 3D-printed two membrane single pass module

Ruijie Tan, Matthias Franzreb

Biotechnology and Bioengineering, 2020, 117, 654-661

DOI: https://doi.org/10.1002/bit.27233

ISSN: 1097-0290

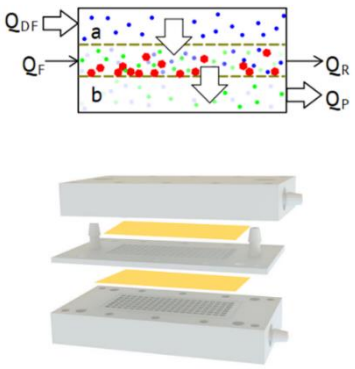

A 3D printed ultrafiltration/diafiltration (UF/DF) module is presented allowing the continuous, simultaneous concentration of retained (bio-)molecules and reduction or exchange of the salt buffer. Differing from the single-pass UF concepts known from the literature, DF operation does not require the application of several steps or units with intermediating dilution.

Continuous single pass diafiltration with alternating permeate flow direction for high efficiency buffer exchange

Ruijie Tan, Fabian Hezel, Matthias Franzreb

Journal of Membrane Science, 2021, 619, 118695

DOI: https://doi.org/10.1016/j.memsci.2020.118695

ISSN: 0376-7388

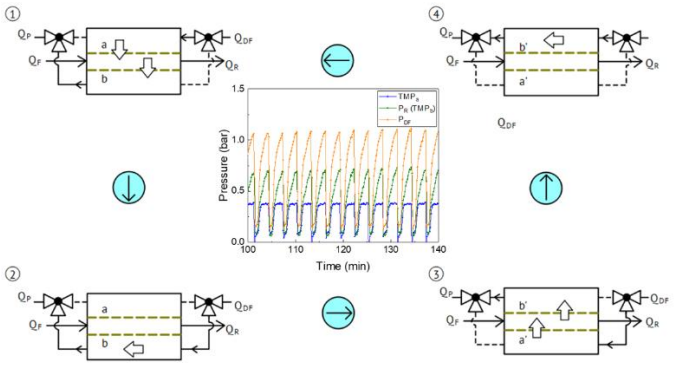

An upscaled 3D-printed membrane module for continuous diafiltration is presented. The module achieves diafiltration efficiencies of 99.3% applying 7 diavolumes (or 99.9% at 14 diavolumes). By this a single unit of the 3D-printed membrane module achieves diafiltration efficiencies surpassing the theoretical optimum of a conventional two stage counter-current SPTFF system. In addition, it is shown that the problem of concentration polarization can be strongly reduced in the device, by the generation of an alternating direction of permeate perfusion through the membranes as process inherent backflush, while continuously conducting the diafiltration without interruption.

Simulation based evaluation of single pass continuous diafiltration with alternating permeate flow direction

Ruijie Tan, Matthias Franzreb

Submitted to journal Chemical Engineering Journal

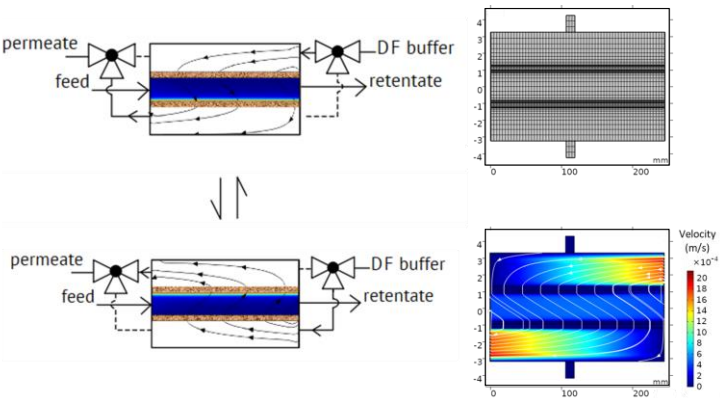

A detailed finite element model of the physical processes within the novel single pass filtration module is presented, predicting key figures such as the obtained diafiltration efficiency and the resulting pressures. The predicted data are validated by experimental results, revealing a good agreement of the qualitative behaviour of the module but also its quantitative characteristics. In addition, a thorough parameter study is conducted, showing that the performance of our single module can match the performance of a conventional three-stage counter-current SPTFF system.

5 Continuous Ultrafiltration/Diafiltration using a 3D-printed two membrane single pass module

Ruijie Tan[1], Matthias Franzreb[1*]

[1]*Institute of Functional Interfaces (IFG), Karlsruhe Institute of Technology (KIT), Hermann-von-Helmholtz-Platz 1, 76344 Eggenstein-Leopoldshafen, Germany*

[*]Corresponding author: matthias.franzreb@kit.edu

Abstract A 3D-printed ultra-/diafiltration (UF/DF) module is presented allowing continuous, simultaneous concentration of retained (bio-)molecules and reduction or exchange of the salt buffer. Differing from the single pass UF concepts known from the literature, DF operation does not require the application of several steps or units with intermediating dilution. In contrast, the developed module uses two membranes confining the section in which the molecules are concentrated while the sample is passing. Simultaneously to this concentration process, the two membranes allow a perpendicular in and outflow of diafiltration buffer reducing the salt content in this section. The module showed the continuous concentration of a dissolved protein up to a factor of 4.6 while reducing the salt concentration down to 47% of the initial concentration along a flow path length of only 5 cm. Due to single pass operation the module shows concentration polarization effects reducing the effective permeability of the applied membrane in case of higher concentration factors. However, because of its simple design and the capability to simultaneously run ultra- and diafiltration processes in a single module, the development could be economically beneficial for small scale UF/DF applications.

Keywords: SPTFF, UFDF, continuous,3D-printing, SPDF

Published in Biotechnology and Bioengineering. 117 (2020) 654-661

5.1 Introduction

Ultrafiltration(UF) is a powerful membrane technology to separate dissolved macromolecules from low molecular weight components [1]. According to their retention properties, UF membranes are especially useful to concentrate dilute product streams in the biotechnological industry. Another common application of UF membranes is within the frame of so-called diafiltration (DF) applied to reduce the ionic strength or change the buffer type in which the retained macromolecules are dissolved [2]. During diafiltration the feed solution buffer is continuously or stepwise diluted by the addition of pure water or a new buffer, while constantly withdrawing a part of the solution as permeate through the UF membrane [3]. During the process of concentration of the biomolecule solution by UF/DF, the permeate flux declines over time mostly because of concentration polarization near the surface of the membrane and the increasing viscosity of the recirculated feed solution[4]. Therefore, the conventional way of operation of UF/DF system in biotechnology is so-called tangential flow filtration (TFF) in which the fluid flows mainly parallel to the plane of the membrane and at relatively high speed, resulting in the prevention of pronounced concentration polarization and membrane fouling. However, the high flow speed leads to only small concentration effects during one passage through the UF/DF system [5,6]. In consequence, frequent recirculation of the feed solution in a loop is required, strongly increasing the energy demand, and resulting in the danger of unwanted temperature increase. The high flow speed and frequent recirculation also increases the shear stress onto the dissolved substances and can result in foaming problems, which may lead to damage or denaturation of sensitive biomolecules [7]. An alternative to TFF is normal flow filtration (NFF), also called dead-end filtration, in which the flow velocity is perpendicular to the plane of the membrane. NFF prevents high shear stress but quickly leads to strong concentration polarization, membrane plugging and very low fluxes through the membrane. As a possible solution to this dilemma single pass tangential flow filtration (SPTFF) has been developed by Gaston de los Reyes in 2005 [8]. Applications of single pass UF with the tangential flow have been reported before, e.g. for blood concentration [9], however, de los Reyes and Mir specially adapted the technology to protein concentration and optimized multi-module setups.

The basic principle of SPTFF is to improve the conversion of a single pass, saying the ratio between the permeate and the feed flow and therefore the concentration factor of the target solute, through increasing the residence time. Increasing the residence time can be accomplished by reducing the feed flow or increasing the flow path length within the membrane module [10]. Although operating with a single pass

of the fluid, compared to dead-end filtration SPTFF still has the advantage of tangential flow having the potential to sweeping away e.g. aggregated molecules from the surface of the membrane and limiting concentration polarization. Additional benefits of SPTFF are the avoidance of additional piping, storage and control instrumentations for the loop section of conventional TFF [5,11,12]. Original SPTFF was mainly used for debottlenecking downstream processes by concentrating process streams between two unit operations, e.g. chromatography steps [13,14]. SPTFF also proved useful for decoupling upstream and downstream process units by inline concentration of clarified cell culture broth [15,16]. Recently, SPTFF has been reported as an interesting tool for continuous diafiltration [17,18]. In this operation mode several SPTFF units are sequentially connected while the diafiltration buffer is added between the units. Passing the first SPTFF unit the feed is concentrated by a certain factor, followed by dilution with diafiltration buffer, usually to a level at which the target biomolecule reaches the concentration originally present in the feed. By this, using an arrangement with three modules, Rucker-Pezzini could demonstrate a continuous buffer exchange > 99.7% with the help of SPTFF. Regarding the required amount of diafiltration buffer, the efficiency of such an arrangement could even be improved by realizing a counter-current principle, in which fresh diafiltration buffer is only applied in the feed of the last SPTFF stage, while the permeate of this stage is used for dilution of the feed of the preceding SPTFF stage [19]. Nevertheless, independent of using con-current or counter-current routing of the buffer, continuous diafiltration using SPTFF requires sequential concentration and dilution of the target biomolecule. If the sequence starts with the concentration step in the first SPTFF module, the degree to which this concentration can be done without the risk of forming aggregates or operating at impracticable low permeate fluxes is limited. If the sequence starts by diluting the feed with diafiltration buffer in front of each SPTFF module, the degree of this dilution is limited by the condition that the required buffer amount should be minimized. Up to now no SPTFF module has been reported, which allows a gentle diafiltration process at constant or slightly increased target molecule concentration, as it is the case in conventional diafiltration with continuous replacement of the permeate volume by fresh diafiltration buffer.

Therefore, it was the purpose of this study to design and investigate a first small prototype of a SPTFF system realizing continuous, and truly simultaneous UF and DF operation by the use of a two-membrane set-up. Applying commercial UF membrane sheets and high-resolution 3D-printing techniques, a device is fabricated in which the feed flows through a narrow channel formed by two adjacent membranes and a porous spacer between. By this, one membrane can operate in SPTFF mode while the second

membrane simultaneously is permeated by pure water or diafiltration buffer, gradually replacing the solution in the channel. Controlling the pressures in the different fluid reservoirs of the device as well as the residence time of the feed solution in the central channel, the degree of concentration as well as buffer exchange can be adjusted independently.

5.2 Material and methods

5.2.1 Protein solution and membrane

The model protein used for UF/DF experiments was bovine serum albumin (BSA, molar weight 66.5 kDa) purchased from PanReac AppliChem (Darmstadt, Germany). The feed solution was prepared by dissolving BSA powder (0.1 g/l) and sodium chloride (100 mM, Merck KGaA, Darmstadt, Germany) in ultrapure water, the pH of the solution was determined as 6.40. The ultrapure water for buffer preparation was produced by a Sartorius arium® pro system (Sartorius, Göttingen, Germany). For buffer exchange a low salt solution containing 5 mM of NaCl was used. The used OMEGA ultrafiltration polyethersulfone (PES) membrane (30 kDa MWCO, OT030SHEET, Lot. #H3186I) was purchased from Pall Life Sciences (Hauppauge, USA). According to the manufacturer, the water permeability and BSA passage of this membrane are given as 458.5 L/(m² h bar) and 0.86%, respectively.

5.2.2 3D printed UF/DF module

All experiments were performed with a self-designed diafiltration module shown in Fig. 5.1. Except for the membrane all parts of the module were 3D printed with a PolyJet system EDEN 260 (Stratasys, Eden Prairie, U.S.A.) using the material VeroWhite. VeroWhite is a UV curable polyacrylate polymer with good chemical resistance. The PolyJet technology offers a nominal resolution of 17 µm in z direction and around 40 µm in x,y direction, delivering the required resolution for smooth surfaces which can be sealed by the membrane and the fine channel structures within the module. The PolyJet technology uses a support material to realize the closed channel structure. After the printing the support material is dissolved by 1M sodium hydroxide solution overnight.

The 3D-printed membrane module is assembled of three parts, two lateral parts and one middle part, which form the required liquid distribution system and provide mechanical support for membranes. The module contains two rectangular membrane sheets, one on each side of the middle part. The size and hold up volume of the central section of the middle part are 20 × 50 × 2 mm^3 and 1.4 ml, respectively. The membrane

is supported by a grid-like structure with 1 mm thick walls at a distance of 3 mm. In order to allow the tangential flow along the membrane, the walls are perforated by 1×2 mm^2 openings. Subtracting the area covered by the printed support grid, an effective membrane area of 0.000532 m^2 results on each side.

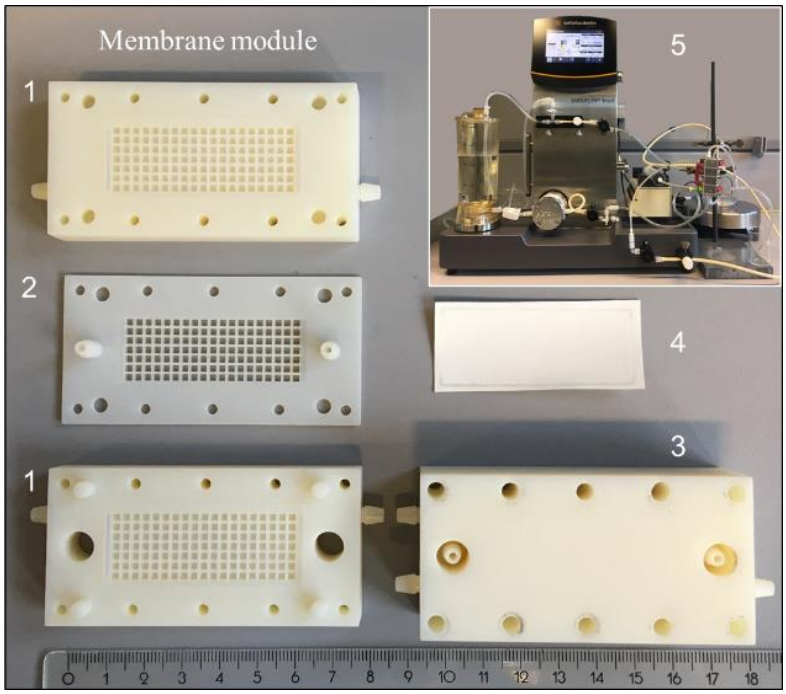

Fig. 5.1 3D-printed UF/DF module for single pass diafiltration: 1. lateral part, 2. middle part, 3. assembled module, 4. commercial OMEGA ultrafiltration membrane, 5. UF/DF peripheral equipment. UF/DF, ultrafiltration/diafiltration

A syringe pump (Pump 11, Harvard Apparatus, Holliston, USA) is used to enter the feed solution into the middle part in a single pass operation mode. Perpendicular to the flow direction of the feed solution, the flow of the exchange buffer is controlled by a conventional lab-scale UF/DF system (SARTOFLOW® Smart, Sartorius, Göttingen, Germany). The use of such a conventional UF/DF system is not mandatory for operating the developed module, however, it allowed the automatic recording of the mass changes of the exchange buffer storage and of the permeate.

5.2.3 Description of the experimental set-up and the monitored parameters

The described membrane module was integrated into an experimental set-up for UF/DF experiments as shown in the scheme of Fig. 5.2. For simultaneous single pass ultra- and diafiltration the feed solution was pumped into the module with a constant volume flow Q_F controlled by a syringe pump. The volume flow Q_R leaving the middle part of the module was controlled by a throttle valve in the outlet and the pressure P_R

was monitored by a sensor. The peristaltic pump of the conventional UF/DF system was used to pump the exchange buffer in a loop through the upper part of module. In the loop two sensors monitored the pressures $P_{DF,in}$ and $P_{DF,Out}$ at the inlet and the outlet of the upper module part. $P_{DF,in}$ and $P_{DF,out}$ were controlled by a throttle valve located downstream of the $P_{DF,out}$ sensor as well as the adjusted flow in the loop. When the pressures $P_{DF,in}$ and $P_{DF,out}$ in the upper module part were adjusted above the pressure P_R in the middle part, a specific flux J_{DF} of exchange buffer passed the UF membrane 'a' between the respective module parts. The exchange buffer storage was placed on a balance allowing accurate monitoring of the volume flow Q_{DF}, which is given by the specific flux J_{DF} times the effective membrane area. The pressure at the lower part of the module was kept at atmospheric pressure, resulting in a pressure difference TMP_P between the middle part and the lower part and a corresponding specific flux Jp through the second membrane 'b'. The resulting permeate volume flow Q_P could leave the lower module part via two outlets and was collected in a small beaker placed on a second balance. In summary the operation of the developed system could be accurately monitored and described by six parameters, the volume flows Q_{DF}, Q_P, Q_F, and Q_R as well as the transmembrane pressures TMP_{DF} and TMP_P. Q_F, TMP_{DF} and TMP_P were given or known from the applied pressure sensors; Q_{DF}, Q_P and Q_R were calculated from the time resolved monitoring of the respective masses m_{DF}, m_P, and m_R.

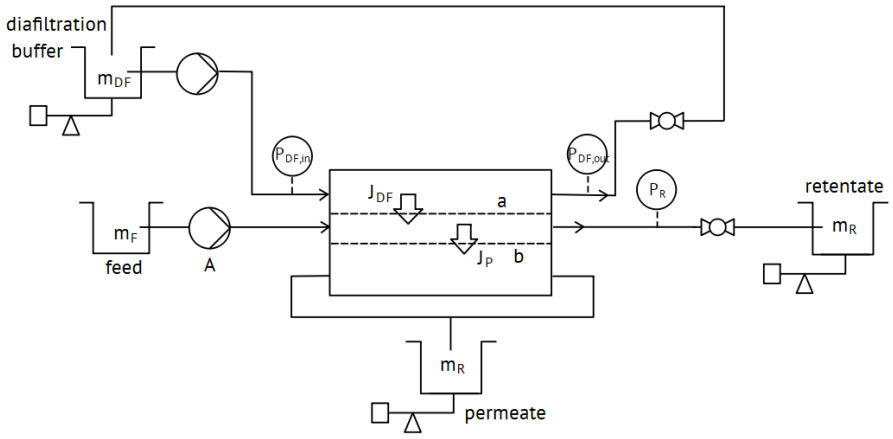

Fig. 5.2 Scheme of the flow paths and different control points of the developed two-membrane module for simultaneous ultra- and diafiltration.

5.2.4 Experimental procedure

Experiments were performed by first adjusting the constant feed volume flow Q_F as 0.5ml/min by the help of the syringe pump and the volume flow in the loop by help of the peristaltic pump of the conventional UF/DF system. Afterwards pressure valves

downstream of the sensors $P_{DF,out}$ and P_R were regulated to set Q_R and the transmembrane pressures TMP_{DF} and TMP_P. Because of the interplay of these parameters, their control required some experience and several readjustments. After the parameters settled at the desired values the system was operated for at least another 30 min to guarantee steady state conditions. In order to check if the dependencies between transmembrane pressures and resulting fluxes follow the rules known from conventional UF/DF systems, the water fluxes passing membranes 'a' and 'b' were determined for different operation conditions. Nine sets of parameter conditions were chosen with TMP_{DF} and TMP_P in a range of 0.07 to 0.3 bar. After adjusting a new parameter set and reaching steady state, the volume flows Q_R, Q_{DF}, and Q_P were determined by averaging over a period of 10 min.

After characterizing the hydrodynamic behavior of the system, a series of experiments with a feed solution containing BSA and NaCl were conducted. The execution of the experiments mainly followed the procedure described in the section above. However, in case of low volume flows Q_R it turned out to be difficult to reliably achieve constant volume flows by the help of the simple throttle valve available. Therefore, another way of controlling the average volume flow Q_R was chosen by completely closing the respective valve for an interval of 2min, 4min, 6min and 12min, respectively and opening and releasing a defined amount of liquid only in short defined intervals in between. Although this operation mode is not fully continuous anymore, it has the advantage of easy control and reliable adjustment of the average flow. In addition to the measurement of the exchange buffer and permeate masses, BSA concentration and conductivity were measured in the collected retentate samples. The concentration of BSA was measured by UV spectroscopy (PerkinElmer Enspire®) based on the absorbance at 280 nm. Conductivity was measured by a conductometer (WTW LF330, Weilheim, Germany) equipped with cell (WTW TetraCon® 325, Weilheim, Germany). In the investigated concentration range the contribution of the concentration of BSA on the conductivity can be neglected, and in good approximation the conductivity is directly proportional to the concentration of NaCl as $c_{NaCl,R} = c_{NaCl,F} \cdot \frac{\lambda_R}{\lambda_F}$, with λ_F, λ_R being the conductivity of the feed and retentate, respectively. In our experiments the feed solution having a concentration of NaCl of 100 mM was partly exchanged by diafiltration buffer (5 mM NaCl) during the single pass through the filtration module. Therefore, the degree of buffer exchange can be calculated from the conductivities by:

$$\text{Buffer exchange (\%)} = \frac{\lambda_F - \lambda_R}{\lambda_F - \lambda_{DF}} \cdot 100\% \qquad (5.1)$$

with λ_{DF} being the conductivity of the diafiltration buffer.

5.3 Results and discussion

5.3.1 Water fluxes and protein concentration dependent permeability

As described, a commercial membrane was used in all experiments of this study. To ensure the validity of water permeability data given by the manufacturer also in the unusual set-up with three pressure levels and membrane ‘a’ operating in a crossflow manner while membrane ‘b’ operating under single pass conditions, the resulting fluxes of pure water were measured for the expected parameter range. Fig. 5.3 shows that the water fluxes of the membranes ‘a’ and ‘b’ increased linearly with the corresponding TMP. From the slope of the linear fit the permeabilities of membrane ‘a’ and membrane ‘b’ were found to be 487.9 ± 8.0 L/(m² h bar) (R^2 =0.998) and 442.5 ± 8.2 L/(m² h bar) (R^2 = 0.997), respectively. Therefore, the permeabilities are equal within an experimental error of less than 10% and closely similar to the value given by the manufacturer 459 (L/m² h bar).

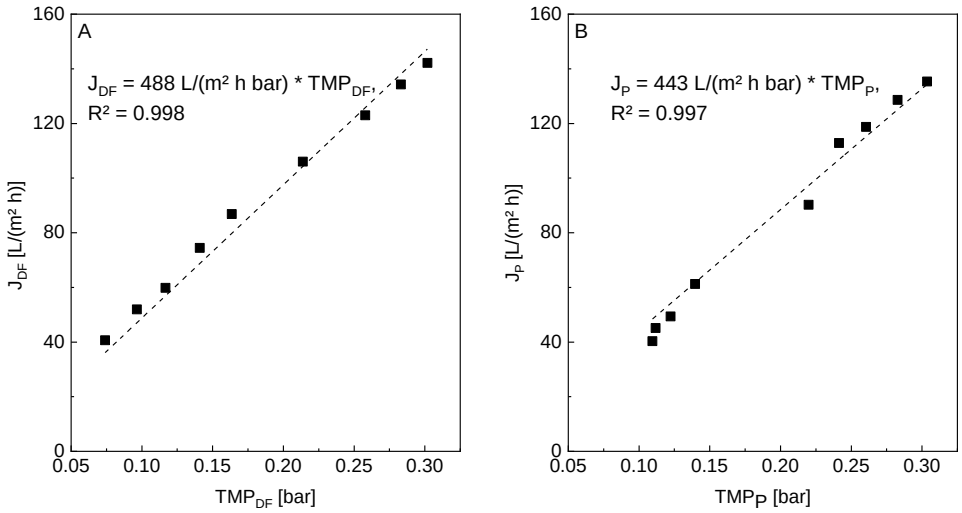

Fig. 5.3 Water flux of membranes 'a' and ‘b’ in the module calculated by mass balances of experiments with different volume flows Q_F and Q_R and different transmembrane pressures TMP_{DF} and TMP_P. (A) membrane 'a‘; (B) membrane 'b'.

SPTFF applies much slower flow velocities within the membrane filtration modules than conventional TFF, which pumps the retentate in a loop. Therefore, the ability to prevent concentration polarization in front of the UF membrane is reduced. In case of our module design which uses an additional perpendicular flow of diafiltration buffer within the module for simultaneous ultra- and diafiltration, this problem is even enhanced, because the flux through membrane b is formed by the sum of the permeate and the diafiltration fluxes. Therefore, additional experiments have been conducted

studying the dependency of membrane permeability on the BSA concentration in the retentate and the applied transmembrane pressure.

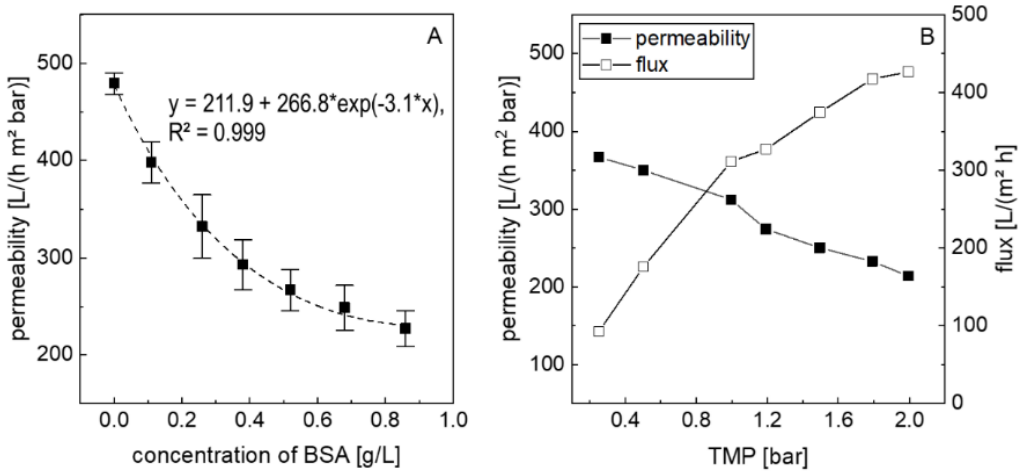

Fig. 5.4 Membrane permeability in dependence of BSA concentration and applied transmembrane pressure. The experiments were conducted in conventional TFF mode using only one membrane. This was achieved by removing the middle part of the module and returning the retentate to the feed tank in a loop. (a) Variation of BSA concentration in the retentate loop. The initial BSA concentration in the loop was 0.1 g/L BSA in 100mM NaCl, except for the first point, which shows the permeability in case of pure water. Afterward, the BSA concentration was increased stepwise by adding increasing volumes of a concentrated BSA stock solution to the loop. The applied transmembrane pressure was constant at 0.75 bar except for the experiment applying pure water (TMP = 0.3 bar). (b) Effect of TMP onto permeability and flux of the used UF membrane, feed solution 0.1 g/L BSA, 100mM NaCl. BSA, bovine serum albumin.

Fig. 5.4A shows the decrease of the permeability of membrane ‘b’ with increasing BSA concentration. The permeability follows the expected trend with an approximately exponential decrease with increasing BSA concentration, however, compared to conventional TFF the decrease is strongly pronounced even at rather low protein concentrations. On the other hand, the decrease seems to level off at a permeability of around 200 L/(h m² bar) in case of BSA concentrations of around one gram per liter. Therefore, the SPTFF with combined ultra- and diafiltration seems to be suitable for low to moderately concentrated protein solutions. In the second series of experiments we investigated to which extent the increase of the transmembrane pressure increases the flux and if an optimal operation point could be identified. Fig. 5.4B shows that within the examined range the flux steadily rises with increasing transmembrane pressure, however, in a nonlinear fashion. The flux curve shows no clear transition point but

rather a constantly decreasing slope, which also indicates in an almost linear decrease of the permeability with increasing transmembrane pressure. Therefore, no clear optimum could be identified and the achievable performance seems to be limited by the pressure resistance of the UF membrane and the 3D-printed SPTFF module.

5.3.2 Time course of the UF/DF experiments

In the following, the time required to reach stationary UF/DF operation conditions has been investigated. For this, experiments with a feed solution containing 0.1 g/l BSA and 100 mM NaCl at a constant feed flow Q_F = 0.50 ml/min were conducted and samples of the effluent Q_R were taken in intervals of 5 or 10 minutes. Because the module was filled with ultrapure water initially, the course of the effluent concentrations of both substances starts at zero and approaches a constant plateau after reaching stationary conditions. Fig. 5.5A shows the time courses of the effluent concentrations of BSA and NaCl in case of an experiment having its focus only on diafiltration ($c_{BSA,R}/c_{BSA,F} \approx 1$). As can be seen, BSA and NaCl reach their plateau after around 40 min. The experiments were conducted in triplicates and the resulting standard deviations indicate that the module performance and its start-up behavior are highly reproducible. According to the records of the weight differences Δm_R, Δm_{DF} and Δm_P determined for every interval, the average volume flows in the membrane module were calculated to be Q_R = 0.42 ml/min, Q_{DF} = 0.50 ml/min, and Q_P = 0.58 ml/min. Together with the applied feed flow of Q_F = 0.50 ml/min the mass balance closes completely if a constant solution density is assumed. A residence time (RT) of the solution of around 3.3 min in the middle grid can be calculated by the division of the free volume of the middle module part (1.4 ml) and the average retentate flow Q_R. Considering the volume of the tubing before and after the module (3 ml and 4 ml), the total residence time increases to 19.5 min. Comparing the residence time and the duration of 50 min to reach stationary conditions, it shows that it requires around two times the residence time to reach a stationary state. This ratio indicates a relatively strong mixing within the middle part of the module, which we think is mainly due to the grid structure and the short length of only 5 cm of the flow path. In this experiment a reduction of the salt concentration down to 52.3% of the inlet concentration was observed, while the ratio between the BSA concentration in the outlet and the one in the inlet approached the expected value of 1.2, indicating that the module was operated in plain diafiltration mode.

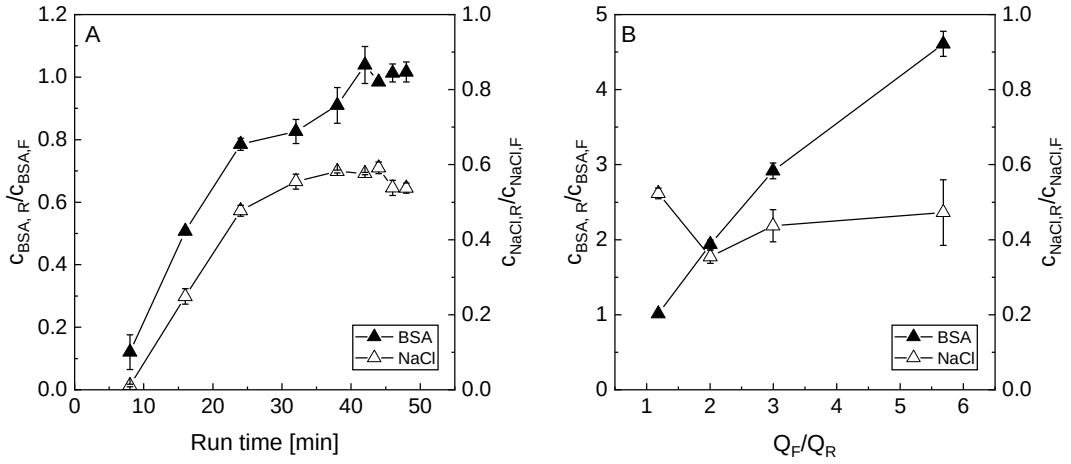

Fig. 5.5 (A) Time course of BSA and NaCl concentration in the retentate for an experiment with Q_F/Q_R = 1.19, Q_P/Q_{DF} = 1.16, TMP_P/TMP_{DF} = 2.07, (B) effect of the volume flow ratio Q_F/Q_R onto the achieved concentration factor of BSA and the resulting reduction of the salt concentration after achieving stationary conditions. Q_F/Q_R = 1.19; 2.01; 3.00; 5.68, Q_{DF}/Q_P = 0.86; 0.88; 0.63; 0.57, TMP_P/TMP_{DF} = 2.07, 4.16; 6.21; 5.04 respectively. Error bars are equal to ±SD.

In case of ideal diafiltration behavior with constant transversal plug flow between the feed inlet and retentate outlet ($Q_R = Q_F$ and therefore also $Q_{DF} = Q_P$) the salt concentration in the retentate can be calculated by (the derivation of this equation is given in the SI part):

$$c_{NaCl,R} = \left(c_{NaCl,F} - c_{NaCl,DF}\right) \cdot exp\left(-\frac{Q_P}{Q_F}\right) + c_{NaCl,DF} \qquad (5.2)$$

If the salt concentration in the diafiltration buffer is zero $(c_{NaCl,DF} = 0)$ Equation (5.2) reduces to a form which is similar to the well-known equation of constant volume diafiltration in a conventional TFF system [5], however, with the volumes of the initial feed and the used diafiltration buffer replaced by the respective volume flows. Equation (5.2) gives a predicted value of $c_{NaCl,R}/c_{NaCl,F}$ = 35%, which is only two third of the experimental value of 52.3%. In fact, the experimental value is much closer to the predicted value, if ideal mixing is assumed within the retentate chamber (see Table 5.1). In this case the local salt concentration in the permeate is constant throughout the module and equals the salt concentration in the retentate. Solving the respective mass balance:

$$\begin{aligned} c_{NaCl,R} &= \left(c_{NaCl,F} \cdot Q_F + c_{NaCl,DF} \cdot Q_{DF}\right)/\left(Q_P + Q_R\right) \\ &= \left(c_{NaCl,F} \cdot Q_F + c_{NaCl,DF} \cdot Q_{DF}\right)/\left(Q_F + Q_{DF}\right) \end{aligned} \qquad (5.3)$$

results in a predicted value of $c_{NaCl,R}/c_{NaCl,F}$ = 52.7%. The good agreement is a clear indication of the backmixing within the short module, corresponding with a reduced diafiltration efficiency.

Table 5.1 Comparison of the measured salt reduction efficiencies with the predictions of the two idealized theoretical models, (i) plug flow and (ii) complete mixing of feed and diafiltration buffer in the module

Flow rate ratio $Q_F \backslash Q_R$ (-)	experimental result, $c_{R,NaCl}$ (mM)	Plug flow[(i)], $c_{R,NaCl}$ (mM)	Complete mixing[(ii)], $c_{R,NaCl}$ (mM)	Q_{DF} (ml/min)	Q_P (ml/min)
1.19	52.3	35.0	52.7	0.5	0.6
2.01	35.5	20.8	41.7	0.8	0.9
3.00	43.7	27.7	56.2	0.5	0.7
5.68	47.2	32.1	60.5	0.3	0.6

(i) $c_R = (c_F - c_{DF}) \cdot exp\left(-\frac{Q_P}{Q_F}\right) + c_{DF}$

(ii) $c_R = \frac{Q_F \cdot c_F + Q_{DF} \cdot c_{DF}}{Q_F + Q_{DF}}$

5.3.3 Concentration and diafiltration with varying volume flow ratios

Finally, a series of experiments was conducted aiming to achieve substantial concentration factors of BSA while simultaneously reducing the salt content and operating in a continuous fashion. Fig. 5.5B shows the expected behavior with the concentration factor of BSA increasing almost linearly with increasing volume flow ratio Q_F/Q_R:

$$\frac{C_{BSA,R}}{C_{BSA,F}} = \frac{Q_F}{Q_R} \tag{5.4}$$

The only exception from the ideal relationship was observed in case of repeated experiments with a Q_F/Q_R ratio above five. In these experiments the concentration factor stayed about 20% below the expectations, assumingly because of the non-ideal BSA retention of the membrane and some BSA accumulation within the module. The influence of this non-ideality starts to grow with increasing concentration and increasing residence time, as it is the case for decreasing retentate flows Q_R while the feed flow Q_F is kept at 0.5 ml/min. Keeping the feed flow Q_F at a constant value and reducing the retentate flow Q_R, it could expect a slight decrease of the remaining salt content in the retentate if the flow of the diafiltration buffer through membrane 'a' Q_{DF} would stay at a constant level. Because of conservation of mass, in this case Q_P would have to increase for decreasing retentate flow, and with increasing Q_P a higher amount of salt would be transferred into the permeate. However, in reality our experiments showed a decrease of the volume flow Q_{DF} with increasing volume flow ratio Q_F/Q_R and a corresponding slight decrease of Q_P. Nevertheless, the experiments show that

the developed module allows setting the levels of protein concentration by ultrafiltration and salt removal by diafiltration independently, by adjusting the input flows and pressures in the module parts. At a given feed flux per membrane area of 56 L/(m² h) our system reached a concentration factor (CF) of 4.5, which compares well with the SPTFF concentration factors reported in literature in case of comparable feed fluxes (CF 3 - 4 in case of a feed flux of 52 L/(m² h) [14], and CF 5 in case of a feed flux of 55 L/(m² h) [16]). As can be seen from Table 5.1, the achieved salt concentrations were in a range between 35 and 52% of the salt concentration in the feed. This degree of salt reduction will be too low for most practical applications requiring diafiltration, however, one has to take into account that the salt reduction is achieved using a very short flow path length in the SPTFF module of only 5 cm. Comparing the experimental results with the predictions of the two idealized SPTFF models introduced in section 5.3.2 one finds that the measured retentate salt concentrations are in-between. Therefore, the flow regime within the SPTFF module seems to be in-between complete mixing and plug flow, with a tendency to complete mixing at low CF values, corresponding with shorter residence times within the module. Nevertheless, increasing the flow path length to e.g. 50 cm while keeping the width constant, the middle part of the module resembles a long narrow channel with permeable walls and it can be expected, that the flow regime approaches plug flow conditions more and more. Using eq. (5.2) and the assumption of a constant flux of diafiltration buffer through membrane ‘a’ per length of the flow path it can be estimated that a single 50 cm SPTFF module of our design should be able to reach diafiltration efficiencies beyond 99%.

5.4 Conclusion and outlook

The data presented show that the developed 3D-printed UF/DF is able to concentrate large biomolecules, e.g. proteins, of a continuous sample feed while simultaneously reducing the salt amount of the sample matrix. This is achieved by the application of two membranes allowing the continuous in- and outflow of pure water or diafiltration buffer perpendicular to the flow direction of the sample stream. This feature clearly differs our set-up from other single pass TFF systems, using only one membrane to split the feed into a permeate and a retentate stream. In order to achieve continuous diafiltration with such systems several units have to be assembled in a row with dilution in between. In our system, the degree of simultaneous dia- and ultrafiltration can be chosen independently by adjusting the pressures in the upper and middle part of the module, as well as the volume flow ratio between the sample feed

and the outlet of the middle part of the module. We are aware that the demonstrated degree of around 55% buffer exchange is much lower than the values of 99 or even 99.9% often requested in biopharmaceutical downstream processes, and that 55% buffer exchange would be easily achievable in a single unit of the known SPTFF systems. However, in order to reach 99% or 99.9% buffer exchange in a single unit of a conventional SPTFF the initial dilution would have to be 100 or even 1000 times, leading to uneconomical amounts of diafiltration buffer and membrane areas required. Therefore, the process has to be divided into several SPTFF units with intermediate addition of diafiltration buffer. In contrast, the developed SPTFF module allows a continuous infiltration of diafiltration buffer throughout the complete flow path. Therefore, future modules having a longer flow path should be able to achieve high degrees of buffer exchange within a single SPTFF unit. In the described setup the flow and the pressure in the upper part of the module are controlled by a conventional UF/DF system. However, optimized future versions of the set-up could use simple pressure controlled reservoirs for a controlled delivery of the diafiltration buffer to the upper part of the module. In addition, besides the described simultaneous UF/DF mode, the module could also be used for plain single pass TFF operation if required. In this case the direction of the flux passing membrane ‘a’ would be reversed by adjusting $P_{DF,in}$ and $P_{DF,out}$ to ambient pressure. By this, the membranes on both sides of the retentate channel will available for ultrafiltration, as it is the case in conventional TFF and SPTFF modules. Finally, stacked versions of multiple 3D-printed cassettes separated by membranes could be realized, with alternating function as buffer delivery, sample concentration, and salt removal sections. Still, we doubt that the simple planar design of the setup is suitable for high-throughput applications. Rather, the direction of future developments will be further size reduction, parallelization and simplified hydraulics of the setup to allow simple buffer exchange and concentration in the area of bioanalytic and high throughput process development.

References

[1] L.J. Zeman, A.L. Zydney, Microfiltration and Ultrafiltration: Principles and Applications, Marcel Dekker Inc., New York, 1996.

[2] W.C. McGregor, ed., Membrane Separations in Biotechnology, Marcel Dekker Inc., New York, 1986.

[3] L. Schwartz, Diafiltration for desalting or buffer exchange processing, Water. (2003).

[4] S.J. Shire, Formulation and manufacturability of biologics, Curr. Opin. Biotechnol. 20 (2009) 708–714. https://doi.org/10.1016/j.copbio.2009.10.006.

[5] H. Lutz, Ultrafiltration for Bioprocessing, (2015) 244. https://doi.org/10.1016/B978-1-907568-46-6.00002-1.

[6] R. van Reis, A. Zydney, Bioprocess membrane technology, J. Memb. Sci. 297 (2007) 16–50. https://doi.org/10.1016/j.memsci.2007.02.045.

[7] R. van Reis, A.L. Zydney, Protein ultrafiltration, in: M.C. Flickinger, S.W. Drew (Eds.), Encycl. Bioprocess Technol. Ferment. Biocatal. Biosep., John Whiley & Sons, Inc., 1999: pp. 2197–2214.

[8] G. de los Reyes, L. Mir, Method and Apparatus for the Filtration of Biological Solutions, US 7,384,549 B2, 2008.

[9] Y. Tamari, R. Nelson, R. Levy, N. Rea, M. Salogub, C. Carolina, M. Hall, C. Moccio, A. Tortolani, Conversion of Dilute Pump Blood to Whole Blood by Single Pass Ultrafiltration, Proceedings. 15 (1983) 126–132.

[10] C. Casey, T. Gallos, Y. Alekseev, E. Ayturk, S. Pearl, Protein concentration with single-pass tangential flow filtration (SPTFF), J. Memb. Sci. 384 (2011) 82–88. https://doi.org/10.1016/j.memsci.2011.09.004.

[11] EMD Millipore, Single-pass tangential flow filtration, (2014) 1–4.

[12] C. Casey, K. Rogler, X. Gjoka, R. Gantier, E. Ayturk, Cadence™ Single-pass TFF Coupled with Chromatography Steps Enables Continuous Bioprocessing while Reducing Processing Times and Volumes,2018. http://www.pall.de/pdfs/Biopharmaceuticals/USD3003_Cadence_SPTFF_ChromSteps_AN.pdf.

[13] C.A. Teske, B. Lebreton, Inline ultrafiltration, Biotechnol. Prog. 26 (2010) 1068–1072. https://doi.org/10.1002/btpr.404.

[14] J. Dizon-Maspat, J. Bourret, A. D'Agostini, F. Li, Single pass tangential flow filtration to debottleneck downstream processing for therapeutic antibody production, Biotechnol. Bioeng. 109 (2012) 962–970. https://doi.org/10.1002/bit.24377.

[15] A. Brinkmann, S. Elouafiq, J. Pieracci, M. Westoby, Leveraging single-pass tangential flow filtration to enable decoupling of upstream and downstream monoclonal antibody processing, Biotechnol. Prog. 34 (2018) 405–411. https://doi.org/10.1002/btpr.2601.

[16] A. Arunkumar, N. Singh, M. Peck, M.C. Borys, Z.J. Li, Investigation of single-pass tangential flow filtration (SPTFF) as an inline concentration step for cell culture harvest, J. Memb. Sci. 524 (2017) 20–32. https://doi.org/10.1016/j.memsci.2016.11.007.

[17] A. Jungbauer, Continuous downstream processing of biopharmaceuticals, Trends Biotechnol. 31 (2013) 479–492. https://doi.org/10.1016/j.tibtech.2013.05.011.

[18] J. Rucker-Pezzini, L. Arnold, K. Hill-Byrne, T. Sharp, M. Avazhanskiy, C. Forespring, Single pass diafiltration integrated into a fully continuous mAb purification process, Biotechnol. Bioeng. 115 (2018) 1949–1957. https://doi.org/10.1002/bit.26708.

[19] A.M.K. Nambiar, Y. Li, A.L. Zydney, Countercurrent staged diafiltration for formulation of high value proteins, Biotechnol. Bioeng. 115 (2018) 139–144. https://doi.org/10.1002/bit.26441.

5.5 Support Information

S1: Details of the experiments to characterize the water fluxes of membranes 'a' and 'b' in the 3D-printed SPTFF module.

No.	TMP_{DF} [bar]	TMP_P [bar]	time [min]	membrane size [cm^2]	Q_F [ml/min]	Δm_{DF} [g]	Δm_P [g]	J_{DF} [L/(h m^2)]	J_P [L/(h m^2)]
1	0.07	0.22	10	5.32	0.5	3.6	8.0	40.6	90.2
2	0.10	0.24	10	5.32	0.5	4.6	10.0	51.9	112.8
3	0.12	0.26	10	5.32	0.5	5.3	10.5	59.8	118.7
4	0.14	0.28	10	5.32	0.5	6.6	11.4	74.4	128.6
5	0.16	0.30	10	5.32	0.5	7.7	12.0	86.8	135.3
6	0.21	0.14	10	5.32	0.5	9.4	5.4	106.0	61.2
7	0.26	0.12	10	5.32	0.5	10.9	4.4	122.9	49.4
8	0.28	0.11	10	5.32	0.5	11.9	4.0	134.2	45.1
9	0.30	0.11	10	5.32	0.5	12.6	3.6	142.1	40.3

S2: Details of the experiments on simultaneous ultra- and diafiltration in section 3.3 Every point in Fig. 5.5A is the average value of three independent experiments for simultaneous concentration of BSA and NaCl buffer dilution.

interval time [min]	TMP_{DF} [bar]	TMP_P [bar]	Q_F [ml/min]	Q_{DF} [ml/min]	Q_R [ml/min]	Q_P [ml/min]	Q_F/Q_R [-]	$c_{BSA,R}$ /$c_{BSA,F}$	$c_{NaCl,R}$ /$c_{NaCl,F}$
2min-1	0.14	0.26	0.50	0.51	0.41	0.63	1.21	1.03	51%
2min-2	0.12	0.29	0.50	0.48	0.43	0.53	1.16	1.03	53%
2min-3	0.12	0.27	0.50	0.46	0.45	0.54	1.11	0.98	N.A.
Average			0.50		0.42		1.19	1.01	52%
SD								±3%	±1%
4min-1	0.31	1.36	0.50	0.61	0.25	0.70	2.00	2.00	33.5%
4min-2	0.31	0.92	0.50	0.97	0.25	1.13	2.00	1.93	36.9%
4min-3	0.31	1.36	0.50	0.86	0.25	0.96	2.02	1.88	36.0%
Average			0.50		0.25		2.01	1.94	35.5%
SD								±6%	±2%
6min-1	0.26	1.35	0.50	0.46	0.17	0.65	2.99	2.80	45.6%
6min-2	0.22	0.93	0.50	0.66	0.17	0.91	3.00	2.95	46.7%
6min-3	0.11	0.88	0.50	0.25	0.17	0.63	3.00	3.00	38.8%
Average			0.50		0.17		3.00	2.92	43.7%
SD								±10%	±4%
12min-1	0.33	1.39	0.43	0.36	0.08	0.47	5.02	4.74	39.9%
12min-2	0.26	1.70	0.50	0.41	0.08	0.65	6.05	4.67	44.9%
12min-3	0.37	0.84	0.50	0.26	0.08	0.70	6.00	4.42	56.9%
Average			0.48		0.08		5.68	4.61	47.2%
SD								±17%	±9%

N.A.: not available.

S3: Details of the experiments to determine membrane permeability in dependence of BSA concentration in the retentate

The given numbers are the average value for three independent experiments.

time [min]	TMP [bar]	c_{BSA} [g/L]	flux [LHM]	permeability [L/ (h m^2 bar)]
0	0.30	0	126.3	479.2
10	0.75	0.12	306.1	407.2
20	0.75	0.23	250.6	334.2
30	0.75	0.36	225.6	299.6
40	0.75	0.48	206.8	276.0
50	0.75	0.63	193.3	256.9
60	0.75	0.80	175.4	232.7

time [min]	TMP [bar]	c_{BSA} [g/L]	flux [LHM]	permeability [L/ (h m^2 bar)]
0	0.30	0	126.3	479.2
10	0.75	0.09	282.0	373.7
20	0.76	0.31	226.3	298.8
30	0.75	0.44	197.4	264.0
40	0.76	0.63	183.3	242.4
50	0.76	0.82	169.2	222.4
60	0.75	1.03	155.1	206.6

time [min]	TMP [bar]	c_{BSA} [g/L]	flux [LHM]	permeability [L/ (h m^2 bar)]
0	0.30	0	126.3	479.2
10	0.76	0.11	312.3	413.0
20	0.76	0.25	275.7	363.6
30	0.76	0.34	237.8	314.7
40	0.75	0.47	212.4	281.6
50	0.75	0.60	200.5	266.2
60	0.75	0.75	181.4	242.4

SD values calculated from the results of Table S3.

time [min]	TMP [bar]	c_{BSA} [g/L]	flux [LHM]	permeability [L/ (h m^2 bar)]
0	0.038	0	15.7	11.2
10	0.002	0.02	16.0	21.2
20	0.005	0.04	24.7	32.5
30	0.004	0.05	20.7	26.0
40	0.003	0.09	15.5	21.2
50	0.005	0.12	16.4	23.1
60	0.003	0.15	13.8	18.5

S4: Derivation of equation 2 of the main text

The following section shows the mathematical derivation of equation 5.2 of the main text:

$$c_{NaCl,R} = \left(c_{NaCl,F} - c_{NaCl,DF}\right) \cdot exp\left(-\frac{Q_P}{Q_F}\right) + c_{NaCl,DF} \qquad (5.5)$$

Figure S5.1 shows a sketch of the module and the fluxes within:

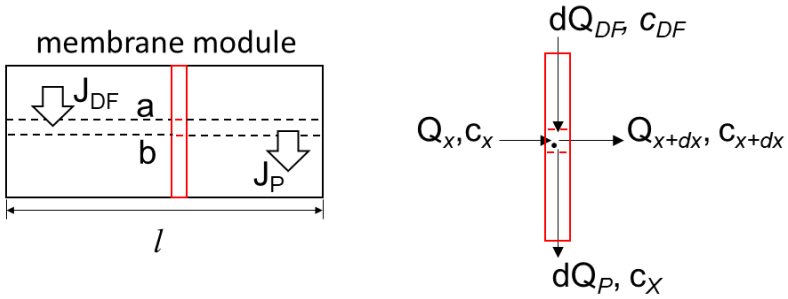

c_x: salt concentration at location x in the middle part of the module,

Q_x: tangential flow within the middle part of the module,

c_{DF}: salt concentration of the diafiltration buffer,

l: membrane module length.

The mass balance of salt within a differential segment of the module is given by:

$$Q_x c_x + dQ_{DF} \cdot c_{DF} = dQ_P \cdot c_x + Q_{x+dx} \cdot c_{x+dx} \qquad (S5.1)$$

Under the assumption of an equal spatial distribution of the flows of diafiltration buffer through membrane 'a' and permeate through membrane 'b' the following relationships hold for the differential flows dQ_{DF} and dQ_P:

$$dQ_{DF} = \frac{Q_{DF}}{l} dx, \;\; dQ_P = \frac{Q_P}{l} dx \qquad (S5.2)$$

In contrast to conventional TFF systems the assumption of an equal distribution of the permeate flow throughout the whole flow path is justified in our module in the case of

pure diafiltration because the protein concentration does not change if the infiltration of diafiltration buffer Q_{DF} through membrane 'a' equals the withdrawal of permeate Q_P through membrane 'b'. Inserting eq. S5.2 into eq. S5.1 results in:

$$Q_x c_x + \frac{Q_{DF}}{l} dx \cdot c_{DF} = \frac{Q_P}{l} dx \cdot c_x + Q_{x+dx} \cdot c_{x+dx} \quad \text{(S5.3)}$$

Together with the condition of pure diafiltration ($Q_{DF} = Q_P$) one gets $Q_x = Q_{x+dx} = Q_F$, meaning the tangential flow within the middle part of the module stays constant, eq. S3 transfers into:

$$Q_F c_x + \frac{Q_{DF}}{l} dx \cdot c_{DF} = \frac{Q_P}{l} dx \cdot c_x + Q_F \cdot c_{x+dx} \quad \text{(S5.4)}$$

Dividing by Q_F and applying Taylor expansion of c_{x+dx} gives:

$$c_x + \frac{Q_{DF}}{Q_F l} dx \cdot c_{DF} = \frac{Q_P}{Q_F l} dx \cdot c_x + c_x + \frac{dc_x}{dx} dx \quad \text{(S5.5)}$$

Which reduces to:

$$\frac{Q_{DF}}{Q_F l} \cdot c_{DF} = \frac{Q_P}{Q_F l} \cdot c_x + \frac{dc_x}{dx} \quad \text{(S5.6)}$$

Case I: If the diafiltration buffer contains no salt, $c_{DF} = 0$, eq. S5.6 simplifies to:

$$-\frac{Q_P}{Q_F l} \cdot dx = \frac{dc_x}{c_x} \quad \text{(S5.7)}$$

Integration between the entrance of the module ($x = 0$, $c_x = c_F$) and the effluent of the module ($x = l$, $c_x = c_R$) gives:

$$-\int_0^l \frac{Q_P}{Q_F l} \cdot dx = \int_{c_F}^{c_R} \frac{dc_x}{c_x} \quad \text{(S5.8)}$$

and finally:

$$c_R = c_F \cdot exp\left(-\frac{Q_P}{Q_F}\right) \quad \text{(S5.9)}$$

Case II: If the diafiltration buffer itself contains small amounts of salt, $c_{DF} \neq 0$, the derivation changes to:

$$-\frac{Q_P}{Q_F l} \cdot dx = \frac{dc_x}{c_x - c_{DF}} \quad \text{(S5.10)}$$

$$dc_x = d(c_x - c_{DF}) \quad \text{(S5.11)}$$

$$-\int_0^l \frac{Q_P}{Q_F l} \cdot dx = \int_{c_F}^{c_R} \frac{d(c_x - c_{DF})}{c_x - c_{DF}}$$

$$-\frac{Q_P}{Q_F} = \ln \frac{c_R - c_{DF}}{c_F - c_{DF}} \quad \text{(S5.12)}$$

$$c_R = (c_F - c_{DF}) \cdot exp\left(-\frac{Q_P}{Q_F}\right) + c_{DF} \quad \text{(S5.13)}$$

which equals eq.5.2 of the main text, remembering that for the sake of simplified notification we used c instead of c_{NaCl} in our notation.

6 Continuous single pass diafiltration with alternating permeate flow direction for high efficiency buffer exchange

Ruijie Tan[1], Fabian Hezel[1], Matthias Franzreb[1*]

[1]*Institute of Functional Interfaces (IFG), Karlsruhe Institute of Technology (KIT), Hermann-von-Helmholtz-Platz 1, 76344 Eggenstein-Leopoldshafen, Germany*

[*]Corresponding author: matthias.franzreb@kit.edu

Abstract Looking at current trends within downstream processing (DSP) of high value bioproducts, it shows that there are ongoing efforts in replacing batch processes by continuous variants. However, a unit procedure which still lacks a simple and compact continuous variant is diafiltration. Here, we present such a single piece of diafiltration equipment achieving continuous buffer exchange of up to 99.90%. The device is composed of a 3D-printed single pass diafiltration (SPDF) module containing two commercial ultrafiltration membranes. While the retentate is flowing through a narrow channel between the two membranes, the channels above and below can supply diafiltration buffer or remove permeate solution. The obtained results illustrate systematically the vulnerability of the device to the effect of concentration polarization at the membrane surface, and that this problem can be strongly reduced using an alternating direction of diafiltration buffer perfusion through the membranes as process inherent backflush. By this, a quasi-stationary operation could be obtained during continuous diafiltration, making the device an interesting option for in-process buffer exchange.

Keywords: diafiltration, continuous processing, single pass tangential flow filtration, buffer exchange, counter-current

Published in Journal of Membrane Science. 619 (2021) 118695

6.1 Introduction

The production of high-quality biological products is widely becoming a key demand in the biomanufacturing industry. Batch processes, as the popular choice of the current commercial-scale production of biological products, are increasingly challenged by new, continuous process variants [1–3]. Several continuous process technologies, including perfusion bioreactors with continuous in- and outflow of materials, single pass tangential flow (SPTFF) units, continuous chromatography and continuous crystallization have been reported for multi-product clarification, purification and formulation [4–8].

There exist also recent developments exploring systems for continuous ultrafiltration (UF) and diafiltration (DF) [9–13]. Compared to conventional tangential flow filtration (TFF) in which the retentate is pumped in a loop and passes the membrane module several times, single pass tangential flow filtration (SPTFF) is more suitable for integration into continuous manufacturing schemes. As early as 2002, Lipnizki [14]and co-workers conducted a theoretical study of batch and continuous diafiltration of a protein solution using between two and ten plate-and-frame membrane modules. They compared three operation modes: (i) batch diafiltration with retentate recycling and all modules operation in parallel, (ii) continuous diafiltration with the retentate passing the modules sequentially and the admixture of diafiltration buffer between the stages, and (iii) continuous counter-current diafiltration injecting fresh diafiltration buffer only once in the final stage and always using the permeate as diafiltration solution of the proceeding stage. It showed that all three operation modes could reach the objective of 98% diafiltration efficiency, with the counter-current diafiltration requiring on the one hand more membrane area, but on the other hand, substantially less diafiltration buffer than the other operation modes. These results are in agreement with later findings reported in the literature [15] demonstrating that continuous counter-current multistage membrane processes result in better purification performances and reduced buffer requirements. However, the achieved purification factors and degrees of buffer exchange were relatively low, compared to the 99.9% diafiltration efficiency often required in biopharmaceutical processes. A first study approaching this limit was conducted by Rucker-Pezzini et al [6] showing the feasibility to obtain a buffer exchange greater than 99.75% using a three-stage single pass diafiltration (SPDF) process, with several repetitive steps of concentrating and diluting. In the same year also Nambiar and Zydney [16] demonstrated an around 350-fold impurity removal (corresponding to approximate 99.7% buffer exchange) applying a flow ratio of 19 between the diafiltration buffer and the feed (19 diavolumes) in a

counter-current two-stage single pass diafiltration system. The latest work reported by the same group exemplified a counter-current three-stage DF system by reconstructing the aforementioned two-stage DF system [17], which allowed to reduce the buffer consumption and accomplished up to 99.9% impurity removal. A different approach is the use of hollow fiber membrane systems originally designed for blood dialysis for counter-current diafiltration of protein solutions. Yehl et al. [18,19] applied a hollow fiber dialyzer for continuously removing the model impurity vitamin B_{12} from concentrated IgG solutions. They achieved around 1000-fold impurity removal at a very small buffer consumption between 2.25 - 4.5 diavolumes. However, to obtain these results the hollow fiber module had to operate at an unusually low specific feed rate of 0.16 L per m² of membrane area and hour. Nevertheless, to the knowledge of the authors, the approach of Yehl and Zydney is the first system achieving continuous, highly efficient diafiltration in a single device, which can be also realized as disposable.

In this work, we present an alternative design of a single pass membrane module, which can achieve comparable diafiltration efficiencies in a single device, however using common membrane sheets and specific feed rates, which are at least an order of magnitude higher than the ones in the mentioned hollow fiber modules. Different continuous DF modes, such as single-direction, alternating co-current and alternating counter-current, have been implemented in two 3D printed prototypes. In addition, the susceptibility to concentration polarization of the model protein at the membrane surface could be reduced to an acceptable level by implementing an alternating direction of the permeate flow through the membranes.

6.2 Material and methods

6.2.1 Feed solution and applied membrane

Bovine serum albumin (BSA) from PanReac AppliChem (Darmstadt, Germany) was used as the model protein in all experiments. BSA powder (1 g/L) was dissolved in 100 mM sodium chloride and 30 mM monosodium phosphate buffer at pH 7.10 (Merck KGaA, Darmstadt, Germany). The used ultrapure water was produced by a Sartorius arium® pro system (Sartorius, Göttingen, Germany). For buffer exchange, either ultrapure water or a diafiltration buffer containing 30 mM monosodium phosphate and 5 mM sodium chloride were used. The OMEGA ultrafiltration polyethersulfone (PES) membrane (30 kDa MWCO, OT030SHEET, Lot. #H3186I) purchased from Pall Life Sciences (Hauppauge, USA) was applied in the 3D-printed membrane modules as described in the next section.

6.2.2 Prototype and scaled-up 3D-printed UF/DF module

The continuous SPTFF experiments were carried out using two versions of a self-designed diafiltration module shown in Fig. 6.1. Both modules were 3D printed using a PolyJet system EDEN 260 (Stratasys, Eden Prairie, USA.) using the material VeroWhite [20]. Each module was composed of two lateral parts and one middle part, all of them housing a narrow hollow-carved structure of 2 mm height allowing a tangential flow along the membranes placed between the parts. The grid-like design of the hollow-carved structure served at the same time as mechanical support for the two membranes. Bounded by these membranes, the middle part forms a channel in which the feed is transferred into the retentate during a single pass. During this passage diafiltration buffer can perfuse into the middle channel via one membrane while simultaneously permeate perfuses through the opposite membrane. Except for the flow path length, the structure of the three parts described was the same in the first prototype module (Fig. 6.1A) and the scaled-up module (Fig. 6.1B).

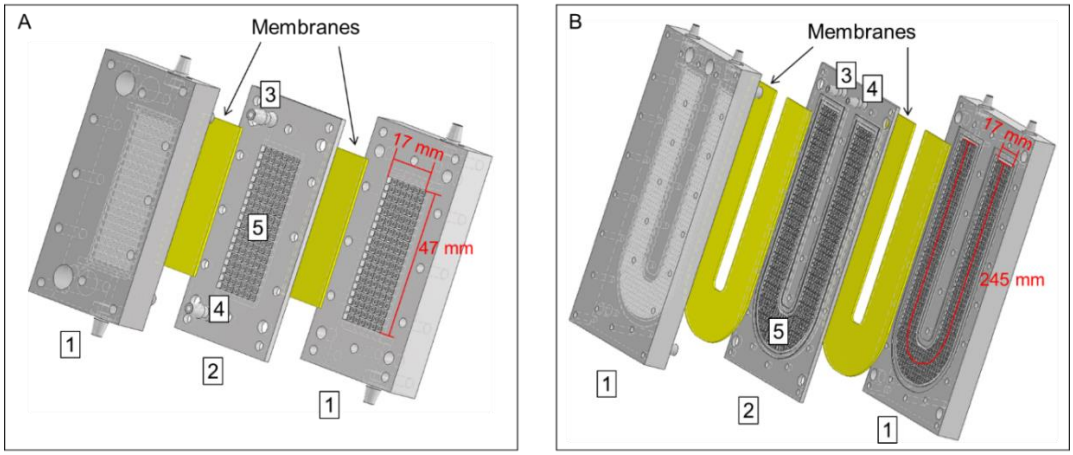

Fig. 6.1 Design of the 3D-printed membrane module for single pass UF/DF. (A) prototype module, (B) scaled-up module. 1: lateral parts for either diafiltration buffer or permeate solution; 2: middle part forming a flow pass for the feed, a membrane is placed between the middle part and the adjacent lateral part on both sides; 3: inlet of the feed flow; 4: outlet of the retentate flow; 5: hollow-carved grid structure to support the membranes. The width of the hollow-carved structure is the same in both modules (17 mm), while the length of the flow path in the scaled-up module is 5.2-fold larger than the one in the short prototype module.

Table 6.1 below illustrates the main dimensions of the modules. Subtracting the area covered by the grid, the effective membrane area of the scaled-up module was 5.2-fold larger than the one of the prototype module. A longer flow path length was built in the scaled-up module in order to prolong the residence time of the retentate in the middle section, offering a practical way to improve the buffer exchange. Additionally,

for the purpose of improving the leak tightness of the assembled module, narrow slots for rubber sealings were added on the inner side of the lateral parts in the scaled-up module.

Table 6.1 Dimensions of the two versions of the 3D-printed SPTFF module

	A. Prototype module	B. Scaled-up module
$V_{\text{lateral part}}$ (ml)	1.25	6.46
$V_{\text{middle part}}$ (ml)	1.18	6.08
$L_{\text{flow path}}$ (cm)	4.70	24.5
$A_{\text{effective, membrane}}$ (mm^2)	532	2972

6.2.3 Experimental set-up

Fig. 6.2 shows the developed experimental set-up for the continuous diafiltration process. The set-up combined the developed SPTFF module with two commercial systems: a FPLC system (ÄKTA purifier UPC 10, GE Healthcare, Uppsala, Sweden) including an additional sample pump and a membrane filtration system Sartorius (SARTOFLOW® Smart, Sartorius, Göttingen, Germany). This combination allowed a detailed and precise control of the operation conditions as well as an online monitoring of the main process parameters. The three high-pressure piston pumps of the FPLC system guaranteed a pressure independent control of the feed, diafiltration buffer, and retentate flows. The multiport valves of the FPLC system allowed an automated switching of the in- and outlet positions of the diafiltration and permeate flows. In addition, the system monitored the UV/Vis and conductivity signals in the retentate.

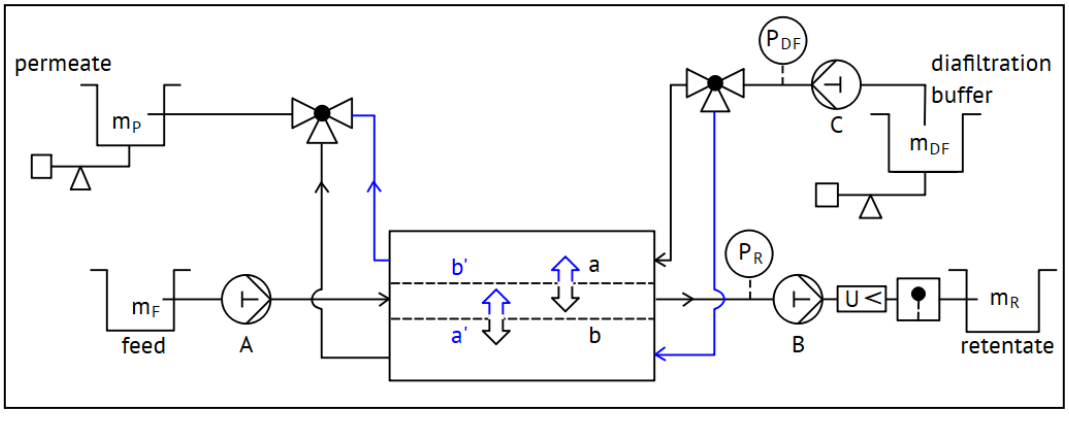

Fig. 6.2 Scheme of the experimental setup. The direction of the flows perfusing membrane a and b could be switched by means of the rotary valves of the FPLC system. The BSA and salt concentration in the retentate were monitored in real-time by UV and conductivity sensors, respectively.

For the control of feed and retentate flows the feature of the Äkta FPLC system originally intended for the execution of salt gradients was used. The Äkta software allows to precisely adjust the sum-flow of pump A and B and the ratio of how this sum-flow is distributed between the two pumps. If the ratio is selected as 1:1, saying the fraction of pump B is set to 50% of the sum-flow, the feed and retentate flows exactly match and the system is operated in pure diafiltration mode. Moreover, if the fraction of pump B is adjusted to less than 50% the system is able to operate in a combined concentration / diafiltration mode. Exemplary concentration factors resulting from different settings of pump B are listed in the supplementary information (see SI Table S6.1). Besides the flows of the feed and retentate controlled by pumps A and B, the flow of the diafiltration buffer was controlled by the sample pump C of the Äkta system. All flow rates were calibrated to the desired value before each experiment by collecting the corresponding effluent during a certain period. BSA concentration was monitored at a wavelength of 280 nm, and diafiltration efficiency was calculated via the conductivity signal (see Fig. S6.1 in the supporting information). For the diafiltration process, fresh diafiltration buffer entered the middle part of the module at a constant flow rate and two rotary valves were applied to adjust the in- and outlet positions of the diafiltration buffer and the permeate at the lateral parts of the module. The pressures at the diafiltration inlet (P_{DF}) and the retentate outlet (P_R) as well as the weight of the diafiltration buffer and permeate reservoirs were monitored using the pressure sensors and scales of the Sartorius system. The developed process mode using an alternating permeate perfusion direction requires a repetitive switching of the valve positions and the flow rate of pump C. The corresponding process sequence was programmed using the software Unicorn 5.20 (GE Healthcare Bio-Sciences, Uppsala, Sweden).

6.2.4 Investigated diafiltration process modes

Different diafiltration studies were executed in order to explore the effect of varying stationary or alternating flow path onto the resulting diafiltration efficiency. First, the stationary two membranes unidirectional DF illustrated in Fig. 6.3A was tested. Through continuously pumping the exchange buffer perpendicular to the flow direction of the feed in the middle chamber, the limitations of this operation mode with unidirectional DF buffer flow were tested. In this mode, membrane a is constantly permeated with a fixed flow of fresh diafiltration buffer, while membrane b was constantly permeated by the solution flowing in the middle part, containing residues of the feed solution and fresh buffer.

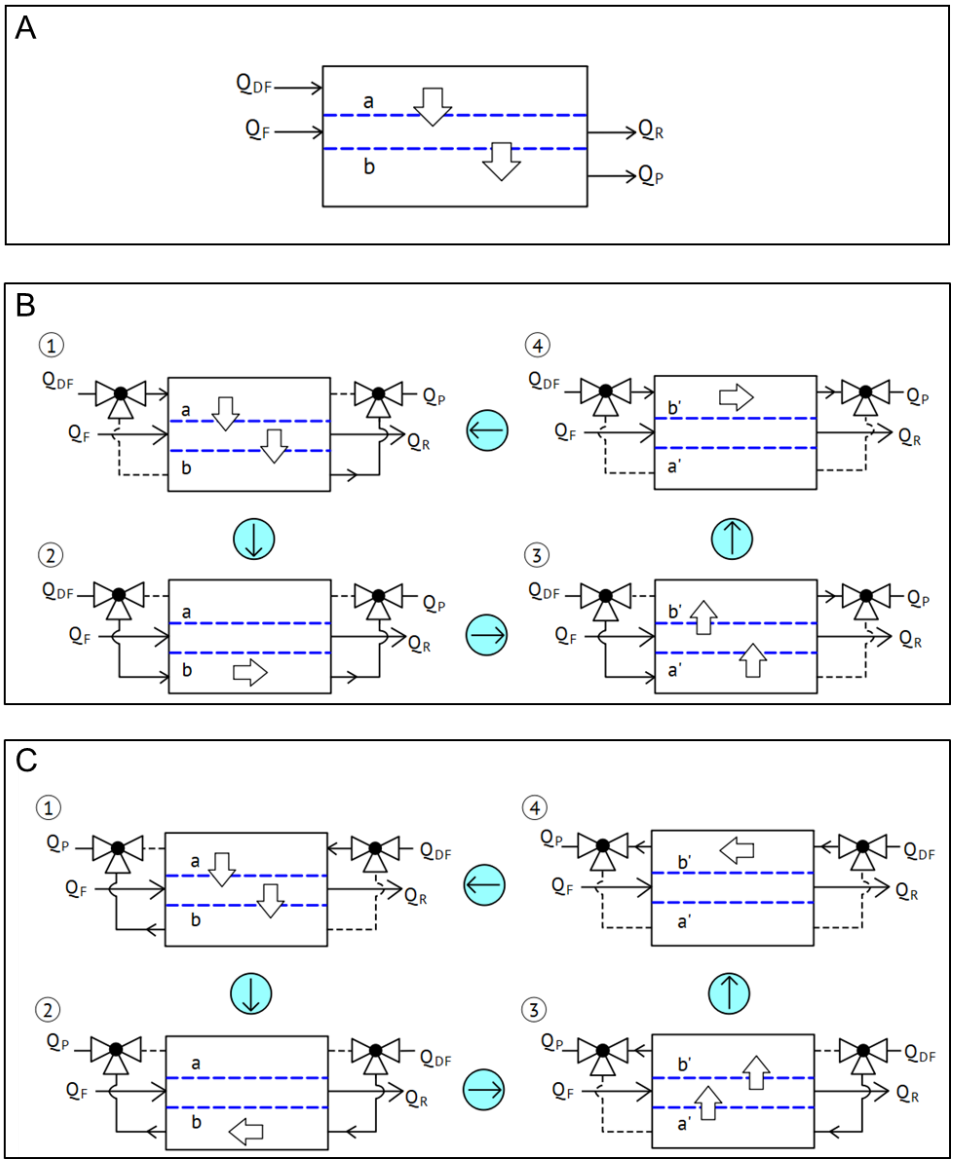

Fig. 6.3 Different continuous DF process modes controlled by switching the rotary valves. (A) Co-current diafiltration applying a unidirectional flow through membranes a and b, (B) Co-current diafiltration applying an alternating flow direction through membranes a and b, (C) Counter-current diafiltration applying an alternating flow direction through membranes a and b. The DF processes (B) and (C) can be executed with or without the flushing steps 2 and 4. The blue dashed lines indicate the membranes and the black dashed lines represent the flow paths which are blocked.

Second, an alternating co-current diafiltration mode illustrated in Fig. 6.3B was investigated. This mode is characterized by a cyclic operation including the repeated use of four steps differing in the adjusted valve positions and resulting in different flow paths. In the first step the left rotary valve is adjusted to connect DF buffer to the inlet of the upper part of the module while the right valve blocks the outlet of this part. In consequence, the DF buffer is pumped from the upper to the middle part of the module.

For plain diafiltration the feed and retentate flows are adjusted exactly at the same flow rate. Therefore, because of the conservation of mass, the permeation of the diafiltration buffer into the middle part enforces the same volume to permeate through membrane b. After a certain interval, the system switches to step 2 by changing the setting of the left valve defining the inlet position of the DF buffer. As a result, the flow path of the DF buffer is changed in a way that it simply flushes the lower part of the module in order to clean it from the permeate remaining after the end of step 1. In the third step, the setting of the right valve defining the position of the permeate outlet is changed in a way that it blocks the simple flushing of the lower part of the module and forces the DF buffer into the middle part crossing the first membrane (now named a' while being membrane b in step 1) and the permeate to cross the second membrane b'. By this the flow direction of the DF buffer is reversed sweeping away the concentration polarization layer formed by retained protein at membrane b (now a') surface during step 1. Finally, in step 4 the setting of the left valve is changed again, resulting in a flushing of the upper part of the module, having the same purpose than the flushing of the lower part during step 2. At the end of step 4, the cycle closes and by switching the setting of the right valve, the system enters a condition resembling the one of step 1. By switching the valves, the flow direction of the DF buffer is reversed again and the concentration polarization layer formed at the surface of membrane b' during step 3 is removed.

The third operation mode tested was an alternating counter-current diafiltration mode as illustrated in Fig. 6.3C. As can be seen, the four steps during a full process cycle of this mode resemble the ones of the co-current diafiltration mode with the difference that the flow direction of the DF buffer and permeate in the upper and lower part of the module is opposite to the flow direction of the retentate in the middle part. In this mode it was also tested if the flushing steps 2 and 4 can be skipped.

6.2.5 Analytical methods

For each diafiltration mode mentioned above, the sequential operating steps were executed repeatedly to approach a quasi-stationary state of the process. The achieved degree of buffer exchange is expressed as:

$$\text{Buffer exchange } (\%) = \left(1 - \frac{c_{Buffer,R}}{c_{Buffer,F}}\right) \cdot 100\% \qquad (6.1)$$

where $c_{Buffer,R}$ and $c_{Buffer,F}$ are the concentrations of the initial buffer in the retentate and the feed (see Fig. S6.1). Two idealized physical models were used to predict the limits of buffer exchange. As shown in our previous work [20], the assumptions of ideal plug flow in all parts of the DF module and co-current flow direction result in an equation

which is analogous to the well-known equation of constant volume diafiltration in a conventional TFF system [21], however, with the volumes of the initial feed and the used diafiltration buffer replaced by the respective volume flows:

$$c_{Buffer,R} = \left(c_{Buffer,F} - c_{Buffer,DF}\right) \cdot exp\left(-\frac{Q_{DF}}{Q_F}\right) + c_{Buffer,DF} \quad (6.2)$$

The second idealized model simply assumes complete mixing of the feed and the diafiltration buffer flows, as it is performed sequentially in the continuous diafiltration approach of Rucker-Pezzini et al. using several conventional SPTFF modules [6]. In this case the resulting concentration $c_{Buffer, R}$ is given by:

$$c_{Buffer,R} = (Q_F \cdot c_{Buffer,F} + Q_{DF} \cdot c_{Buffer,DF})/(Q_F + Q_{DF}) \quad (6.3)$$

Besides, although the focus of our work was on continuous diafiltration, also the concentration factor (CF) of the used model protein BSA was defined using equation (4).

$$CF = \frac{c_{BSA,R}}{c_{BSA,F}} \quad (6.4)$$

where $c_{BSA, R}$ and $c_{BSA, F}$ is the concentration of BSA in the retentate and the feed, respectively. The main purpose of CF is to see the time course of BSA and the degree to which BSA is retained in the diafiltration module due to membrane fouling and/or concentration polarization.

6.3 Results and discussion

6.3.1 Co-current diafiltration with unidirectional permeate flow

The first test series was designed to verify the accuracy of the flow control of the developed system and to study the influence of the flow rate of the diafiltration buffer onto the degree of buffer exchange. In the experiments the small prototype module was used in co-current mode and unidirectional flow of the DF buffer and the permeate through the membranes. Both the feed and retentate flow rates were kept at $Q_F = Q_R$ = 0.5 ml/min (56.4 L m^{-2} h^{-1}) over the course of the experiments, while increasing the diafiltration buffer flow rate Q_{DF} by 0.1 ml/min in every step from 0 to 0.5 ml/min. Standard deviations were analyzed by conducting every step in triplicates.

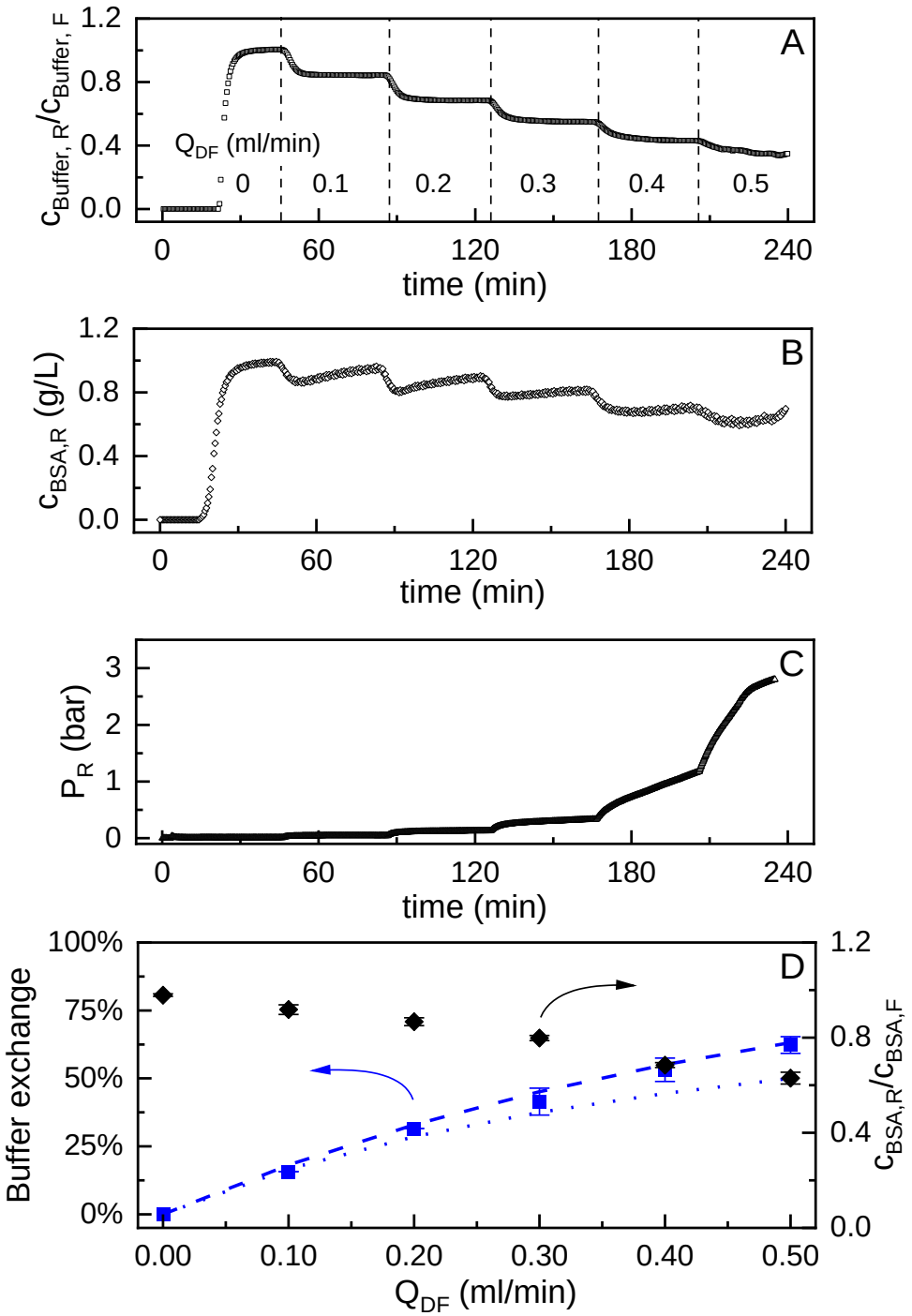

Fig. 6.4 Degree of buffer exchange of the co-current DF process with unidirectional flow through the membranes. In the course of the test series the flow rate of DF buffer was increased stepwise from 0 to 0.5 ml/min in steps of 0.1 ml/min, while the feed and retentate flow were kept constant at 0.5 ml/min. (A) Normalized concentration of the components of the original buffer remaining in the retentate, (B) Concentration of BSA in the retentate, (C) Pressure in the middle part of the membrane module, (D) Degree of buffer exchange and concentration factor of BSA plotted versus the flow rate Q_{DF}. The dashed lines represent the theoretical buffer exchange values corresponding to the idealized models of complete mixing (·····) and plug-flow (– – –), respectively.

In the experiments the concentrations of BSA and buffer in the retentate, as well as the pressure in the middle part of the module were monitored during the continuous operation (see Fig. 6.4A - C). In addition, Fig. 6.4D shows the resulting buffer exchange and CF values for different flow rates of the diafiltration buffer Q_{DF}, and the theoretical values calculated using eq (6.1) and eq (6.4), respectively. The plot of the feed buffer content remaining in the retentate in dependence of the applied Q_{DF} shows the expected picture (Fig. 6.4A). If no diafiltration buffer is applied, the feed buffer concentration in the retentate shows a steep increase to the level of the buffer concentration in the inlet after a short delay determined by the residence time of the liquid in the middle part of the module. The steep increase also indicates that in this case the flow profile in the middle part approximates an ideal plug flow. With increasing Q_{DF} the feed buffer concentration in the retentate starts to decline. By using accurate flow control of Q_F, Q_R, and Q_{DF} instead of the more common pressure control, the incompressibility of water enforces that the permeate flow through membrane b equals Q_{DF} in the case of the boundary condition $Q_F = Q_R$, which was applied in all experiments of Fig. 6.4. Together with the permeate flow a certain amount of the feed buffer is removed through membrane b resulting in the decreased level of this buffer in the retentate. However, Fig. 6.4B and 6.4C directly reveal the problems arising with the unidirectional flow through the membranes. During the initial period ($Q_{DF} = 0$) the BSA concentration in the retentate shows the expected steep increase. Because BSA is not able to penetrate the membranes and the ratio of $Q_R/Q_F = 1$ is not changed, in the ideal case, c_{BSA} would stay constant at this level throughout the complete experiment. That said, Fig. 6.4B shows that c_{BSA} deviates from this ideal behavior. After each increase of Q_{DF} the signal of c_{BSA} shows a sharp dip followed by a slow return to the original level. Beyond $Q_{DF} = 0.2$ mL/min the applied step duration is insufficient for the return, resulting in c_{BSA} in the retentate permanently staying below the feed level. In consequence BSA shows an ongoing accumulation within the module. This observation is consistent with the time course of P_R shown in Fig. 6.4C. During the initial steps ($Q_{DF} = 0$ - 0.3 ml/min) P_R stays at plateau levels below 0.3 bar, with the level of the plateau showing a small increase each time Q_{DF} is increased by 0.1 mL/min. The increase is caused by the simple fact, that after each step also the amount of permeate which has to penetrate membrane b is increased, requiring a larger transmembrane pressure (TMP). When Q_{DF} increased to 0.4 and 0.5 mL/min, the picture changes in a way, that within the monitored step duration no constant plateau of the pressure is reached, but the pressure displays a constant increase. This reveals that, besides the proportionally increased TMP required for higher Q_{DF}, an additional pressure drop results from the concentration polarization of BSA at the surface of

membrane b. Finally, the resulting buffer exchange is plotted in Fig. 6.4D and compared with the theoretical values calculated based on the plug flow as well as the complete mixing model (detailed values are shown in the SI part, Table S6.2). As can be seen, the experimental values lie between the two idealized models with a tendency to be closer to the plug flow results, something that can be expected to take into account the steep breakthrough observed in Fig. 6.4A. Nevertheless, the achieved buffer exchange of around 63% at $Q_{DF}/Q_F = 1$ is too low to be of practical use. In order to achieve higher levels of buffer exchange, the flow of the diafiltration buffer must be increased further. Unfortunately, the attempt to follow this direction quickly leads to an inadmissible increase of the pressure within the middle part of the module.

6.3.2 Co-current diafiltration with alternating flow direction through the membrane

As described above, the use of a unidirectional permeate flow through membrane b of our module quickly resulted in a constantly rising pressure within the middle part of the module when the flow of the diafiltration buffer approached a ratio of Q_{DF}/Q_F around one. In order to avoid this problem, we introduced a single pass filtration with alternating flow direction of the diafiltration buffer. As in the case of the experiments described in section 6.3.1, the short prototype module was used and the flow rates of the feed Q_F and the retentate Q_R were adjusted at 0.5 ml/min (56.4 L m^{-2} h^{-1}) while the diafiltration buffer flow rate Q_{DF} was increased by 0.1 ml/min steps, starting at an initial value of 0.1 ml/min up to a maximum of 0.8 ml/min. Every parameter set was operated for 30 minutes, with a switching time of the alternating flow direction through the membrane of 10 min. After switching the inlet position of the diafiltration buffer, the remaining permeate was flushed with high flow rate of 10 ml/min for 10 seconds (for details see operation mode ‘B’ in Fig. 6.3, section 6.2.4). Since this operation mode resulted in a cyclic backflush of the accumulated concentration polarization layer of BSA, the signal detected by the UV sensor showed strong fluctuations. Hence, in order to get representative analytical results for each parameter set, the retentate was collected during the corresponding 30 min period and the average concentrations of BSA and feed buffer residues in the retentate were determined from this sample.

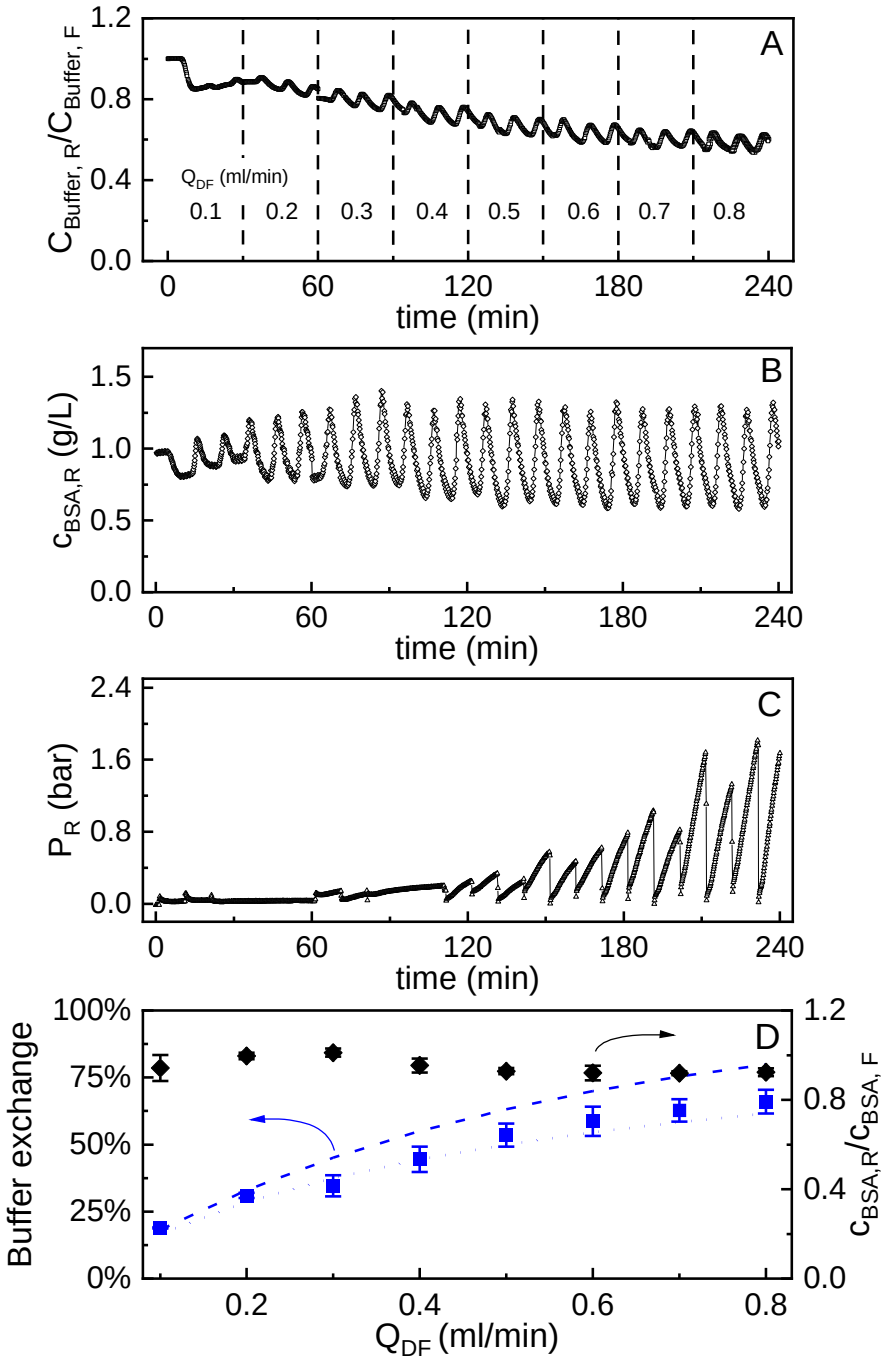

Fig. 6.5 Degree of buffer exchange of the co-current DF process with alternating flow direction through the membrane. In the course of the test series the flow rate of DF buffer was increased stepwise from 0.1 to 0.8 ml/min in steps of 0.1 ml/min, while the feed and retentate flow were kept constant at 0.5 ml/min. (A) Normalized concentration of the components of the original buffer remaining in the retentate, (B) Concentration of BSA in the retentate, (C) Pressure in the middle part of the membrane module, (D) Degree of buffer exchange and concentration factor of BSA plotted versus the flow rate of diafiltration buffer Q_{DF}. The dashed lines represent the theoretical buffer exchange values corresponding to the idealized models of complete mixing (· ····) and plug-flow (– ––), respectively.

Fig. 6.5A shows the same trend of slowly decreasing residues of the feed buffer in the retentate with increasing Q_{DF}. However, the decrease does not show one clear step after increasing Q_{DF} by 0.1 ml/min, but a relatively smooth decrease superposed by a wiggle of the buffer concentration caused by the switching events of the alternating flow direction of the DF buffer. While this wiggle is relatively small in the case of the buffer concentration, it is much more pronounced for the BSA concentration in the retentate (Fig. 6.5B). Beyond a Q_{DF} of approx. 0.3 ml/min c_{BSA} in the retentate fluctuates between 0.6 and 1.3 g/L. Besides this short-term fluctuation, the average BSA concentration in the retentate is close to 1 g/L and therefore almost equal to the feed concentration. The minima of the concentration fluctuations show a slightly decreasing trend, which is likely caused by the fact that higher Q_{DF} result in a stronger concentration polarization during the 10 min intervals between the reversals of the DF buffer flow direction. Nevertheless, Fig. 6.5B is a first indication that the inherent backflushing caused by the cyclic reversal of the flow of the diafiltration buffer may result in the desired effect of limiting the accumulation of BSA within the filtration module. Looking at Fig. 6.5C it shows that also the pressure in the middle part of the module shows strong fluctuations in the case of higher Q_{DF}. Comparing the pressure peaks in Fig. 6.5C with the pressure plateaus in Fig. 6.4C one has to keep in mind that in Fig. 6.4 Q_{DF} increased stepwise to only 0.5 ml/min while in Fig. 6.5 the steps went up to a final diafiltration flow of 0.8 ml/min. Comparing the average pressure at Q_{DF} = 0.5 ml/min in both experiments, the $\overline{P_R}$ values are 2.24 bar and 0.24 bar in the case of the unidirectional and the alternating flow direction of the diafiltration buffer. This shows that the alternating flow operation mode is able to temporarily reduce the pressure build-up caused by the concentration polarization layer by sweeping this layer away. However, especially in the case of the highest Q_{DF} of 0.8 ml/min the reformation of the polarization layer at the opposite membrane after the switching event is quite fast, resulting in a pressure increase of more than 1.6 bar within a 10 min period. Finally, when looking at Fig. 6.5D, it must be concluded that the alternating DF flow operation mode did not result in an improved buffer exchange. Actually, in the case of the same Q_{DF} the buffer exchange of the alternating DF flow operation mode was even slightly less than the buffer exchange achieved with unidirectional DF flow mode (see SI Table S6.3). The explanation for this decrease is threefold. First, as can be expected, the alternating DF flow direction increases the mixing within the middle part of the module. Therefore, the buffer exchange moves closer to the lower boundary values given by the model assumption of complete mixing. Second, during the short flushing periods being part of the switching cycle, no diafiltration buffer enters the middle part of the module while the feed solution is continuously pumped into this region. And third, the

flushing time of 10 seconds may not be long enough to remove all residues of the permeate. Therefore, in the initial phase after switching the flow direction the diafiltration buffer entering the middle part of the module may be contaminated by these residues. In conclusion, the results of Fig. 6.5 show that the alternating DF flow operation mode does not improve buffer exchange if the same parameters are applied as in the case of the unidirectional flow mode. However, the frequent reduction of the accumulated concentration polarization layer opens a wider window of possible operation parameters if the switching times are adjusted accordingly. In the next section, we discuss the results of different test series in which this parameter space was explored in order to find optimum operation conditions for the buffer exchange of our system.

6.3.3 Optimization of co-current diafiltration with alternating DF flow direction

The first parameter investigated was the flushing time applied for washing out the permeate residues from the lateral module part which serves for delivering the diafiltration buffer after the switching of the flow direction through the membranes. The investigated flushing times were 5, 10, 15 and 20 s while keeping the switching interval time at 10 min and the volume flows at $Q_F = Q_R = Q_{DF} = 0.5$ ml/min (56.4 L m^{-2} h^{-1}). Each flushing parameter was investigated for 30 min, which means reversing the direction of DF flow for three times.

The experiments showed the highest buffer exchange of around 50% in the case of a flushing time of 15 s, and no significant difference of buffer exchange between 10, 15 and 20 s flushing time (see Table 6.2). When a flushing time of only 5 s was applied, the buffer exchange dropped significantly to 46%. Based on the hold-up volume of the section of the lateral module part which stays in contact to the membrane (1.25 ml) and the high flow rate during the flushing step (10 ml/min) the residence time of the liquid in this section can be approximated to 7.5 s. Therefore, a flushing time of 15 s corresponds to approx. two times the residence time and should guarantee an almost complete removal of permeate residues.

Table 6.2 Degree of buffer exchange as a function of flushing time

Flushing time (s)	Buffer exchange	SD
5	45.8%	0.01
10	48.4%	0.03
15	48.8%	0.03
20	48.2%	0.004

The next parameter investigated was the duration of the interval between the switching events of the DF flow direction. On the one hand, within long intervals the pressures in the module may approach a critical level. On the other hand, short intervals and frequent switching will increase the mixing in the module and the amount of DF buffer which is consumed for flushing. In order to investigate these relationships, we conducted two initial test series with increasing Q_{DF} (0.1 ml/min steps) applying switching intervals of 10 min and 5 min. Again Q_F and Q_R were kept constant at 0.5 ml/min. The respective Fig. S6.2 in the SI part shows that at low Q_{DF} the buffer exchange in the case of a switching interval of 5 min is slightly worse than the buffer exchange in the case of a switching interval of 10 min. This observation is within our expectation, because in the case of 5 min switching intervals the related detrimental effects, like mixing and short periods without diafiltration buffer entering the middle part of the module, occur more frequently. However, in the case of higher Q_{DF} values this trend seems to be reversed. A possible explanation for this effect is that in the case of higher Q_{DF} values longer intervals between the flow reversals will lead to an enhanced concentration of BSA at the membrane surface. If BSA reaches very high concentrations it starts forming a gel like structure which hampers also the perfusion of hydrated ions and the sieving coefficient of the salt of the buffer drops below one, reducing the efficiency of buffer exchange.

Despite the small detrimental effect of short switching intervals, they offer the chance to increase Q_{DF} further. From our idealized plug flow model, it is known that a ratio of at least $Q_{DF}/Q_F = 7$ is needed for a buffer exchange around 99.9%. Therefore, an experiment having a Q_{DF}/Q_F of 7.2 was conducted, in order to see how far the conditions of the co-current diafiltration with alternating DF flow can approach. Because the required Q_{DF} turned out to be too high in the case of Q_F = 0.5 ml/min (56.4 L m^{-2} h^{-1}), we reduced the feed flow to 0.25 ml/min (28.2 L m^{-2} h^{-1}) and adjusted Q_{DF} at 1.8 ml/min. In addition, the switching interval was reduced to 3 min.

Fig. 6.6A shows the resulting time course of the buffer exchange for this experiment. Because of the reduced feed flow, the system requires a longer duration to approach quasi-stationary conditions, however, after 80 min a stable buffer exchange of around 92% could be achieved. This is the first time we succeeded to get a buffer exchange above 90% using the developed single pass filtration module. This enables potential applications having only moderate requests regarding the degree of diafiltration, such as reducing the salt content between two ion exchange chromatography steps.

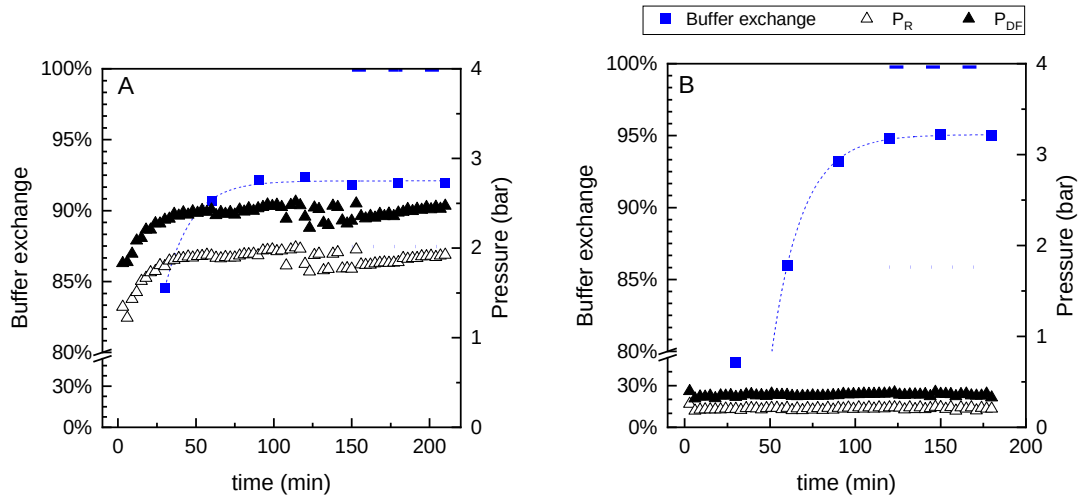

Fig. 6.6 Time course of the buffer exchange and the pressures in the middle (P_R) and the lateral (P_{DF}) part of the module for co-current diafiltration and alternating flow direction of the DF buffer through the membranes. The flushing time for the lateral part and the switching interval were 15 s and 3 min in both experiments. (A) small prototype module with a 5 cm flow path length, (B) scaled-up module with 25 cm flow path length. The dashed lines represent the theoretical buffer exchange value corresponding to the idealized models of complete mixing (·····) and plug-flow (– – –), respectively.

Besides the time course of the degree of buffer exchange, Fig. 6.6A also shows the pressures in the middle (P_R) and the lateral (P_{DF}) part of the module. Because of the short switching interval of 3 min, plotting the complete time course of the pressures results in a rather turbulent picture showing more than 70 narrow pressure peaks for P_R and P_{DF} (see Fig. S6.3 in the SI). Therefore, Fig. 6.6A only shows the average pressure values observed in each of the switching intervals. After an initial phase, the average pressure P_R in the middle part approaches 2 bar with a very small incline during the duration of the experiment of 3.5 h. The pressure P_{DF} in the lateral part of the module which is connected to the inlet of the diafiltration buffer is around 0.5 bar higher than P_R and follows exactly the same trend. The consistency of the transmembrane pressure resulting from the difference between P_{DF} and P_R indicates, that the permeability of the membranes for pure diafiltration buffer stays constant and there is no permanent fouling of the membranes within the duration of the experiment.

6.3.4 Co-current diafiltration with alternating DF flow direction using a scaled-up module

While the increase of the Q_{DF}/Q_F ratio to around 7 resulted in a clear improvement of buffer exchange, the value of 92% is still rather far from the theoretical optimum. Comparing our prototype module with other SPTFF modules, the very short flow path

length of only 47 mm is an obvious difference hampering high buffer exchange. Therefore, the next stage in our stepwise optimization was the design of a scaled-up module having a flow path length of 245 mm. Using this new module, an experiment applying the same parameters (Q_F = Q_R = 0.25 ml/min; Q_{DF} = 1.8 ml/min) than the preceding one with the small module was conducted. In consequence, the feed flux per membrane area was reduced from 28.2 L/(m^2 h) to 5.05 L/(m^2 h), which is about 10 times less than conventional SPTFF systems used in multistep diafiltration. As can be seen in Fig. 6.6B, the buffer exchange in the scaled-up module increased to 95%, while using the same amount of diavolumes (7.2). More pronounced than this increase in buffer exchange is the strong drop in the maximum pressures achieved during the switching intervals, staying constant at P_R = 0.21 bar and P_{DF} = 0.35 bar throughout the experiment. Comparing these pressures with the ones appearing in the small module, it can be seen that while the pressure difference between P_{DF} and P_R reduced only by approx. a factor of 3.6, the pressure in the middle part of the module (retentate chamber) dropped by almost a factor of 10. This shows, that besides the direct effect of the reduced specific flows, in the scaled-up module the pressure build-up in the middle part is also reduced due to a diminished concentration polarization. Again, detailed time courses of P_{DF} and P_R are displayed in the SI Fig. S6.3. It reveals, that in contrast of the time courses observed in the small module, the pressures in the scaled-up module reach a plateau after approx. 2 min and remain practically constant afterwards. Even when the diafiltration flux Q_{DF} was further increased from 1.8 ml/min to 3.6 ml/min (14.4 DV), the pressure P_{DF} in the module quickly reached a stable value of only about 1 bar. In case of this high diafiltration flux, the degree of buffer exchange reached up to 98.2% (see SI Fig. S6.4).

6.3.5 Counter-current diafiltration with alternating DF flow direction using a scaled-up module

For the unidirectional operation mode, as it is illustrated in Fig. 6.3A, the inlet position of the diafiltration buffer does not matter, because the complete upper lateral part of the module is filled with pure diafiltration buffer. However, in the case of the operation mode with alternating DF flow this situation changes. Now, after a switching event permeate residues are present in the lateral part which is entered by the diafiltration buffer, and the mutual alignment of the flow directions of Q_F and Q_{DF} makes a difference. From general engineering principles but also from the literature on single pass diafiltration [17,18] it is known that a counter-current design should have inherent advantages. Therefore, we explored the buffer exchange of our scaled-up module in case it is operated in counter-current mode with alternating DF flow direction, as it is

explained in section 6.2.4 Fig. 6.3C. Three variants of counter-current DF were tested, differing in the application or the omission of the flushing step after switching the DF flow direction and the selected feed flow. The first two experiments were conducted under the same conditions: $Q_F = Q_R = 0.25$ ml/min, $Q_{DF} = 3.6$ ml/min at a switching interval of 3 minutes and a flushing flow rate of 26 ml/min for 15 s (if flushing was applied). For these operation conditions, the idealized models calculate theoretical buffer exchange of 93.5% and 100.0% in the case of complete mixing and plug-flow, respectively.

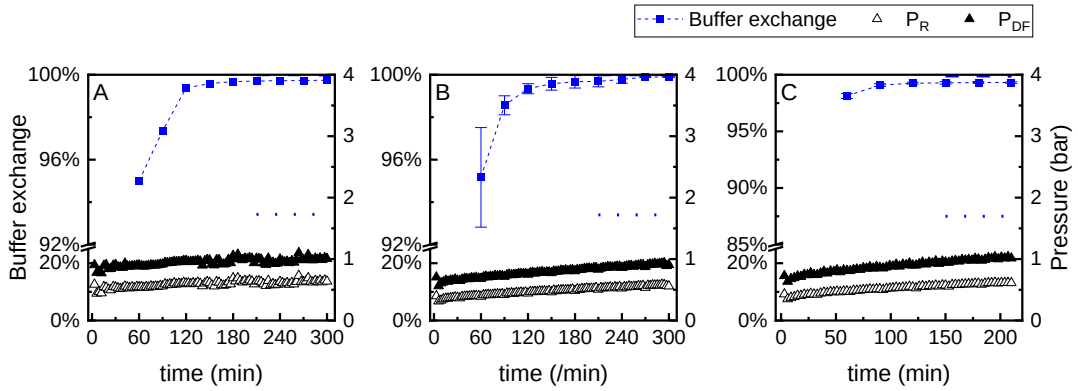

Fig. 6.7 Degree of buffer exchange and average pressures in the middle (P_R) and the lateral (P_{DF}) part of the module during the counter-current diafiltration with alternating flow direction of the DF buffer through the membranes. $Q_{DF} = 3.6$ ml/min, switching interval 3 minutes. (A) $Q_F = Q_R = 0.25$ ml/min, with flushing steps applying 26 ml/min for 15 s, (B) $Q_F = Q_R = 0.25$ ml/min, without flushing steps. (C) $Q_F = Q_R = 0.5$ ml/min, without flushing steps.

In the experiments applying counter-current mode with alternating DF flow direction the buffer exchange attained 99.7% with flushing steps applied (Fig. 6.7A). When compared with a corresponding experiment using exactly the same operation parameters but co-current flow (see SI Fig. S6.4) it shows that the performance of the counter-current mode is clearly better (99.7% compared to 98.2% buffer exchange). While the difference may not look very significant at first glance, one has to be aware, that this means that the retentate resulting from the co-current operation contained six times more (1.8%:0.3%) remaining ‘impurities’ than the retentate resulting from the counter-current operation. When the intermittent flushing steps were omitted in the counter-current mode, the degree of buffer exchange even reached 99.9% (Fig. 6.7B). These results demonstrate the strong improvement that can be obtained if permeate residues in the lateral parts of the module are pumped towards the feed inlet because of the applied counter-current mode. Thus, if they penetrate back into the middle part after reversal of the DF flow direction, they dilute the high feed buffer concentration in the region of the feed inlet instead of contaminating the already desalted (diluted)

solution close to the retentate outlet. The reason for the detrimental effect of the application of flushing steps is not fully understood yet. One possible explanation could be that the high volume flows occurring during the flushing result in an enhanced pressure gradient along the flow path in the respective lateral part of the module. In combination with the very low pressure in the middle part of the module during the flushing step[1] some unwanted circulating flows between the flushed lateral part and the middle part may occur, increasing axial dispersion and slightly reducing the buffer exchange. Another reason is that during the flushing step the actual diafiltration process in the middle part of the module comes to a temporary stop. Either way, the possibility to skip the flushing steps strongly simplifies the system control and saves the required volume of DF buffer. Taking the DF buffer used into account for flushing, the actual Q_{DF}/Q_F ratio of the experiment with flushing increases to 21.3, compared to 14.4 without flushing. Looking at the time course of the pressures, it shows that although the experiments ran for more than 5h, the average value of P_{DF} and P_R showed only a slight increase and stayed below 1.1 bar in all cases. The maximum pressures occurring during the whole diafiltration process were less than 1.5 bar (see SI Fig. S6.5). Because the use of 14.4 diavolumes would result in a rather high buffer consumption in larger systems, we finally tested counter-current mode with alternating DF flow direction while switching back to the application of 7.2 diavolumes by doubling the feed flow. The resulting buffer exchange dropped slightly to 99.3% corresponding to a 140-fold removal of the impurities in the feed. If compared with the buffer exchange of a countercurrent staged diafiltration using several SPTFF units and the same amount of diavolumes (see Fig. 3 in [16]) it shows that our single 3D-printed membrane module achieves a buffer exchange being located between the ones of two- and three-stage SPTFF systems. It can be expected that after a further increase of the flow path length in our module, it will be able to challenge the buffer exchange of a three-stage SPTFF system in a single device.

6.4 Conclusion and outlook

The experimental data presented in our study clearly show that the new design of a 3D-printed single pass filtration module housing two membranes is able to achieve diafiltration efficiencies up to 99.9% without the need of coupling several modules and/or intermediate dilution and mixing steps. For this achievement, the module design and its operation mode required a systematic stepwise optimization, leading to a

[1] During the flushing $Q_F = Q_R$ still holds in the middle part and no permeate has to be pushed through the membrane. Therefore, P_R drops to practically zero.

system with 245 mm flow path length running in counter-current diafiltration mode with an alternating DF flow direction. Operating at 5 - 10 L/(m^2 h) the specific feed rate of our system is located between the corresponding values of commercial SPTFF systems [4] and the hollow fiber dialysis systems used by Yehl et al. [18]. Compared to our first paper, which reported the continuous diafiltration of BSA at feed concentrations of only 0.1 g/L, we increased the feed concentration tenfold in this work and preliminary experiments with higher concentrations indicate that the 3D-printed module also works fine at feed concentrations of 5 g/L. However, there is still another tenfold increase of the feed concentration needed in order to reach protein feed concentrations commonly applied during formulation. We expect that the module will be able to achieve high DF efficiencies also in this case, but it is likely that the specific feed rate has to be reduced to round 1 - 2 L/(m^2 h). Nevertheless, the productivity would stay in the range of around 25 g/(m^2 h), being in the same order of magnitude compared to the productivity reported by Yehl and Zydney (30 g/(m^2 h). Therefore, we think that our design might be suitable for cases in which small volumes must be diafiltrated and one wants to avoid the complexity of multi-stage SPTFF diafiltration, but also the large membrane area and hold-up volumes of the hollow-fiber system. The unconventional design of our system allows a cyclic reversal of the flow directions of DF buffer and permeate through the two membranes while continuously pumping the feed solution into the module. Thus, we can conduct an inherent backflush in order to reduce the concentrated protein layer formed by concentration polarization at the membrane surface, during continuous operation. In future research we are going to test the limits of this approach regarding the admissible protein concentration in the feed, in order to demonstrate the suitability of the system at protein concentrations as they are encountered e.g. in the case of formulation steps during downstream processing.

References

[1] A.L. Zydney, Continuous downstream processing for high value biological products: A Review, Biotechnol. Bioeng. (2016). https://doi.org/10.1002/bit.25695.

[2] A. Jungbauer, Continuous downstream processing of biopharmaceuticals, Trends Biotechnol. 31 (2013) 479–492. https://doi.org/10.1016/j.tibtech.2013.05.011.

[3] A.L. Zydney, Perspectives on integrated continuous bioprocessing - opportunities and challenges, Curr. Opin. Chem. Eng. 10 (2015) 8–13. https://doi.org/10.1016/j.coche.2015.07.005.

[4] J. Dizon-Maspat, J. Bourret, A. D'Agostini, F. Li, Single pass tangential flow filtration to debottleneck downstream processing for therapeutic antibody production, Biotechnol. Bioeng. 109 (2012) 962–970. https://doi.org/10.1002/bit.24377.

[5] N.A. Bleckwenn, H. Golding, W.E. Bentley, J. Shiloach, Production of recombinant proteins by vaccinia virus in a microcarrier based mammalian cell perfusion bioreactor, Biotechnol. Bioeng. 90 (2005) 663–674. https://doi.org/10.1002/bit.20423.

[6] J. Rucker-Pezzini, L. Arnold, K. Hill-Byrne, T. Sharp, M. Avazhanskiy, C. Forespring, Single pass diafiltration integrated into a fully continuous mAb purification process, Biotechnol. Bioeng. 115 (2018) 1949–1957. https://doi.org/10.1002/bit.26708.

[7] A. Vancleef, S. Seurs, J. Jordens, T. Van Gerven, L.C.J. Thomassen, L. Braeken, Reducing the induction time using ultrasound and high-shear mixing in a continuous crystallization process, Crystals. 8 (2018). https://doi.org/10.3390/cryst8080326.

[8] S. Xu, J. Gavin, R. Jiang, H. Chen, Bioreactor productivity and media cost comparison for different intensified cell culture processes, Biotechnol. Prog. 33 (2017) 867–878. https://doi.org/10.1002/btpr.2415.

[9] A. Arunkumar, N. Singh, M. Peck, M.C. Borys, Z.J. Li, Investigation of single-pass tangential flow filtration (SPTFF) as an inline concentration step for cell culture harvest, J. Memb. Sci. 524 (2017) 20–32. https://doi.org/10.1016/j.memsci.2016.11.007.

[10] C. Casey, T. Gallos, Y. Alekseev, E. Ayturk, S. Pearl, Protein concentration with single-pass tangential flow filtration (SPTFF), J. Memb. Sci. 384 (2011) 82–88. https://doi.org/10.1016/j.memsci.2011.09.004.

[11] D. Barba, F. Beolchini, D. Cifoni, F. Veglió, Whey protein concentrate production in a pilot scale two-stage diafiltration process, Sep. Sci. Technol. 36 (2001) 587–603. https://doi.org/10.1081/SS-100102948.

[12] J.C. Martínez-Alvarado, B. Torrestiana-Sánchez, M.G. Aguilar-Uscanga, Isolation of steviol glycosides by a two-step membrane process operating under sustainable flux, Food Bioprod. Process. 101 (2017) 223–230. https://doi.org/10.1016/j.fbp.2016.11.013.

[13] A. Simon, L. Vandanjon, G. Levesque, P. Bourseau, Concentration and desalination of fish gelatin by ultrafiltration and continuous diafiltration processes, Desalination. 144 (2002) 313–318. https://doi.org/10.1016/S0011-9164(02)00333-8.

[14] F. Lipnizki, J. Boelsmand, R.F. Madsen, Concepts of industrial-scale diafiltration systems, Desalination. 144 (2002) 179–184. https://doi.org/10.1016/S0011-9164(02)00309-0.

[15] J.C. Te Lin, A.G. Livingston, Nanofiltration membrane cascade for continuous solvent exchange, Chem. Eng. Sci. 62 (2007) 2728–2736. https://doi.org/10.1016/j.ces.2006.08.004.

[16] A.M.K. Nambiar, Y. Li, A.L. Zydney, Countercurrent staged diafiltration for formulation of high value proteins, Biotechnol. Bioeng. 115 (2018) 139–144. https://doi.org/10.1002/bit.26441.

[17] M.G. Jabra, C.J. Yehl, A.L. Zydney, Multistage continuous countercurrent diafiltration for formulation of monoclonal antibodies, Biotechnol. Prog. 35 (2019) 6–11. https://doi.org/10.1002/btpr.2810.

[18] C.J. Yehl, M.G. Jabra, A.L. Zydney, Hollow fiber countercurrent dialysis for continuous buffer exchange of high-value biotherapeutics, Biotechnol. Prog. 35 (2019) 1–5. https://doi.org/10.1002/btpr.2763.

[19] C.J. Yehl, A.L. Zydney, Single-use, single-pass tangential flow filtration using low-cost hollow fiber modules, J. Memb. Sci. 595 (2020) 117517. https://doi.org/10.1016/j.memsci.2019.117517.

[20] R. Tan, M. Franzreb, Continuous ultrafiltration/diafiltration using a 3D-printed two membrane single pass module, Biotechnol. Bioeng. (2019). https://doi.org/10.1002/bit.27233.

[21] H. Lutz, Ultrafiltration for Bioprocessing, (2015) 244. https://doi.org/10.1016/B978-1-907568-46-6.00002-1.

6.5 Support Information

Calibration curves for the conversion of conductivities into fractions of feed buffer concentration remaining in the retentate

The conversion of conductivities measured by an online sensor in the retentate into residues of the original feed buffer after diafiltration was conducted by the help of calibration curves determined from standards of known concentrations. In all experiments the feed solution contained 30 mM NaH_2PO_4 and 100 mM NaCl. In the initial series of diafiltration experiments, also the diafiltration buffer contained 30 mM NaH_2PO_4 but only 5 mM NaCl. Therefore, even a 100% exchange of the original feed buffer with diafiltration buffer does not reduce the conductivity of the retentate down to values close to zero. This fact was taken into account by preparing the standards by dilution with increasing amounts of diafiltration buffer (Fig. S6.1A). At a later point in the study pure water was used as diafiltration buffer, because even at very low ionic strength no detrimental effect onto the dissolved BSA could be observed. On the one hand this simplifies the preparation of calibration standards, on the other hand the calibration curve had to be divided into two sections (see Fig. S6.1B), because a single straight line is not a good fit of the required correlation if the conductivity stretches over several orders of magnitude.

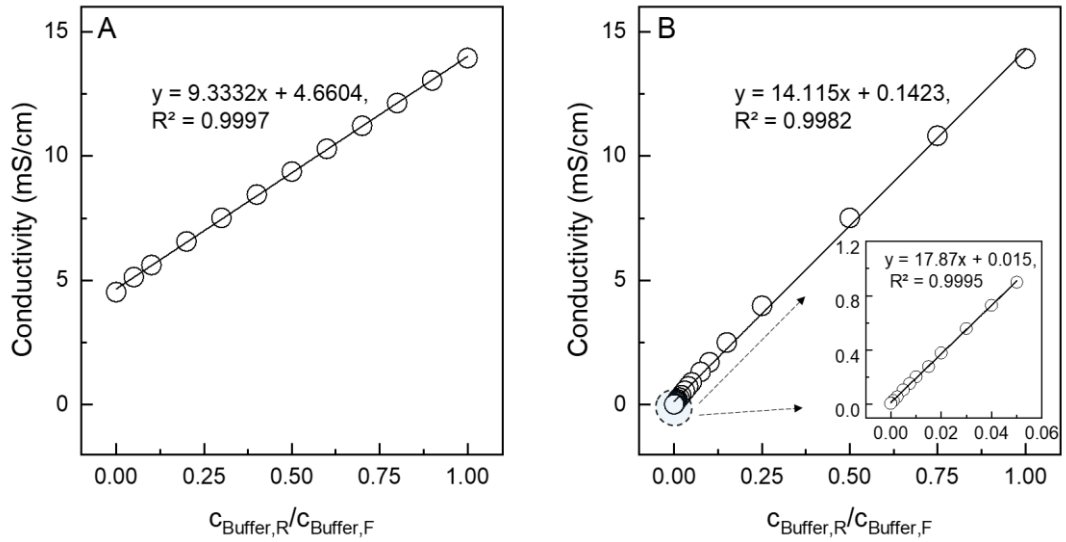

Fig. S6.1 Calibration curves for the conversion of conductivities into fractions of feed buffer concentration remaining in the retentate

Exemplary concentration factors resulting from different settings of pumps A and B of the chromatography system

The Äkta system was used in a way that pump A controlled the feed rate and pump B controlled the retentate rate. In the Äkta software the two feed rates are defined by the sum-flow of pumps A and B and the percentage X defining how much of this sum-flow is pumped by pump B. The pump rate of pump A is automatically set to (100 - X)% of the sum-flow. Dividing the resulting flow rates of pumps A and B will give the theoretical values of the concentration factor listed in Table S6.1.

Table S6.1 Theoretical concentration factors controlled by adjusting the percentages of pump A and pump B of the Äkta system

Percentage of pump A (%)	Percentage of pump B (%)	Concentration factor
50	50	1
66.7	33.3	2
75	25	3
80	20	4

Details of measured and theoretical buffer exchange in the experiments applying co-current diafiltration with unidirectional and alternating flow of the diafiltration buffer

The theoretical values listed in Table S6.2 and Table S6.3 are calculated using two idealized models based on the assumption of (i) complete mixing and (ii) plug flow.

Table S6. 2 Measured and theoretical buffer exchange in the experiment applying co-current diafiltration with unidirectional flow

Flow rate ratio Q_{DF}/Q_F (-)	Experimental result, buffer exchange (%)	SD	Complete mixing, buffer exchange (%)	Plug flow, buffer exchange (%)
0	0	0.000	0	0
0.2	15.7	0.000	16.7	18.1
0.4	31.6	0.049	28.6	33.0
0.6	41.5	0.043	37.5	45.1
0.8	53.2	0.031	44.4	55.1
1.0	62.3	0.000	50.0	63.2

Table S6. 3 Measured and theoretical buffer exchange in the experiment applying co-current diafiltration with alternating flow of the diafiltration buffer

Flow rate ratio Q_{DF}/Q_F (-)	Experimental result, buffer exchange (%)	SD	Complete mixing, buffer exchange (%)	Plug flow, buffer exchange (%)
0.2	18.9	0.003	16.7	18.1
0.4	31.0	0.010	28.6	33.0
0.6	34.6	0.040	37.5	45.1
0.8	44.5	0.047	44.4	55.1
1.0	53.5	0.043	50.0	63.2
1.2	58.7	0.054	54.5	69.9
1.4	62.7	0.042	58.3	75.3
1.6	66.0	0.045	61.5	79.8

Co-current diafiltration with alternating DF flow direction: degree of buffer exchange as a function of switching interval times

For co-current diafiltration with alternating DF flow direction Fig. S6.2 shows the influence of the applied switching interval time onto the buffer exchange and the maximum pressure build-up. For low Q_{DF} the dependency shows the expected order, with longer switching intervals resulting in a higher pressure build-up but at the same time slightly better buffer exchange. The higher buffer exchange is assumed to be related to the detrimental mixing effects originating from the switching event. However, above a Q_{DF} of 0.7 ml/min, the buffer exchange order changes, saying the buffer exchange of the experiment with the shorter switching interval is slightly higher. The reason for this unexpected behavior is not clear yet.

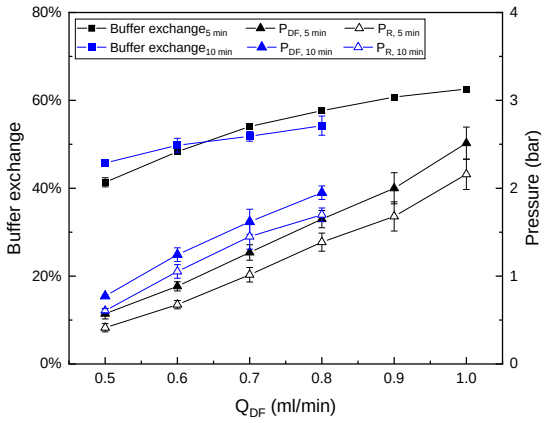

Fig. S6.2 Degree of buffer exchange and pressures in the membrane module as a function of various switching interval times. $Q_F = Q_R = 0.5$ ml/min (56.4 L m^{-2} h^{-1}), flushing time 15 s at 10 ml/min.

Co-current diafiltration with alternating DF flow direction: Detailed time courses of the degree of buffer exchange as well as P_R and P_{DF} within the small and scaled-up module

For co-current diafiltration with alternating DF flow direction Fig. S6.3 shows the detailed time courses of buffer exchange and the pressures P_R and P_{DF} for long-term experiments in the small and scaled-up module.

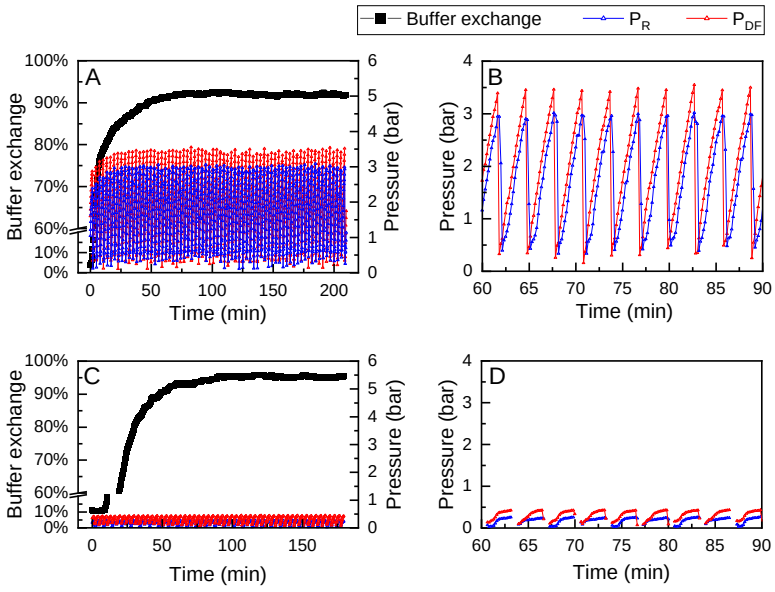

Fig. S6. 3 Detailed time courses of buffer exchange as well as P_R and P_{DF} during co-current diafiltration with alternating DF flow direction. $Q_F = Q_R = 0.25$ ml/min, $Q_{DF} = 1.8$ ml/min (7.2 DV), switching interval 3min, flushing time 15 s; (A) full-time course of the experiment using the small module, (B) zoomed out the section of the time course of the experiment using the small module, (C) full-time course of the experiment using the scaled-up module, (D) zoomed out section of the time course of the experiment using the scaled-up module.

Co-current diafiltration with alternating DF flow direction: Detailed time courses of the degree of buffer exchange as well as P_R and P_{DF} within the scaled-up module

Fig. S6.4 shows the results of an experiment applying co-current diafiltration with alternating direction of the permeate flow. During the experiment, operation conditions applying 7.2, 12, and 14.4 diavolumes were tested.

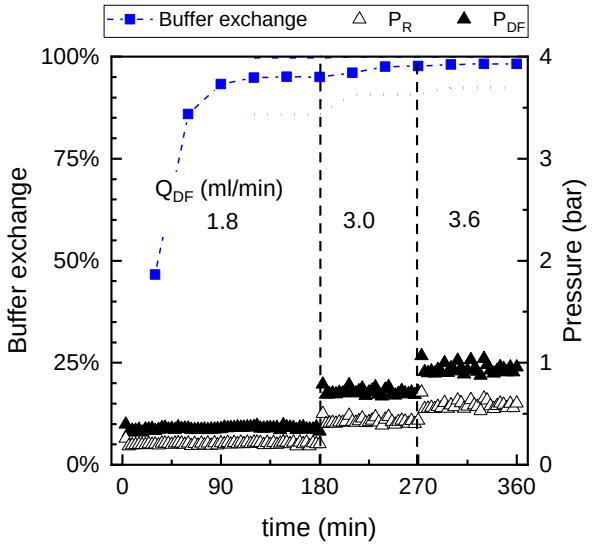

Fig. S6. 4 Time course of the buffer exchange and the pressures in the middle (P_R) and the lateral (P_{DF}) part of the module for co-current diafiltration with alternating DF flow direction in the scaled-up membrane module. The diafiltration flow flux was increased from 1.8 to 3.6 ml/min during the experiment. The dashed lines represent the theoretical buffer exchange value corresponding to the idealized models of complete mixing (▪ ▪ ▪ ▪ ▪ ▪) and plug-flow (— — —), respectively.

Counter-current diafiltration with alternating DF flow direction: Detailed time courses of the degree of buffer exchange as well as P_R and P_{DF} within the scaled-up module

For counter-current diafiltration with alternating DF flow direction Fig. S6.5 shows the detailed time courses of the buffer exchange and the pressures P_R and P_{DF} for long-term experiments with and without flushing step as well as different feed flow rates in the scaled-up module.

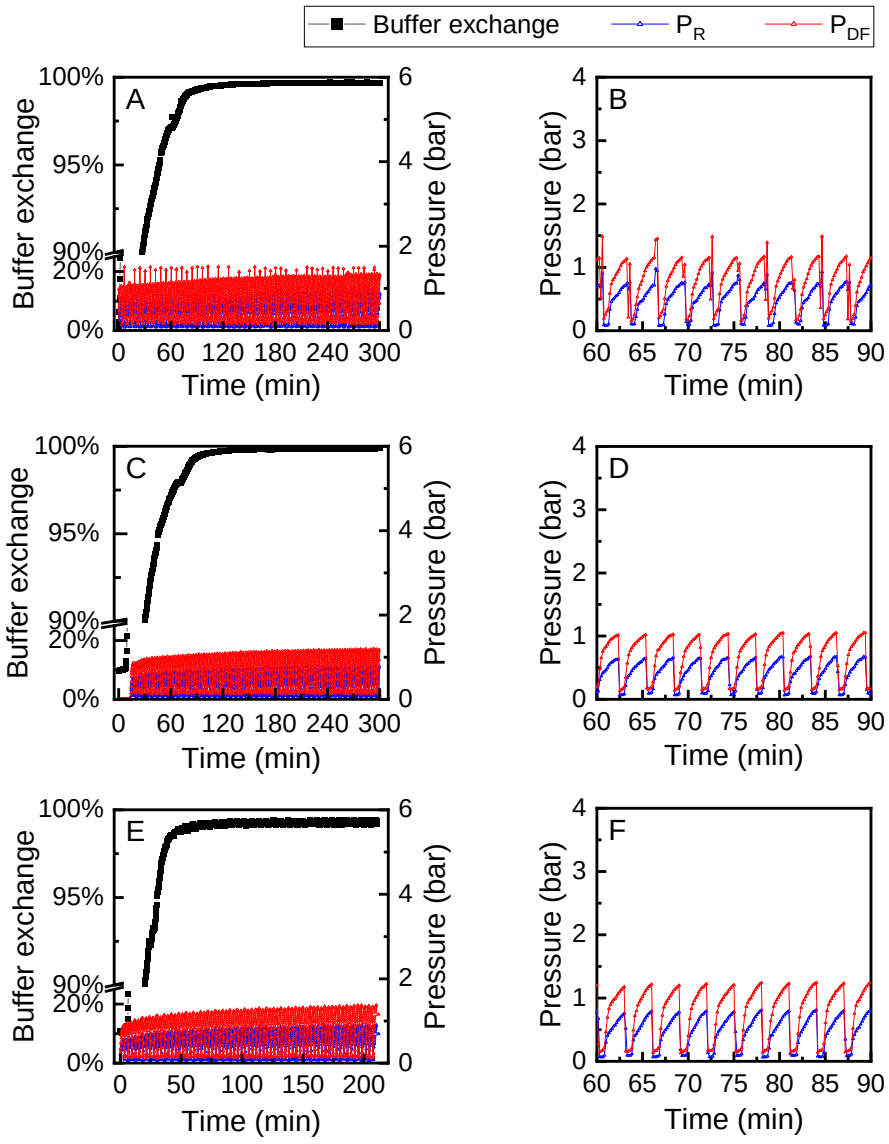

Fig. S6.5 Detailed time courses of buffer exchange as well as P_R and P_{DF} during counter-current diafiltration with alternating DF flow direction using the scaled-up module. The flow rate Q_{DF} and switching interval were 3.6 ml/min and 3 min respectively in these experiments. A and B: With flushing steps, $Q_F = Q_R = 0.25$ ml/min (5.05 L m^{-2} h^{-1}), DV 21.3), (A) full-time course of the experiment, (B) zoomed out section of the time course of pressures in the module. C and D: Without flushing steps, $Q_F = Q_R = 0.25$ ml/min (DV 14.4), (C) full-time course of the experiment, (D) zoomed out the section of the time course of pressures in the module. E and F: Without flushing steps, $Q_F = Q_R = 0.5$ ml/min (10.1 L m^{-2} h^{-1}), DV 7.2), (E) full-time course of the experiment, (F) zoomed out the section of the time course of pressures in the module.

7 Simulation based evaluation of single pass continuous diafiltration with alternating permeate flow direction

Ruijie Tan[1], Matthias Franzreb[1*]

[1]*Institute of Functional Interfaces (IFG), Karlsruhe Institute of Technology (KIT), Hermann-von-Helmholtz-Platz 1, 76344 Eggenstein-Leopoldshafen, Germany*

[*]Corresponding author: matthias.franzreb@kit.edu

Abstract In the framework of modern bioprocessing continuous ultrafiltration/diafiltration (UF/DF) is getting increasingly popular. However, while continuous UF can be easily implemented using a so-called single pass tangential flow filtration (SPTFF) module, continuous DF requires a more complicated setup including several SPTFF modules and intermittent dilution steps. Recently, we introduced a novel module design for continuous DF allowing simultaneous delivery of fresh buffer while withdrawing the permeate, thus achieving high degrees of buffer exchange within a single unit. In addition, the system allows to cyclically switch the flow direction of DF buffer through the membranes. Those uncommon features, however, also make it more difficult to determine an operation optimum experimentally by means of trial and error. Therefore, here a detailed finite element model of the physical processes within the module is presented, predicting key figures such as the obtained diafiltration efficiency and the resulting pressures. Because within the module all flow channels are filled by a 3D-printed porous grid supporting the membranes from both sides, the Brinkman equation was used to simulate the hydrodynamics, while common mass balance differential equations including accumulation, convection, and an anisotropic dispersion term were used for the simulation of concentration profiles of dissolved species. The predicted key figures are in good agreement with experimental results, obtained for feed solutions including up to 5 g/L of protein and being operated with and without switching the flow direction of the diafiltration buffer. A thorough parameter study reveals that the module shows the best performance for unidirectional flow of the diafiltration buffer, reaching diafiltration efficiencies independence to the applied diavolumes which are comparable to the ones of a conventional multi-stage setup using three SPTFF modules. Therefore, the simulation-based evaluation of optimum operation conditions reveals that the new module design has the potential to realize truly continuous diafiltration setups with high efficiency, requiring only one unit and no extra external piping for returning diafiltration in counterflow. Such simplified setups

should be especially useful in small, flexible processing plants as they are increasingly demanded in the biopharmaceutical industry.

Keywords: diafiltration, continuous processing, SPTFF, modelling, concentration profiles

---

Submitted to journal Chemical Engineering Journal.

7.1 Introduction

Membrane-based separation processes, including microfiltration (MF), ultrafiltration (UF), diafiltration (DF), and reverse-/forward osmosis (RO/FO), are indispensable separation technologies in diverse fields such as biopharmacy, biotechnology, dairy industry or water treatment [1–4]. For the formulation of high value bioproducts, UF is usually used for concentrating the protein, while DF is used for exchanging the buffer in which the protein is dissolved. One limiting factor for the productivity of these processes is the fact that the retained molecules accumulate on the membrane surface [5] (Fig. 7.1A). During ultrafiltration, the accumulating process is undergoing two periods: concentration polarization (CP) and membrane fouling [6–9]. Concentration polarization occurs immediately when the filtration process starts, however, the formed proteinaceous layer is reversible and releases back into the bulk when the applied flux through the membrane is diminished. The accumulated proteins may change the effective MWCO of membrane, hence deteriorating the membranes hydraulic permeability and selectivity [10]. When the protein concentration at the membrane surface exceeds the solubility limit, irreversible fouling phenomena can be observed. Various types of membrane fouling have been reported, such as adsorption, pore-blocking, and deposition of solidified solute [8,11–13].

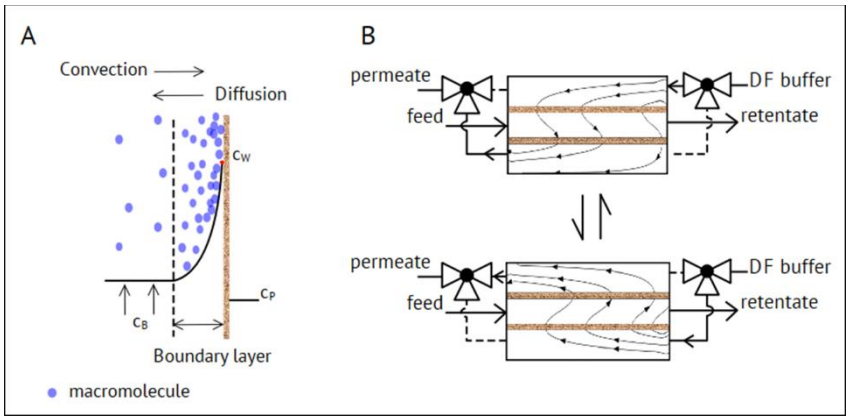

Fig. 7.1 Microscopic accumulation phenomena and macroscopic flow patterns in the newly developed single pass tangential flow filtration module. A. Concentration polarization of macromolecules at the surface of an ultrafiltration membrane. c_B: concentration of the macromolecules in the bulk; c_W: t concentration at the membrane surface; c_P: concentration in the permeate stream. B. Diafiltration operation modes of a single pass tangential flow filtration module containing two membranes. The module can apply an alternating direction of the perfusion of diafiltration buffer as inherent backflush to reduce the concentration polarization effects.

The usual way to limit CP is the application of so-called tangential flow filtration. In this operation mode the feed solution is pumped in parallel to the membrane surface at high velocities, in order to reduce the thickness of the CP layer. The high velocities result in short residence times and only small diafiltration effects during this duration. Therefore, the retentate has to be recycled in a loop and pumped through the module several times. In contrast, so-called single pass tangential flow filtration (SPTFF) uses only one pass of the feed solution. However, in this case the flow velocity has to be reduced strongly in order to achieve long enough residence times for efficient ultrafiltration [14–16]. If the systems are used for diafiltration, several of the modules are used with intermittent dilution steps with diafiltration (DF) buffer. The application of a single pass simplifies the setup and enables truly continuous operation. However, the low tangential flow velocities amplify the problem of concentration polarization. In order to reduce the accumulation phenomena, we recently developed a novel continuous single pass diafiltration system [17] (Fig. 7.1B). Within this system, the middle channel guiding the retentate flow is bounded by two membranes. By this, it is possible to supply fresh DF buffer and discharge the permeate at the same time and along the complete flow path of the retentate. This allows to reach high diafiltration efficiencies within a single module, while commercial SPTFF modules need a series of two, or in many cases three, modules and intermittent mixing steps in order to reach high diafiltration efficiency. In addition, the new system allows the optional operation mode of alternating direction of the perfusion of the membranes (see Fig. 7.1B). When the direction of perfusion is reversed during continuous operation, this acts as inherent backflush. Applying this operation mode and counter-current flow directions between the middle and the lateral flow channels a single module of this type is able to achieve a continuous diafiltration efficiency of more than 99% with a diavolume of 7.2.

Besides its effectiveness, the new SPTFF module containing two membranes offers a higher number of process parameters that can be controlled in order to optimize the performance for a specific diafiltration task. Next to the common parameters, such as feed flux and the applied diafiltration volumes, these include the choice between co-current or counter-current operation and the frequency of the optional switches of the perfusion direction through the membranes during continuous operation. Because of the additional complexity caused by the increased number of process parameters, the experiments also revealed that the duration until the quasi-stationary conditions of the process are fully developed may take a high number of switching intervals and therefore long times. In consequence, the experimental optimization of the process conditions of the new SPTFF module is a time consuming and laborious undertaking, which is why we decided to develop a simulation tool that

predicts the performance of the system and allows a better understanding of its special properties.

Looking into literature, there is no model reported which would allow the simulation of a two-membrane system with simultaneous perfusion of fresh DF buffer and permeate discharge, as well as cyclic switches of the perfusion directions. Nevertheless, there exist several excellent publications about modelling approaches towards ultrafiltration, which represent the state-of-the-art and give helpful advice about modelling dynamic phenomena, such as concentration polarization. Those models have been used to predict fluxes, pressure profiles, concentration distributions, shear stresses, and mass transfer as well as accumulation phenomena. Respective models are available for different setups, such as dead-end modules [3,8,18,19], flat sheet cross-flow rigs [20,21], hollow fiber modules [7,22] and multistage SPTFF units [23,24]. In the last two decades, the description of the accumulation phenomena during UF developed from a static, mostly qualitative to a dynamic quantitative analysis in order to better understand the important process limitations resulting. The development was accompanied by improved experimental technologies to visualize the accumulation process near the membrane [3]. In 2002, Ghosh [19] developed a pulse injection technique applying BSA to study membrane fouling. Later, Fernández-Sempere et al. [8] utilized holographic interferometry to visualize the effects of concentration polarization *in-situ*. They also predicted concentration profiles and permeate fluxes by modeling using an empirical equation based on the global convection-diffusion mechanism.

In contrast to the above mentioned global correlations, models based on computational fluid dynamics (CFD) using e.g. finite volume (FVM) or finite element (FEM) techniques enable to consider complex system geometries and predict local concentration and flow patterns [25]. Marcos et al. [22] presented a 2D FEM model using the software COMSOL Multiphysics (COMSOL Inc, Burlington, USA) to simulate transient flow and concentration profiles based on the equations of momentum and mass conservation for a hollow fiber cross-flow UF. They applied a resistance-in-series model to consider reversible as well as irreversible CP and fouling effects at the membrane surface. They also introduced an empirical correlation predicting a linear increase of the fluid viscosity with the concentration of the accumulated proteins. In a separate study by Schausberger et al. [21], also a 2D CFD model was used to assess the total flux and fouling by surface adsorption under various feed volume flows, pH and protein concentrations for UF using a flat-sheet cross flow rig. The results show that CP phenomena have to be considered even at low transmembrane fluxes, because otherwise significant membrane-solute-solvent interactions would be ignored.

They suggested replacing the individual convection-diffusion equations for proteins and ionic species with alternative multi-component transport equations. The same point was also stressed by Rajabzadeh et al. [7] in their study introducing a model for hollow fiber cross-flow UF of soy protein extracts. Recently, Aguirre-Montesdeoca et al. [20] introduced the local critical flux to demonstrate the CP phenomena along the membrane length. By using a model based on the modified Maxwell Stefan equation expressed as a function of volume fractions of both protein (BSA) and accompanying ions, they predicted the permeate flux, volume fractions of BSA on the membrane surface and the osmotic pressure difference over the membrane under different pH and ionic strengths in the feed solution. Haribabu et al. [18] pointed out the importance to show the non-uniformity of parameters like local transmembrane pressure, flow velocity, and concentration at different positions of the membrane in the cross-flow filtration. They advised using a multi-dimensional numerical treatment instead of a one dimensional or area-averaged models.

As will be described in detail in the next section, also our 2D-CFD model is based on common equations for conservation of mass and momentum. Namely, the Brinkman equations for the fluid flow and mass conservation equations for the salt and protein species containing convective and dispersion terms. However, instead of describing the transient behavior of the local transmembrane pressure (TMP) by a resistance in series approach, we consider the effect of CP directly within the fluid compartments in the vicinity of the membranes. In contrast to hollow fiber modules, where the inner volume of the fibers but also the void volume of the containment housing the fibers is open space only filled by the fluid, all flow channels of our module are filled by a grid supporting the membranes on both sides (see SI Fig. S7.1). Although the grid is relatively coarse, it can be looked at as a porous structure causing a pressure drop in dependence of the viscosity and velocity of the fluid that flows through its pores. Therefore, next to the constant permeability of the membranes themselves, we use a correlation linking the local fluid viscosity to the protein concentration and thereby getting a dynamic description of the flow resistance in certain regions of the module in dependence of the built-up concentration polarization. By this, the local flow resistance is always directly coupled to the prevailing protein concentration, which is an important feature in few of the fact that a reversal of the direction of perfusion of the membranes results in an almost instantaneous degradation of the CP layer at the membrane surface. Currently our model does not account for irreversible membrane fouling, however the implementation should be straightforward adding a transient resistance to the constant membrane resistance, following e.g. the approach of Marcos et al. [22].

7.2 Materials and methods

7.2.1 Materials and SPTFF set-up

The model protein bovine serum albumin (BSA, molecular weight of 67 KDa) was purchased from PanReac AppliChem (Darmstadt, Germany). A mixture of 100 mM sodium chloride and 30 mM mono-sodium phosphate buffer at pH 7.10 (Merck KGaA, Darmstadt, Germany) was used as carrier phase for the BSA in the feed solution. The ultrapure water used to exchange the feed buffer and all ultrapure water used in the experiments was prepared by a Sartorius arium® pro system (Sartorius, Göttingen, Germany). The polyethersulfone (PSE) 30 kDa cutoff membrane manufactured by Pall Life Sciences (Hauppauge, USA) was mounted in the 3D-printed membrane module for continuous UF/DF. The module used here was a scaled-up one which also has been introduced detailly in previous study [17]. In brief, the module is composed of three parts, including two lateral parts containing either the diafiltration buffer or the permeates, and a middle part which includes the inlet of feed and the outlet of retentate (Fig. 7.1B). Between the middle and the lateral part there are two membranes of the same type, both facing with their selective layer towards the middle channel. Due to size exclusion, the protein entering with the feed can only move within the channel confined by the middle part and the adjacent membranes. Each membrane has an effective area of 2972 mm^2 along a flow path length of 24.5 cm. For operation, the module was integrated into a FPLC Äkta system (purifier UPC 10, GE Healthcare, Uppsala, Sweden) including an additional sampling pump as well online detectors for UV/Vis adsorption, conductivity and pH (see SI Fig. S7.2). The three double-piston high pressure pumps were able to adjust precise flow rates of feed, retentate and DF buffer, and thus also fixing the flow rate of the permeate due to the incompressibility of the fluids. Therefore, in contrast to common UF systems having pressure dependent permeate fluxes, our set-up controls the fluxes while the pressures in the different parts of the module result from the transient permeabilities. The system was operated in plain diafiltration mode, saying the feed and effluent flow rates always were kept identical. As a consequence, also the permeate flow rate directly corresponded to the flow rate of the DF buffer. In addition, the multiport valves of the FPLC system allowed an easy switching of the perfusion directions through the membranes, as illustrated in Fig. 7.1B. Finally, the pressure in the diafiltration inlet was recorded by an external pressure sensor.

7.2.2 Analytical methods

In the effluent of the retentate, the concentrations of BSA and salt were measured and recorded online using a UV/Vis sensor at the absorbance wavelength of 280 nm and a conductivity meter, respectively. Two key parameters were calculated to evaluate the system with respect to transient protein accumulation and diafiltration performance: concentration factor (CF) and diafiltration efficiency (DE). The factor CF was defined as the ratio of concentration of BSA in the retentate and the feed:

$$CF = \frac{c_{BSA,R}}{c_{BSA,F}} \tag{7.1}$$

Since the retentate and feed flow had the same flow rates in all experiments, the idealized value of CF always has been equal to one, assuming no built-up of concentration polarization occurring during the filtration process. The factor DE was calculated based on the equation (7.2).

$$DE\ (\%) = \left(1 - \frac{c_{salt,R}}{c_{salt,F}}\right) \times 100\% \tag{7.2}$$

where $c_{salt,R}$ and $c_{salt,F}$ are the concentrations of salt in the retentate and feed solution, respectively.

7.2.3 Modelling

7.2.3.1 Governing equations for fluid dynamics

The Brinkman equations were used to compute fluid velocity and pressure fields within the porous grid structure of the module parts as well as within the membranes. The Brinkman equations extends Darcy's law to describe the dissipation of the kinetic energy by viscous shear, similar to the Navier-Stokes equations. Depending on the intensity of this shear, the resulting flow patterns are located between pure plug flow in a porous structure with small pores and the laminar flow profile of an open channel. The Brinkman equations can be written [26]:

$$\nabla \boldsymbol{p} = -\frac{\mu}{\kappa}\boldsymbol{u} + \frac{\mu}{\varepsilon}\nabla^2\boldsymbol{u} \tag{7.3}$$

with κ being the intrinsic permeability of the porous media permeated by the fluid and μ is the viscosity of the fluid. The first term on the right side represents the common Darcy equation while the second one was added by Brinkman. An important feature of the introduction of the second term is, that it allows satisfying a no-slip condition when the porous media is confined by a solid wall. In addition, it also enables the formulation of a "self-consistent" set of equations when a volume is only partly filled by a porous media and the other part is e.g. an open channel in which laminar flow conditions prevail. In order to calculate the flow and pressure profiles the equation describing the

conservation of mass for an incompressible fluid with constant density is required in addition:

$$\nabla \boldsymbol{u} = 0 \tag{7.4}$$

For the estimation of the intrinsic permeability of the porous grid structure, the Kozeny-Carman equation using a porosity of $\varepsilon_g = 0.6$ and a characteristic length $L_g = 1$ mm is used.

$$\kappa_g = \frac{L_g^2 \cdot \varepsilon_g^3}{180\,(1-\varepsilon_g)^2} \tag{7.5}$$

The intrinsic permeability of the membranes κ_m could be calculated from the hydraulic tests of the membrane with pure water:

$$\kappa_m = \frac{Q \cdot \mu \cdot d_m}{TMP \cdot A} \tag{7.6}$$

where Q is the flow rate, d_m is the thickness of the membrane, TMP is the transmembrane pressure, and A is the membrane area. With respect to the boundary conditions, our model specifies the volume flows with fully developed flow profile in all four inlets and outlets, instead of the common specification of a fixed pressure in the retentate and permeate outlet. The first reason for this choice is given by the fact that we operate the system at fixed volume flows by the help of the double piston pumps of the setup, independent of the occurring pressures. The second reason results from the possibility to easily implement the change of the perfusion direction through the membrane this way. For switching the flow direction, the inlet of DF buffer changes its position and at the same time the former inlet is closed by a valve (see Fig. 7.1B). The same holds for the former and new position of the permeate outlet. In our model this switching can simply be achieved by a periodic rectangle function controlling the flows in the in- and outlets. However, as can be expected, the control of all in- and outlets of a closed compartment in combination with the assumption of an incompressible fluid unavoidable leads to numerical problems. Because of the assumption of incompressibility even very tiny differences in the sums of in- and outlet flows would result in physically senseless pressures and aborting of the program. Therefore, as will be explained in more detail in the SI Fig. S7.3, we introduced an additional artificial outlet in the model, which however, has only a very low permeability. The boundary condition is set in a way that the outlet is at ambient pressure. Because of the low permeability the flux in this outlet is completely negligible in the mass balance and the flow profiles, nevertheless it prevents that the model is overdetermined and allows the calculation of meaningful transmembrane pressures.

7.2.3.2 Governing equations for the transport of dissolved species

Mass transfer of both, BSA and salt, is simulated by the 'transport of diluted species' physics of COMSOL. Convective flux caused by the flow patterns, diffusive flux caused by concentration gradients and dispersive effects are the contributors to species transport. Accordingly, the mass balance accounting for species accumulation and transport is given as:

$$\frac{\partial(\varepsilon c_i)}{\partial t} + \nabla \cdot \boldsymbol{J_i} + \boldsymbol{u} \cdot \nabla c_i = 0 \tag{7.7}$$

where $\boldsymbol{J_i}$ is the effective diffusive flux vector given by equation (7.8).

$$\boldsymbol{J_i} = -(\boldsymbol{D_{D,i}} + D_{e,i})\nabla c_i \tag{7.8}$$

In eq. (7.8) $\boldsymbol{D_{D,i}}$ and $D_{e,i}$ are the dispersion tensor and the effective diffusivity, respectively. The effective diffusivities of the species in the grid structure are related to the diffusivities in free solution by:

$$D_{e,i} = \frac{\varepsilon}{\tau} D_{F,i} \tag{7.9}$$

where τ is the tortuosity and $D_{F,i}$ is the binary diffusion coefficient of the species in water. For the tortuosity the correlation of Millington & Quirk for an ideal porous material is used [27]:

$$\tau = \varepsilon^{-1/3} \tag{7.10}$$

For the dispersion tensor a simplified form is used, which only contains the terms $D_{D,x}$ and $D_{D,y}$ of the main diagonal. As can be seen in Table 7.1 the used values for these two terms differ strongly. While this would be rather unusual for common porous media encountered in biotechnology, such as e.g. a chromatography bed or a monolith, one has to keep in mind that our structured, 3D-printed grid is highly anisotropic. In x-direction, the flow has to pass about 80 cube shaped chambers of 2 × 2 × 2 mm^3 with only a narrow window of about 1x1 mm^2 in the walls between the chambers. Such an arrangement results in strongly varying path lengths of different streamlines and therefore strong eddy diffusion effects in x-direction with a characteristic structure dimension of about 1mm. The situation is completely different if one looks at the flow path in y-direction. In y-direction the grid forms short, completely open quadratic channels, without any obstacles for the flow (see SI Fig. S7.4). Therefore, in first approximation one could assume that there are no eddy diffusion effects for the flow in y-direction. However, in reality there is some coupling, so that also in y-direction a weak eddy diffusion, resulting in a low $D_{D,y}$, has to be taken into account. When, implementing such eddy diffusion phenomena into a model in form of dispersion terms, it is important to remember that eddy diffusion is independent of the flow velocity as

long as the laminar flow regime holds. However, the dispersion term in the model shows an effect which is inversely proportional to the flow velocity. In order to compensate for this, in first approximation, the dispersion coefficient representing eddy diffusion is defined with a linear dependency on flow velocity [28]. If a dispersion coefficient is determined for a certain flow velocity u_0 it can be extrapolated to another flow velocity u simply by multiplying with the factor u/u_0, which also equals the ratio of the applied flow rates Q/Q_0.

Table 7.1 parameters for the molecular diffusion and eddy dispersion of molecules in the grid structure

	i= BSA	i= salt	
	middle part	middle part	lateral part
$D_{F,i}$ (m²/s)	5E-11	1.5E-9	1.5E-9
$D_{D,i,x}$ (m²/s)	1.2E-5 × Q_F / Q_{F0}	1.2E-5 × Q_F / Q_{F0}	1.2E-5 × (0.5 × Q_{DF}) / Q_{F0}
$D_{D,i,y}$ (m²/s)	2.0E-9 × Q_F / Q_{F0}	2.0E-9 × Q_F / Q_{F0}	2.0E-9 × (0.5 × Q_{DF}) / Q_{F0}

In case of BSA, we assume that the molecule is completely retained by the membrane while the fluid can permeate. As a result, the phenomenon of concentration polarization occurs, meaning BSA accumulates in the vicinity of the membrane and the local concentration strongly increase. This happens until an equilibrium is reached in which the diffusive flux back into the bulk solution matches the convective flux transporting BSA towards the membrane. The phenomenon of concentration polarization is accompanied by an increased flow resistance. As mentioned in the introduction, we do not use the more common resistance in series approach to consider this effect, but we simulate the increased flow resistance by means of an increased effective viscosity in a region which stretches 150 µm above the membrane. Within this region the viscosity is not a constant but a function of the local BSA concentration (see section 7.3.2.2). Because of the fact that we model all our flows as flow through a porous grid (Eq. 7.1), the increased viscosity automatically results in an increased flow resistance. By this approach the flow resistance can dynamically follow the local BSA concentration close to the membrane. This concentration increases due to accumulation during normal operation but also abruptly drops when the flow direction through the membrane is switched.

7.3 Results and discussion

7.3.1 Hydrodynamics characterization

For the investigation of the plain hydrodynamic behavior of the module, in the beginning, idealized experiments without the presence of BSA were conducted. In this case, solely a buffer exchange between the salt in the feed flow and pure water, serving as DF buffer, took place.

7.3.1.1 Simulation of the dynamic salt profiles

To explore the influence of periodic switching of the flow direction of DF buffer in single-pass counter-current diafiltration, a representative simulation applying a salt concentration of $c_{F,salt}$ = 100 mol/m³ at a feed flow rate of Q_F = 0.25 ml/min was conducted. Fig. 7.2 displays the simulated transport of salt in the module while alternating the flow direction of DF buffer every 180 s. The chosen value of 7.2 diavolumes results in a degree of buffer exchange of around 95%. As can be seen for the concentration contour at 170 s the DF buffer flowing from the top lateral part of the module to the bottom one shifts the salt downwards to the lower membrane during the first interval. The DF buffer enters at the upper right inlet and leaves the module at the lower left outlet (see also Fig. 7.1B). So, the overall flow direction of the DF buffer is from right to left, however, during the passage of the middle part of the module, the flow direction from top to bottom is superimposed by the flow of the feed respectively retentate from left to right. Therefore, the streamlines show a kind of zig-zag profile. At the switching times there is a very short transition period in which the flow direction of the DF-buffer changes in a way that it now enters at the lower right inlet and leaves at the upper left outlet.

By this, the DF buffer flow through the membranes changes its direction, however, the overall flow direction of the DF buffer is still countercurrent to the direction of the feed flow. Mainly because of the convection of the DF buffer across the membrane, but partly also because of diffusion effects caused by the concentration difference of salt between the middle and the lateral parts, most of the salt entering with the feed stream is transported into the upper lateral part of the module in the period between 180 and 360 s. Note that while penetrating the upper membrane and entering the upper lateral part, the majority of the salt stays in the vicinity of the membrane while flowing towards the effluent. This is because the flow in the x-direction is strongly dominating in the lateral parts and there is only little mixing of the fluid compartments in the y-direction. While this characteristic is of minor significance in a non-alternating operation mode, it reduces the efficiency if the flow direction through the membrane is switched periodically. Changing the flow direction will transport fluid compartments containing

high salt loads back from the lateral part into the middle part. This behavior can be observed e.g. by looking at the stream lines in the lower lateral part in the plots between 190 s and approx. 250 s.

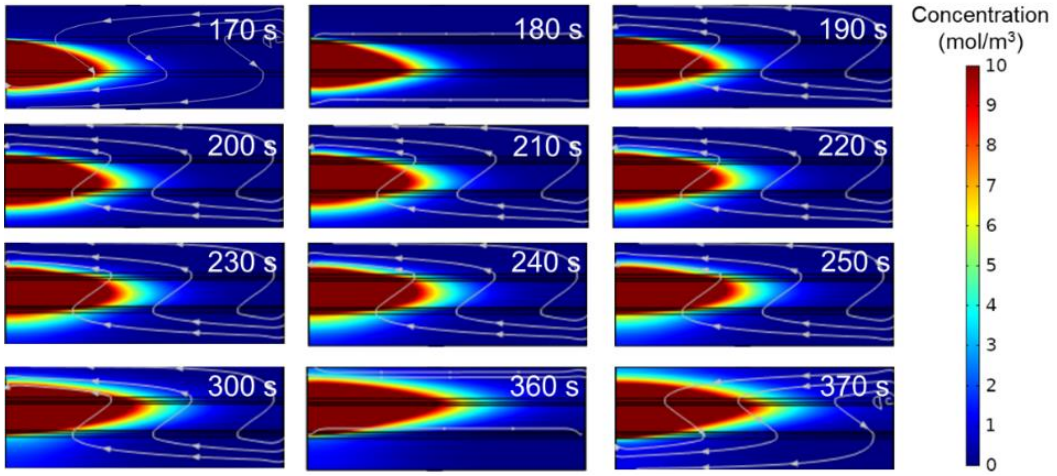

Fig. 7.2 Representative salt concentration profiles in the module before and after switching the flow direction of DF buffer. Parameter settings of the simulation: $c_{F,salt}$ = 100 mol/m³, Q_{DF} = 1.8 ml/min, Q_F = 0.25 ml/min and t_S = 180 s. The color legend of the contour plot of the salt concentration is restricted to the range between 0 and 10 mol/m³ in order to give a better picture of the spatial distribution of the lower salt concentrations dominating at the investigated degrees of buffer exchange. In addition to the contour plot streamlines of the flow profile in the module are plotted to illustrate the abruptly changing flow pattern at the switching events.

About 120 s after the switching event at 180 s (corresponding to the plot at 300 s) the salt in the lower lateral part is mainly flushed away by fresh DF buffer entering this part. However, at 360 s the next switch of the flow direction is initiated, now transporting salt from the upper lateral part back into the middle part (see the plot at 370 s). Therefore, each switching event causes a reduction of the buffer exchange efficiency lasting for a certain time. If the period between the switching events is long enough, this temporary disturbance does not interfere too much the overall performance. However, according to the simulation, for short switching intervals a severe reduction of the buffer exchange performance can be expected. Besides, the concentration of salt detected in the retentate shows a wave-like trend due to the periodic switching of the flow direction of DF buffer (see in SI Fig. S7.4). There may be cases of continuous downstream processing where even such short fluctuations are unwanted. However, integrating a small mixing vessel in the effluent having an average residence time in the range of 2-3 switching periods could easily solve this problem.

7.3.1.2 Model validation

As discussed above, the model predicts an increasing reduction of the buffer exchange performance, when the period between the switching events gets shorter. In this section, this forecast is compared to experimental data, in order to see if the developed model is able to satisfyingly predict the relationship quantitatively. For this, a series of experiments with two feed flow rates and varying switching intervals between 100 and 600 s were conducted. As in the case of the idealized simulation, the experiments were run with plain buffers without the presence of BSA.

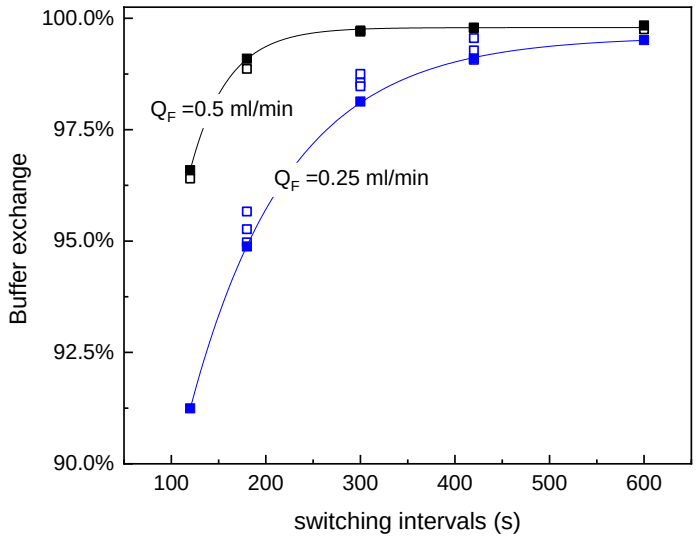

Fig. 7.3 Achieved degrees of buffer exchange in single pass countercurrent diafiltration experiments with periodic switching of the flow direction of DF buffer through the membranes. The figure shows the experimentally obtained and simulated degrees for two different feed flow rates Q_F and various values of the switching interval of the DF buffer direction. The flow rate of the DF buffer was adjusted to the Q_F in order to achieve a constant diavolume of 7.2. Higher Q_F and longer switching intervals result in a better buffer exchange performance. Open symbol: experimental value, filled symbol: simulated value.

As shown in Fig. 7.3, with increasing switching intervals and volumetric feed flow rate, both modeling and experimental results show in good agreement that the buffer exchange efficiency increased. As shown in the previous section, after each switching event there follows a period in which a part of the salt already transported into the permeate in the lateral part of the module is pushed back into the middle part of the module. In case of longer switching intervals the fraction of this period in relation to the total interval is not large and therefore the disturbing influence is low. With increasing switching intervals, the buffer exchange efficiency reaches a plateau value corresponding to the buffer exchange efficiency of unidirectional operation at the same

amount of diavolumes. The dependence of the buffer exchange efficiency on the feed flow rate seems to be counter-intuitive on first sight. Assuming the same flow patterns in case of a constant ratio between Q_{DF} and Q_F (same diavolumes) one could expect a constant degree of buffer exchange, despite the higher absolute flow rates. However, the experimental as well as the simulation results show a clearly improved efficiency if higher flow rates are applied at the same switching intervals. The explanation for this behavior can be found in the fact that a higher Q_{DF} shortens the period which is required to flush out residual salt in the lateral part after switching. In first approximation it can be assumed that doubling Q_{DF} will cut the time approximately in half. If this assumption holds, the buffer exchange efficiency of an experiment Q_F = 0.25 ml/min and 400 s switching interval should be the same than in case of Q_F = 0.5 ml/min and 200 s. As can be seen in Fig 7.3, this is nearly the case, in the simulation as well as in the experiment. Overall, the comparison between the experimental and simulated data shows that the developed FEM model is able to reliably predict the hydrodynamic behavior of our diafiltration module in case the dissolved substances are able to freely pass the membranes. In the next section, the model will be extended to the case that the feed also contains macromolecules being retained by the membranes.

7.3.2 Concentration polarization and pressure build-up

In the above section it was shown, that in the absence of any retained macromolecules and under the assumption of a constant number of diavolumes applied, increasing feed flow rates would result in increasing buffer exchange efficiencies for a given switching interval of the flow direction of DF buffer. However, in the presence of macromolecules such as BSA, the applicable feed and DF buffer flows are limited by the maximum pressure the diafiltration module can tolerate. Therefore, a realistic model of the device must be able to predict the effects of concentration polarization of retained macromolecules, especially the resulting pressure build-up.

7.3.2.1 Simulated time course of BSA concentration within the module

Fig. 7.4 shows the simulated time course of the BSA concentration profiles, again in the period between 170s and 370 s for an experiment having a switching interval of 180 s. Because our model assumes a complete retention of BSA by the membranes, BSA concentration profiles only differ from zero in the middle part of the module. The single plots show snapshots of the contour of the BSA concentration for t = 170 s, 180 s, … 370 s. Consequently, the plots show the contour shortly before the first switching event and for the time period between the first and the second switching event. During these times, the operation of the module has not reached a quasi-stationary state and

the plots show the situation when the BSA concentration profiles propagate through the module. Comparable plots of BSA concentration contours in quasi-stationary operation can be found in the SI Fig. S7.5. In the plot at 170 s it can be seen that the DF buffer flow pointing from the upper lateral part of the module towards the lower lateral part pushes BSA towards the lower membrane in the inlet region of the middle part. However, in contrast to the behavior of salt discussed in Fig. 7.3, BSA cannot penetrate the UF membrane. Therefore, a rapid accumulation of BSA and a corresponding concentration polarization is predicted by the model (details see in SI Fig. S7.6). In case of constant operation conditions with unidirectional flow of DF buffer through the membranes, the concentrated BSA layer would slowly propagate through the module until its end reaches the effluent of the middle part and a stationary state is reached.

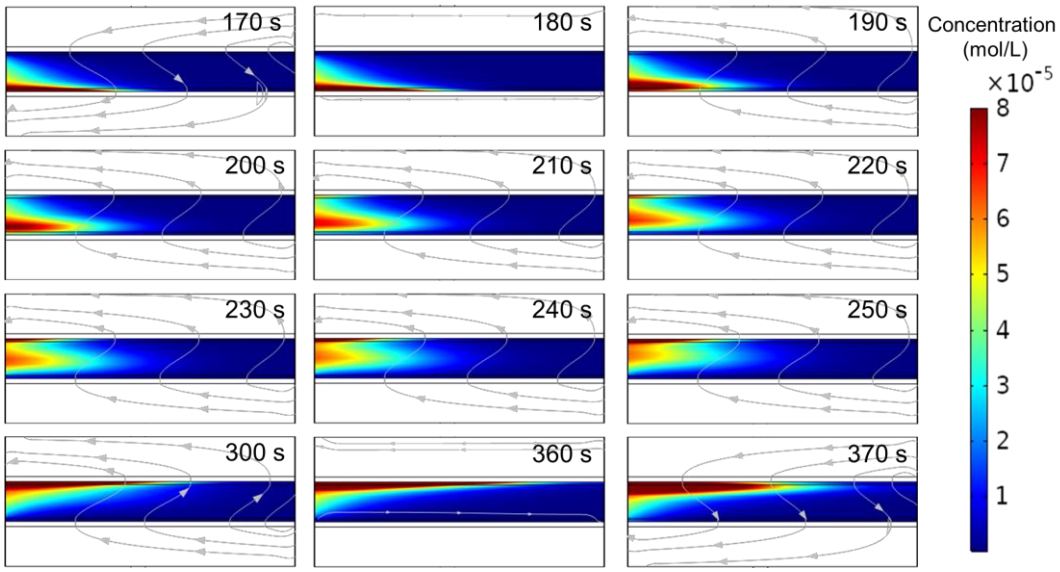

Fig. 7.4 Representative protein BSA concentration profiles in the module before and after switching the flow direction of DF buffer applying BSA ($c_{F,\,BSA}$ = 5 g/L) and salt ($c_{F,\,salt}$ = 100 mol/m³) in the feed stream. The modeling is simulated under the identical parameter settings as in section 3.1.1. The colorful surface and gray streamline represent the BSA concentration distribution and flow direction, respectively.

However, in the presented case, the direction of DF buffer flow is abruptly changed at 180 s. In the following snapshots taken at 10 s intervals it shows that the accumulated BSA layer detaches from the lower membrane and, driven by the vertical component of the DF buffer flow, slowly moves towards the upper membrane. In addition, while passing the central region of the module, the liquid compartments with highly concentrated BSA are also moved in positive x-direction towards the effluent of the middle part. Finally, because of dispersion effects, the concentrated region also

starts to blur. However, when the ‘bubble’ of concentrated BSA hits the upper membrane the accumulation and concentration polarization quickly restore and about 120 s after the switching a new, almost stationary concentration profile is obtained which slowly propagates towards the effluent. It is obvious, that the duration of the intermediate state, represented by the concentrated bubble moving vertically through the module, depends on the flow rate of DF buffer. Looking at the progression of the simulated pressure in the middle part of the module during the operation phase it shows that the formation of an accumulation layer of BSA is accompanied by a rapid increase of the pressure (Fig. S7.7). However, each switching event results in an almost instantaneous drop of the pressure towards the level caused by the flux of pure DF buffer through the membrane. In the following interval, the pressure recovers because of the renewed BSA accumulation on the opposite membrane until the increase is stopped by a new switching event. If switching is omitted, the pressure increases up to a plateau value (see Fig. S7.8). This situation corresponds with a stationary accumulation and concentration polarization profile in the module. In case of a conventional ‘constant pressure’ operation of an UF module, the formation of a highly concentrated accumulation layer at the membrane decreases the permeate flux through the membrane. However, in the developed system all flow rates are kept constant by the application of high-pressure double piston pumps guaranteeing a constant flow also in case of increased back pressures. After a switching event, the concentrated BSA is pushed back into the retentate and subsequently a part of it builds up on the opposite membrane while the other part appears in the effluent of the retentate. This explains the wave-like trend of the effluent concentration of BSA observed in the experiments (see Fig. S7.6 and the respective graphs in [17]).

7.3.2.2 Model validation

All simulations were conducted applying pure diafiltration, saying the retentate flow rate was exactly matching the feed flow rate, resulting in the average concentration of BSA in the effluent being the same than the one in the feed, when the system reaches its quasi-stationary state. Therefore, for validation it is more useful to compare the simulated and experimental results of the maximum pressure built-up caused by the accumulated BSA. The maximum pressure occurring during quasi-stationary operation is also of high practical interest, because in order to guarantee a reliable operation of our 3D-printed diafiltration system, the pressures in all parts of the module must not exceed a pressure limit of 3 bar. This limitation is comparable to the recommended pressure limits of many UF processes for proteins, because transmembrane pressures above 2 - 3 bar normally do not result in higher permeate fluxes [13,29,30]. When

investigating the observed pressures, the special structure of our system with two membranes must be considered. Assuming the flow direction of DF buffer from top to bottom, the different pressures in the module can be defined as illustrated in Fig. 7.5[2].

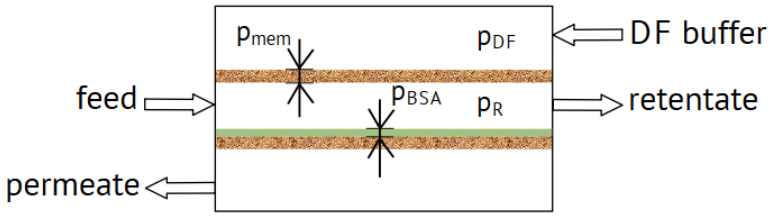

Fig. 7.5 Schematic of pressures in each part of the module. For a given flux of DF buffer the pressure drop of the membrane p_{mem} is a constant value determined by the intrinsic properties of membrane.

Soon after the accumulation layer starts to form, the pressure in the middle part is mainly related to the concentrated BSA at the membrane surface. In addition, the pressure drops caused by the permeate passing the lower membrane adds to the total transmembrane pressure between the middle and the lower lateral part of the module. In contrast, the transmembrane pressure between the upper lateral part and the middle part is only caused by the DF buffer passing the upper membrane. Because the upper and lower membranes are identical and the additional salt in the permeate does not have a significant influence on the permeability, the pressure drop of the membrane itself (p_{mem}) is the same for both membranes. Therefore, the transmembrane pressures can be calculated by equation (7.11) and (7.12).

$$TMP_{upper} = p_{mem} = p_{DF} - p_R \tag{7.11}$$

$$TMP_{lower} = p_R = p_{BSA} + p_{mem} \tag{7.12}$$

By substituting equation (7.12) into equation (7.11) one obtains:

$$p_{DF} = p_{BSA} + 2 * p_{mem} \tag{7.13}$$

This shows that the pressure required to pump the DF buffer into the module is defining the maximum load onto the 3D-printed material and therefore is used for the comparison. Fig. 7.6 shows the maximum experimental and simulated values of p_{DF} for two different feed flow rates and various switching intervals. All experiments and simulations were conducted at a constant value of 7.2 diavolumes and a concentration of BSA in the feed of 5 g/L. While for the higher flow rates the simulated pressures

[2] As it is common praxis, we us the expression 'pressure' in the sense of pressure difference against the ambient pressure of 1 bar. Because there is no restrictor valve in the permeate effluent, the pressure in this part of the module is assumed to be zero and the TMP of the lower membrane reduces to P_R.

reach up to more than 7 bar, the experimental data had to be restricted to values slightly higher than the mentioned limit of 3 bar. As can be expected, higher feed flow rates but also longer switching intervals result in higher values of $p_{DF,max}$. The slope of the increase of $p_{DF,max}$ is steeper in case of Q_F = 0.5 ml/min (10.1 LMH) than in case of 0.25 ml/min (5.05 LMH). However, looking e.g. at the relative difference of $p_{DF,max}$ between t_S = 200 s and 400 s, it shows that both curves increased by about the same factor of two. In order to obtain a quantitative prediction of the pressure, the relation between the viscosity and the BSA concentration in the accumulation layer at the membrane surface had to be fitted once. However, thereafter all simulated results have been obtained with the following correlation:

$$\mu = 1 \cdot 10^{-3} Pa \cdot s + 3.39 \cdot 10^{7} Pa \cdot s \times \left(\frac{c_{BSA}}{c_{BSA,max}}\right)^2 \quad (7.14)$$

The parameter $c_{BSA,max}$ was set to 6.9 mol/m^3 (460 g/L), which was reported to be the gelling point of BSA [21]. It should be mentioned that the correlation between viscosity and BSA concentration of this fit is orders of magnitude larger than the relationship experimentally measured for bulk BSA solutions of different concentrations [31–33]. This shows that the real effects causing a strong pressure increase because of BSA accumulating at the membrane surface are much more complex than our simple picture of viscosity increase in a porous boundary layer. Nevertheless, after fitting once, our model is able to predict the dependence of the dynamic pressure built-up onto different operation parameters to a satisfying degree, as can been seen by a comparison of the simulated (filled cycles) and experimental (open cycles) values in Fig. 7.6. Note that $p_{DF,max}$ was lower than the allowed pressure limit for all tested switching intervals at Q_F = 0.25 ml/min. When doubling Q_F to 0.5 ml/min the simulated values of $p_{DF,max}$ reached up to more than 7 bar for t_S = 600 s, however, when choosing a switching interval of around 180 s, the exceeding of the pressure limit could be avoided. This shows, that on the one hand, the new operation mode with alternating direction of the DF buffer flow through the membranes allows to operate the system at feed flow rates which, without switching, would quickly exceed the allowed pressure limits. On the other hand, as seen in Fig. 7.3 short switching intervals clearly deteriorate the achievable diafiltration efficiency. The question if there exists an optimum set of Q_F and t_S-values will be investigated more deeply in section 7.3.3.2.

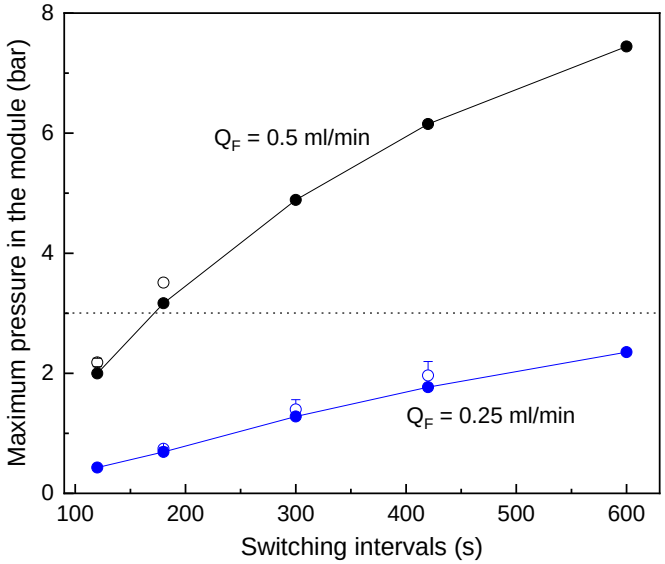

Fig. 7.6 Effect of the duration of the switching interval for on the maximum pressure built-up in the developed diafiltration module. $c_{F,BSA}$ = 7.52·10^{-2} mol/m³ (5 g/L), DV = 7.2, Q_F = 0.25 ml/min and 0.5 ml/min, respectively. The dotted line at $p_{DF,max}$ = 3 bar marks the pressure limit of the module. Open symbols: experimental values, filled symbols: simulated values. Error bars are equal to ± standard deviation, the error bar for switching interval 180 s at Q_F = 0.25 ml/min is within the size of the symbol.

7.3.3 Model based parameter screening

7.3.3.1 Unidirectional DF buffer flow

From the data presented in Fig. 7.3 it became obvious that the highest degrees of buffer exchange are obtained for the longest switching intervals. Consequently, it is worth to investigate the case with no switching events, synonymous to infinitely long switching intervals, in more detail. As shown in Fig. 7.6, long switching intervals in combination with the presence of BSA in the feed stream can quickly lead to the pressure limit being exceeded. Therefore, it is interesting to screen for parameter combinations Q_F, $c_{F,BSA}$, DV at which the final maximum pressure $p_{DF,max}$, obtained without switching the flow direction of the DF buffer, just approaches the allowed pressure limit. In order to speed-up this screening process, we extracted a semi-empirical correlation from the complete set of experimental data (see SI Fig. S7.10 in the supporting information). The multi-parameter correlation describes a relation between the maximum pressure $p_{DF,max}$ and the parameters $c_{F,BSA}$, Q_F, Q_{DF}, as well as t_S. Evaluating this correlation for $t_S \rightarrow \infty$ allows to quickly find suitable starting parameters for the precise screening using the COMSOL model.

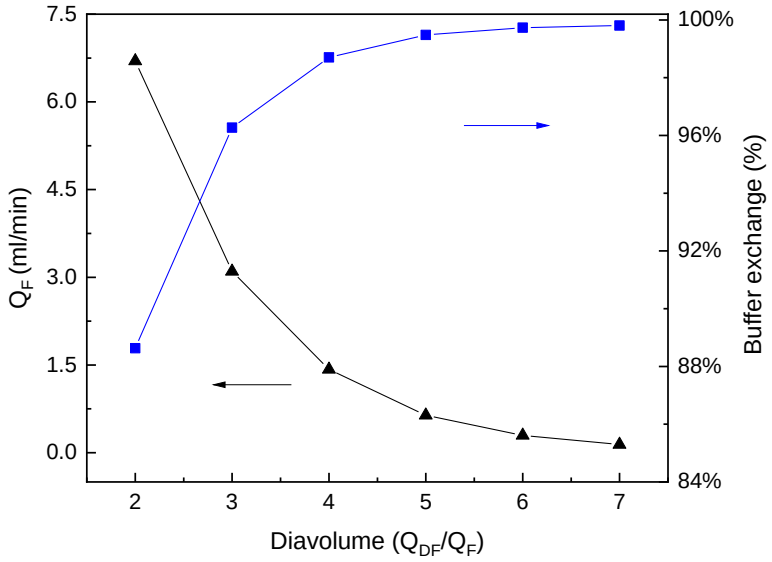

Fig. 7.7 Effect of the used amount of diavolumes on the maximum feed flow rate Q_F applicable without exceeding the pressure limit of $p_{DF,max}$ = 3 bar. On the right y-axis the corresponding degree of buffer exchange is plotted. The simulated feed solution contains 5 g/L BSA and 100 mol/m³ salt.

As mentioned, the boundary conditions of this first parameter study were to find parameter combinations Q_F, DV which approach the pressure limit of 3 bar when applying the non-switching diafiltration mode (see Fig. 7.7). There are two ways to interpret the presented curves. First, one can start with a given feed flux at the left y-axis. Then the black line with the filled triangles will give the maximum number of diavolumes, corresponding with the maximum applicable Q_{DF}, which is allowed without exceeding the pressure limit. In case of Q_F = 1.5 ml/min this number is approx. four diavolumes. Knowing DV the blue line together with the right y-axis will tell the degree of buffer exchange which can be expected for our module and the given feed concentration of BSA. In our example, this would be a buffer exchange of approx. 98.5%. The second way to interpret the Figure is to start with a desired buffer exchange efficiency on the right y-axis. The blue line then tells the required amount of diavolumes, and with this the black line in combination with the left y-axis shows the maximum Q_F possible. For example, a requested buffer exchange of 96% requires approx. 3 diavolumes, and allows a maximum Q_F of approx. 3 ml/min. When the applied Q_F is lower than this maximum Q_F, the resulting final pressure will be lower than the pressure limit (see Fig. S7.8).

7.3.3.2 Switching flow direction of DF buffer

Fig. 7.6 shows that by introducing an alternating flow direction of the DF buffer, the maximum pressure built-up in the module can be restricted. The shorter the intervals

between the switching events, the lower is the maximum pressure obtained during operation. Therefore, for a given Q_F the application of an alternating DF buffer direction will allow to apply higher values of Q_{DF} than in the case of unidirectional DF buffer flow, without exceed the pressure limit. Higher ratios of Q_{DF}/Q_F correspond to a higher number of diavolumes. Therefore, on the one hand one could expect that the application of the switching mode will enable to reach higher diafiltration efficiencies for a given Q_F, while staying within the given pressure limits. On the other hand, Fig. 7.3 clearly shows the negative influence of frequent switches of the DF buffer direction onto the diafiltration efficiency. In order to answer the question if these opposing effects will result in an optimum switching interval with optimal diafiltration efficiency we extended our parameter study to cases with various Q_F, DV, and t_S values. Fig. 7.8A indicates the switching interval required in order to obtain a certain number of diavolumes (DV) for a given feed flow rate Q_F without exceed the pressure limit. In order to allow comparability to other UF/DF modules, we plotted the feed flux, saying the feed flow rates related to the effective membrane area, of our module on the x-axis, with an absolute Q_F value of 0.5 ml/min corresponding to Q_F/A = 10.1 LMH. The vertical lines mark the Q_F/A values below which no switching is required for a certain DV. E.g. in case of a requested DV of 5, no switching is required if Q_F/A values below 13 LMH are applied. However, if this value is exceeded, the blue line indicates the switching intervals that must be applied to guarantee that the pressure limit is not surpassed. Therefore, in case of 20 LMH and DV = 5 a switching interval of approx. 180 s is required. Looking at the feed flux numbers one has to be aware, that in the case of our module the feed flux is decoupled from the permeate flux which physically flows through the membrane. In conventional diafiltration, the permeate flux is only a fraction of the feed flux, getting close to one in its maximum. In contrast, in the presented diafiltration module, the permeate flux is related to the independently applied flow rate of DF buffer. For example, in case of DV = 5, the permeate flux which has to penetrate the membrane is five times the feed flux Q_F/A.

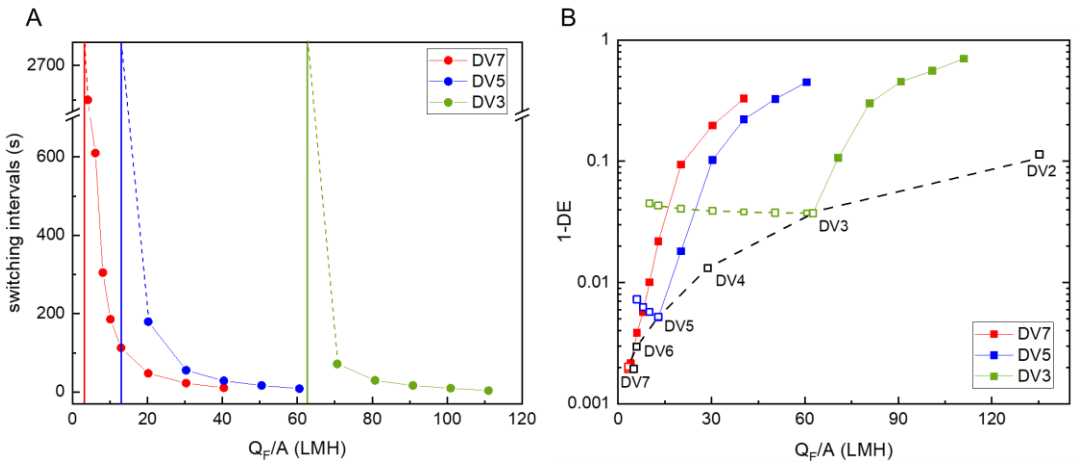

Fig. 7.8 Required switching intervals in dependence of the applied feed flux (Q_F/A) and the number of diavolumes. When the feed flux is lower than the vertical line, the operating mode changes from switching to unidirectional DF buffer flow; B. Simulated buffer exchange efficiency applying various feed fluxes, switching intervals, diavolumes and operation modes. In all cases the concentration of BSA in the feed stream was fixed at 5 g/L. The filled symbols correspond to the operation mode with switching direction of the DF buffer flow, the open symbols correspond to the operation mode with unidirectional DF buffer flow.

The stated feed flux therefore corresponds to the amount of original feed solution which can be treated by the module per time, while the physical flux impinged to the membrane is several times higher. Fig. 7.8B shows the predicted diafiltration efficiencies (DE) for multiple simulation runs with constant $c_{F,BSA}$ = 5 g/L and $p_{DF,max}$ = 3 bar but various parameter sets for Q_F, DV and t_S. In order to get a detailed picture of the system behavior at high diafiltration efficiencies, the values of 1-DE are plotted in a logarithmic scale on the y-axis. This value can also be looked at as the fraction of the original buffer in the feed remaining in the retentate. Therefore, low numbers of 1-DE are equivalent to high diafiltration efficiencies. The black dashed line results for the limiting case of unidirectional flow of DF buffer and therefore corresponds to the blue line in Fig. 7.7. Starting from this boundary, the lines with fully colored square symbols show the predicted diafiltration efficiencies for decreasing switching intervals t_S but a constant number of diavolumes. In accordance to Fig. 7.8A, decreasing switching intervals allow higher Q_F values for a given maximum pressure. However, they also result in lower diafiltration efficiencies, corresponding to higher 1-DE values. In case of the lines for DV = 3 and DV = 5 the plot also shows the calculated 1-DE values if Q_F values smaller than the limiting value for unidirectional DF buffer flow are applied. The respective results are indicated by open squares, because the conditions of these runs differ in a way that the achieved maximum pressure is below the limiting pressure. From the calculations with unidirectional DF buffer flow it can be seen, that when

keeping DV constant, a reduction of Q_F does not improve diafiltration efficiency. Instead, the obtained DE values show a slightly decreasing trend (increasing 1-DE), which may be caused by the decreasing dispersion coefficient in the y-direction. However, the question if the introduction of a periodic switch of the direction of DF buffer flow can improve DE is of higher relevance for this work. As explained, the period switch allows higher fluxes through the membranes. This can be used to increase Q_F and keep DV constant, as in case of the colored lines with filled squares, but also to keep Q_F constant and increase DV. In the Figure, keeping Q_F constant is equivalent to moving along a vertical line defined by a given Q_F value. For example, one could start at the point where the blue line meets the black dashed line (DV = 5, unidirectional DF buffer flow, $Q_F/A \approx 15$ LMH) and move vertically until the intersection with the red line for DV = 7. This means, by introducing a periodic switching of the direction of DF buffer flow, one can increase the number of applied diavolumes from 5 to 7, while keeping Q_F/A and the maximum pressure constant. However, in order to meet the red line one has to move upwards in the Figure, showing that the diafiltration efficiency decreases despite the increased number of DV. In order to obtain a better DE in case of the switching mode, the slope of a line with constant DV would have to be lower than the slope of the black dashed line. From Fig. 7.8B it becomes obvious that, at least in the investigated parameter range, this is never the case. Therefore, with respect to the achievable DE, unidirectional flow of the DF buffer without any switching events is the optimum way of operation.

In Fig. 7.9, the simulated buffer exchange efficiency of our system is compared to different designs of single pass diafiltration systems reported in the literature. These include dialysis modules [34] as well as multistage continuous countercurrent diafiltration [35]. In addition, the black dash dot line indicates the diafiltration efficiency predicted by the well-known equation of constant volume diafiltration in a conventional TFF system [36]. As shown by Tan and Franzreb [37], the same correlation between the applied diavolumes and the resulting dilution efficiency holds for the investigated module with two membranes if one assumes pure plug flow in all parts of the module and neglects the effects of dispersion. Looking at the red line in Fig. 7.9, displaying the results of the COMSOL simulations for the operation mode with unidirectional DF buffer flow, it shows that up to the application of approx. five diavolumes, the diafiltration efficiency is slightly better than the estimation based on the simplified assumption of pure plug flow. However, both lines follow the same linear trend in this plot using a logarithmic scale on the y-axis.

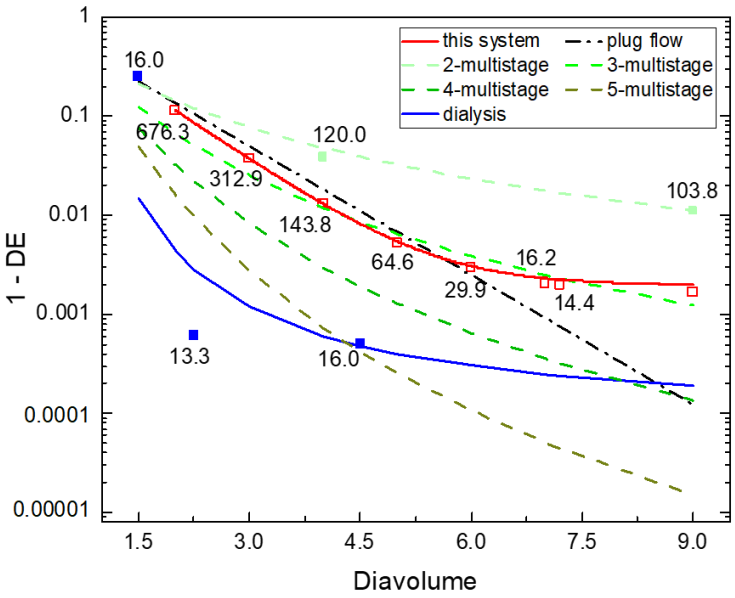

Fig. 7.9 Effect of the number of diavolumes applied on the achieved degree of buffer exchange for different continuous diafiltration processes. Values beside the symbols indicate the corresponding protein load per membrane area, e.g. expressed in g/(m² h). Open symbol: simulated value, filled symbol: experimental value.

At first sight, it may be surprising that the predictions of the detailed simulation of our module accounting for diffusion/dispersion effects could exceed the predicted diafiltration efficiencies of an idealized model which accounts for convections mass transport only. However, in case of a counter-current operation dispersion effects perpendicular to the flow direction can be advantageous. An impressive confirmation of this assumption is given by the blue trend line, which shows the predicted dilution efficiencies in case of pure dialysis operated in counter-current mode [34]. Although, in the used hollow-fiber dialysis module the transport of salt across the membrane is driven by diffusion only, even low numbers of diavolumes can achieve high dilution efficiencies, albeit at very low surface loads of the module. The trend that systems operated in counter-current mode can surpass the dilution efficiency of conventional constant volume diafiltration at the same number of diavolumes can also be seen for the plotted lines representing multistage continuous countercurrent diafiltration [24]. However, it requires at least three stages to match the performance of our single module or constant volume diafiltration. Beyond approx. six diavolumes all systems applying counter-current operation show the trend, that the increase in diafiltration efficiency with increasing diavolumes starts to level off. For an evaluation of the efficiency of a diafiltration system, the applicable protein load per membrane area, e.g. expressed in g/(m^2 h), is an important aspect in addition to the dilution efficiency. Therefore, we added exemplary numbers of the predicted load for our module as well

as for diafiltration experiments reported in the stated literature. Comparing, e.g. the predicted and reported loads at around four diavolumes, it shows that our system could handle about the same protein load per membrane area as the two-stage counter-current SPTFF setup, however at a better dilution efficiency. The dialysis system achieves even better dilution efficiencies, however, at the expense of protein loads which are around an order of magnitude lower. If dilution efficiencies beyond 99% are required, the simulation predicts a relatively sharp decrease of the permitted protein load of our module, dropping below 20 g/(m^2 h) beyond approx. 6.5 diavolumes.

7.4 Conclusion and outlook

In this work, a 2D finite element model of our recently developed SPTFF module for continuous diafiltration was developed. The unconventional module contains two membranes allowing a simultaneous withdrawal of permeate and delivery of fresh DF buffer, throughout the whole flow path of the retentate. The module allows a unidirectional flow of DF buffer through the membrane as well as an operation mode applying an alternating flow direction of DF buffer, switching periodically at certain intervals. Especially, the second operation mode results in a complex hydrodynamic behavior and dynamically changing concentration profiles within the module. The purpose of the model was to predict the diafiltration efficiency in dependence of various operation parameters and to elucidate the dynamic concentration polarization and pressure built-up phenomena. Different from common UF models often applying a resistance-in-series approach, a porous boundary layer above the membrane was introduced, where accumulated macromolecules, such as proteins, result in an increased pressure drop when a convective flow is forced through the boundary layer. A direct correlation between the protein concentration and the resulting pressure drop is achieved by introducing a hypothetical viscosity. The dependence of this hypothetical viscosity on the protein concentration is purely empirical, however, after fitting once to the experimental results, the fixed correlation is able to predict the dynamic pressure within the module at good accuracy for various conditions. Besides the simulated pressures, also the simulated diafiltration efficiencies are in good accordance to the experimental results. The results show that for a fixed number of diavolumes longer intervals between switch the flow direction of the DF buffer correspond to higher diafiltration efficiencies. Therefore, on the one hand frequent switching is detrimental to the performance of module, on the other hand it limits the pressure-built and allows higher flow rates of DF buffer without exceeding the pressure limit of the system. A thorough, computer-based analysis of this antagonistic effects

showed that, at least within the investigated parameter range, the first effect prevails and the module achieves its best performance in case of unidirectional DF buffer flow. While from a scientific view it may have been more interesting if an optimum would exist for dynamic alternating conditions, the operation with unidirectional flow strongly simplifies the setup and control of the new SPTFF module, thus increasing its commercial potential. As illustrated in the comparison with other setups for continuous diafiltration, the presented single module approaches the diafiltration efficiency of a counter-current multistage setup applying three conventional SPTFF modules. Although, in this work the protein concentration in the feed was increased to 5 g/L, the applicability of the new SPTFF module for significantly higher protein concentrations remains a question, which must be investigated experimentally in further studies. Nevertheless, extrapolating our model to higher proteins concentrations the simulations predict that also the allowable protein loads per membrane area should be comparable to the ones obtained in counter-current multistage setups.

Reference

[1] C. Gavazzi-April, S. Benoit, A. Doyen, M. Britten, Y. Pouliot, Preparation of milk protein concentrates by ultrafiltration and continuous diafiltration: Effect of process design on overall efficiency, J. Dairy Sci. 101 (2018) 9670–9679. https://doi.org/10.3168/jds.2018-14430.

[2] C. Casey, T. Gallos, Y. Alekseev, E. Ayturk, S. Pearl, Protein concentration with single-pass tangential flow filtration (SPTFF), J. Memb. Sci. 384 (2011) 82–88. https://doi.org/10.1016/j.memsci.2011.09.004.

[3] E. Iritani, Y. Mukai, E. Hagihara, Measurements and evaluation of concentration distributions in filter cake formed in dead-end ultrafiltration of protein solutions, Chem. Eng. Sci. 57 (2002) 53–62. https://doi.org/10.1016/S0009-2509(01)00362-1.

[4] S.P. Agashichev, Modelling temperature and concentration polarization phenomena in ultrafiltration of non-newtonian fluids under non-isothermal conditions, Sep. Purif. Technol. 25 (2001) 355–368. https://doi.org/10.1016/S1383-5866(01)00063-6.

[5] C. Sharma, D. Malhotra, A.S. Rathore, Review of computational fluid dynamics applications in biotechnology processes, Biotechnol. Prog. 27 (2011). https://doi.org/10.1002/btpr.689.

[6] R. Wu, K. Su, Z. Wang, T. Hao, S. Liu, A comprehensive investigation of filtration performance in submerged hollow fibre membrane modules with different fibre geometries, Sep. Purif. Technol. 221 (2019) 93–100. https://doi.org/10.1016/j.seppur.2019.03.082.

[7] A. Reza, C. Moresoli, B. Marcos, Fouling behavior of electroacidified soy protein extracts during cross-flow ultrafiltration using dynamic reversible – irreversible fouling resistances and CFD modeling, J. Memb. Sci. 361 (2010) 191–205. https://doi.org/10.1016/j.memsci.2010.05.057.

[8] J. Fernández-Sempere, F. Ruiz-Beviá, P. García-Algado, R. Salcedo-Díaz, Visualization and modelling of the polarization layer and a reversible adsorption process in PEG-10000 dead-end ultrafiltration, J. Memb. Sci. 342 (2009) 279–290. https://doi.org/10.1016/j.memsci.2009.06.046.

[9] T. Chaabane, S. Taha, M. Taleb Ahmed, R. Maachi, G. Dorange, Coupled model of film theory and the Nernst-Planck equation in nanofiltration, Desalination. 206 (2007) 424–432. https://doi.org/10.1016/j.desal.2006.03.577.

[10] W.C. McGregor, Membrane Separations in Biotechnology, Marcel Dekker Inc., New York, 1986.

[11] E. Iritani, N. Katagiri, Developments of blocking filtration model in membrane filtration, KONA Powder Part. J. 2016 (2016) 179–202. https://doi.org/10.14356/kona.2016024.

[12] I.M. Griffiths, A. Kumar, P.S. Stewart, A combined network model for membrane fouling, J. Colloid Interface Sci. 432 (2014) 10–18. https://doi.org/10.1016/j.jcis.2014.06.021.

[13] A.R. Rajabzadeh, C. Moresoli, B. Marcos, Fouling behavior of electroacidified soy protein extracts during cross-flow ultrafiltration using dynamic reversible-irreversible fouling resistances and CFD modeling, J. Memb. Sci. 361 (2010) 191–205. https://doi.org/10.1016/j.memsci.2010.05.057.

[14] C. Casey, T. Gallos, Y. Alekseev, E. Ayturk, S. Pearl, Protein concentration with single-pass tangential flow filtration (SPTFF), J. Memb. Sci. 384 (2011) 82–88. https://doi.org/10.1016/j.memsci.2011.09.004.

[15] J. Dizon-Maspat, J. Bourret, A. D'Agostini, F. Li, Single pass tangential flow filtration to debottleneck downstream processing for therapeutic antibody production, Biotechnol. Bioeng. 109 (2012) 962–970. https://doi.org/10.1002/bit.24377.

[16] T. Elich, E. Goodrich, H. Lutz, U. Mehta, Investigating the combination of single-pass tangential flow filtration and anion exchange chromatography for intensified mAb polishing, Biotechnol. Prog. 35 (2019). https://doi.org/10.1002/btpr.2862.

[17] R. Tan, F. Hezel, M. Franzreb, Continuous single pass diafiltration with alternating permeate flow direction for high efficiency buffer exchange, J. Memb. Sci. 619 (2021) 118695. https://doi.org/10.1016/j.memsci.2020.118695.

[18] M. Haribabu, D.E. Dunstan, G.J.O. Martin, M.R. Davidson, J. Dalton, E. Harvie, Simulating the ultrafiltration of whey proteins isolate using a mixture model, J. Memb. Sci. 613 (2020) 118388. https://doi.org/10.1016/j.memsci.2020.118388.

[19] R. Ghosh, Study of membrane fouling by BSA using pulsed injection technique, J. Memb. Sci. 195 (2002) 115–123. https://doi.org/10.1016/S0376-7388(01)00550-6.

[20] V. Aguirre-Montesdeoca, A.E.M. Janssen, A. Van der Padt, R.M. Boom, Modelling ultrafiltration performance by integrating local (critical) fluxes along the membrane length, J. Memb. Sci. 578 (2019) 111–125. https://doi.org/10.1016/j.memsci.2019.02.040.

[21] P. Schausberger, N. Norazman, H. Li, V. Chen, A. Friedl, Simulation of protein ultrafiltration using CFD: Comparison of concentration polarisation and fouling effects with filtration and protein adsorption experiments, J. Memb. Sci. 337 (2009) 1–8. https://doi.org/10.1016/j.memsci.2009.03.022.

[22] B. Marcos, C. Moresoli, J. Skorepova, B. Vaughan, CFD modeling of a transient hollow fiber ultrafiltration system for protein concentration, J. Memb. Sci. 337 (2009) 136–144. https://doi.org/10.1016/j.memsci.2009.03.036.

[23] M.J. Huter, J. Strube, Model-based design and process optimization of continuous single pass tangential flow filtration focusing on continuous bioprocessing, Processes. 7 (2019). https://doi.org/10.3390/pr7060317.

[24] M.J. Huter, C. Jensch, J. Strube, Model validation and process design of continuous Single Pass Tangential Flow Filtration focusing on continuous bioprocessing for high protein concentrations, Processes. 7 (2019) 1–18. https://doi.org/10.3390/pr7110781.

[25] A. Subramani, S. Kim, E.M.V. Hoek, Pressure, flow, and concentration profiles in open and spacer-filled membrane channels, J. Memb. Sci. 277 (2006) 7–17. https://doi.org/10.1016/j.memsci.2005.10.021.

[26] D.A. Nield, A. Bejan, Convection in porous media, 2017. https://doi.org/10.1007/978-3-319-49562-0.

[27] J.P. Quirk, Permeability of porous solids, (1960).

[28] F. Chung, C.Y. Wen, Longitudinal dispersion of liquid flowing through fixed and fluidized beds, 14 (n.d.) 857–866.

[29] M.A. Monfared, N. Kasiri, A. Salahi, T. Mohammadi, CFD simulation of baffles arrangement for gelatin-water ultrafiltration in rectangular channel, Desalination. 284 (2012) 288–296. https://doi.org/10.1016/j.desal.2011.09.014.

[30] C. Gavazzi-April, S. Benoit, A. Doyen, M. Britten, Y. Pouliot, Preparation of milk protein concentrates by ultrafiltration and continuous diafiltration : Effect of process design on overall efficiency, J. Dairy Sci. 101 (2018) 9670–9679. https://doi.org/10.3168/jds.2018-14430.

[31] M.J. Huter, J. Strube, Model-based design and process optimization of continuous single pass tangential flow filtration focusing on cntinuous bioprocessing, Processes. (2019). https://doi.org/10.3390/pr7060317.

[32] W.N. Gill, D.E. Wiley, C.J.D. Fell, A.G. Fane, Effect of viscosity on concentration polarization in ultrafiltration, AIChE J. 34 (1988) 1563–1567. https://doi.org/10.1002/aic.690340919.

[33] P. Uitrafiitration, G. Example, B.L. Filtration, Protein Ultrafiltration : A general example of boundary layer filtration, 18 (n.d.) 1030–1040.

[34] C.J. Yehl, M.G. Jabra, A.L. Zydney, Hollow fiber countercurrent dialysis for continuous buffer exchange of high-value biotherapeutics, Biotechnol. Prog. 35 (2019) 1–5. https://doi.org/10.1002/btpr.2763.

[35] M.G. Jabra, C.J. Yehl, A.L. Zydney, Multistage continuous countercurrent

diafiltration for formulation of monoclonal antibodies, Biotechnol. Prog. 35 (2019) 6–11. https://doi.org/10.1002/btpr.2810.

[36] H. Lutz, Ultrafiltration for Bioprocessing, (2015) 244. https://doi.org/10.1016/B978-1-907568-46-6.00002-1.

[37] R. Tan, M. Franzreb, Continuous ultrafiltration/diafiltration using a 3D-printed two membrane single pass module, Biotechnol. Bioeng. (2019). https://doi.org/10.1002/bit.27233.

7.5 Supporting Information

Schematic structure of the developed membrane module

Fig. S7.1 shows an exploded view of the developed membrane module allowing continuous single pass diafiltration. The module consists of three 3D-printed parts (one middle part and two lateral parts) enclosing two commercial UF membranes. The lateral parts hold the flow channels for either diafiltration (DF) buffer or permeate, and the middle part provides the flow channel for feed respectively retentate. In order to increase the flow path length in a compact design, the flows are guided by U-shaped channels. All flow channels are filled by a grid structure providing a mechanical support for the membranes from both sides.

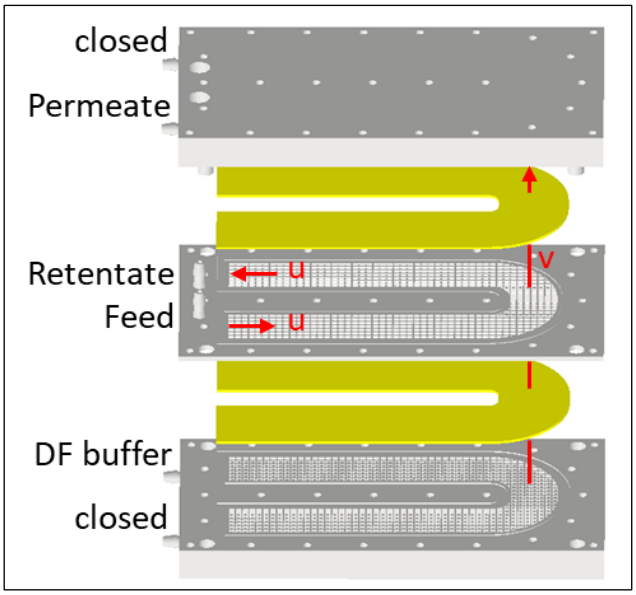

Fig. S7. 1 Exploded view of the developed membrane module. The grid structures in the middle and lateral parts provide flow channels and at the same time mechanical support for the membranes.

Piping and instrumentation diagram of the experimental setup

Fig. S7.2 shows the piping and instrumentation diagram of the experimental setup used to test the developed diafiltration module. With the double piston pumps A, B, and C, the flow rates in the system can be adjusted precisely, independently of the occurring pressures. Switching of the flow direction of DF buffer is achieved by two computer controlled multi-port valves. The system includes two pressure sensors for online monitoring of the pressures in the retentate outlet as well as the DF buffer inlet. In addition, the system allows recording of the UV-signal at 280 nm and the conductivity of the retentate.

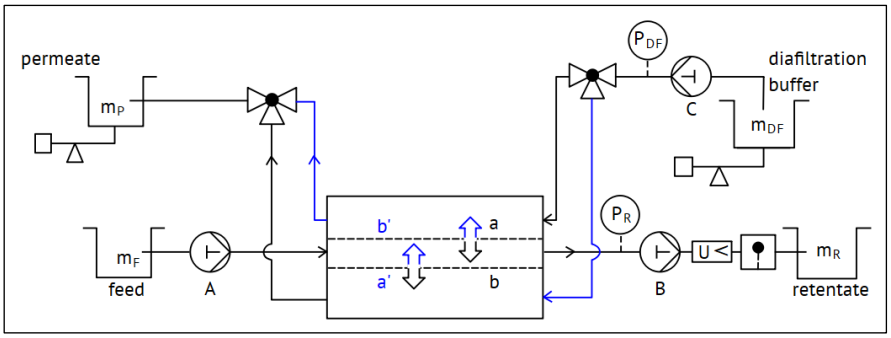

Fig. S7. 2 Piping and instrumentation diagram of the experimental setup. The direction of the flows perfusing membrane a and b could be switched by means of the multiport valves of the FPLC system. The BSA and salt concentration in the retentate were monitored in real-time by UV and conductivity sensors, respectively. Adapted from Ref. [17].

Applied FEM mesh and simulated flow pattern in the module

For the simulations a quadratic mesh with inhomogeneous meshing is used. In order to reproduce the steep concentration profiles resulting during concentration polarization a very fine mesh is used in the vicinity of the membranes (see Fig. S7.3B). Fig. S7.3A shows a typical flow pattern of the simulated runs. The flow in the middle part is constant along the module length and, due to the pressure drop caused by the grid, shows only small variations in the y-direction. The flow rate in the upper lateral part decreases from its initial value in the DF buffer inlet down to zero at the left outlet, which is closed by a valve during this period. Along the module, the DF-buffer gradually permeates through the membrane into the middle part. The same amount of fluid leaves the middle part and leads to a gradual increase of the flow rate in the lower module part along the length of the module. The simulated flow patterns also clearly show that the flow velocity in the two artificial outlets is practically zero and that the flow pattern in the lateral parts is not influenced when flowing by.

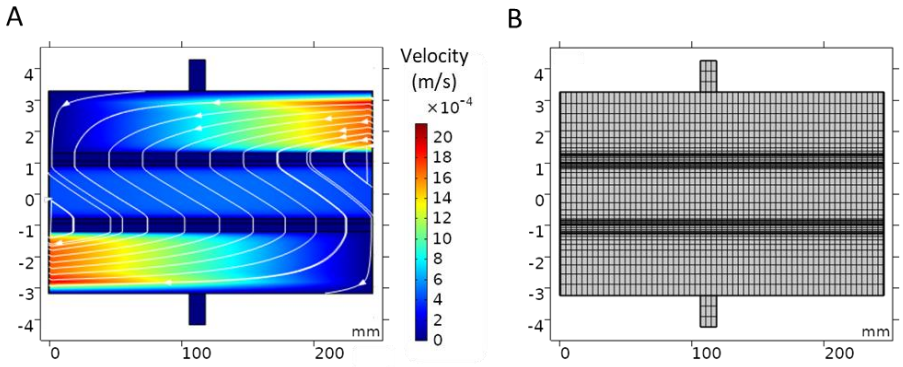

Fig. S7. 3 Flow distribution within the membrane module and the applied mesh of the FEM calculations. A. Velocity field and flow path contours when applying the DF buffer from top to bottom; B. Generated quadratic mesh with increased mesh density in the vicinity of the membranes.

Detailed view of the 3D-printed grid structure within the flow channels of the module

The flow channels are filled by a hollow-carved grid with quadratic combs. The combs allow a free fluid flow in y-direction while the flow in x-direction is diverted and splitted by staggered holes in the grid walls.

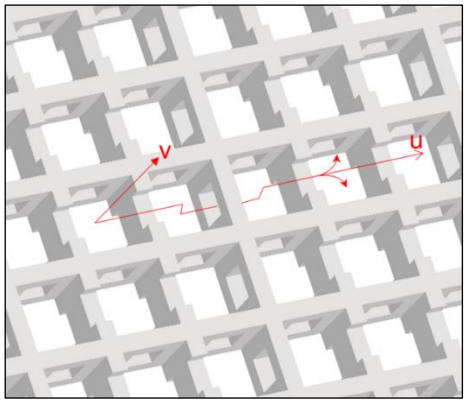

Fig. S7. 4 Close-up of the grid structure supporting the membranes in the module from both sides. The flow in y-direction is without any obstacles while the flow in x-direction results in strong eddy diffusion effects.

Typical time course of the salt concentration in the retentate effluent

The concentration of salt detected in the retentate shows a wave-like fluctuation caused by the periodic switching of the flow direction of DF buffer. In the shown example the flow direction of DF buffer was switched every 180 s at a feed flow rate of 0.25 ml/min and 7.2 diavolumes. The simulated concentration of salt in the retentate varies from about 3.5 to 5.8 mol/m³. The average concentration is about 5 mol/m³, corresponding with a diafiltration efficiency of 95%.

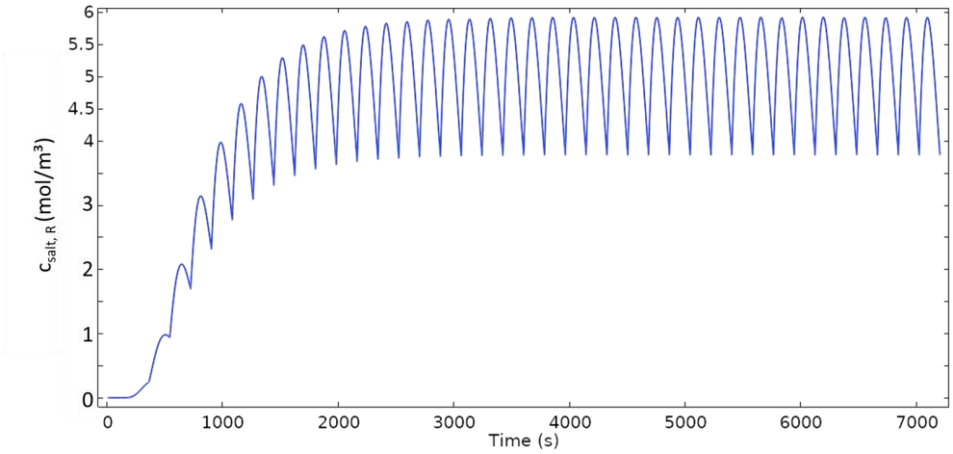

Fig. S7. 5 Periodic fluctuations of the concentration of salt in the retentate for a simulated experiment with: $c_{F,salt}$ = 100 mM, Q_{DF} = 1.8 ml/min, Q_F = 0.25 ml/min and t_S = 180 s.

Representative BSA concentration contours in the quasi-stationary status

After simulation times of about three times the fluid residence time in the middle channel, the BSA concentration in the retentate is close to the one in the feed solution because the same feed and retentate flow rates are applied. At this quasi-stationary state, the freshly accumulated BSA amount in the boundary layer at the membrane surface equals the BSA amount leaving the module in the retentate. Shortly after switching the DF buffer flow direction, BSA moves to the opposite membrane in form of a concentrated fluid compartment stretching across the whole module.

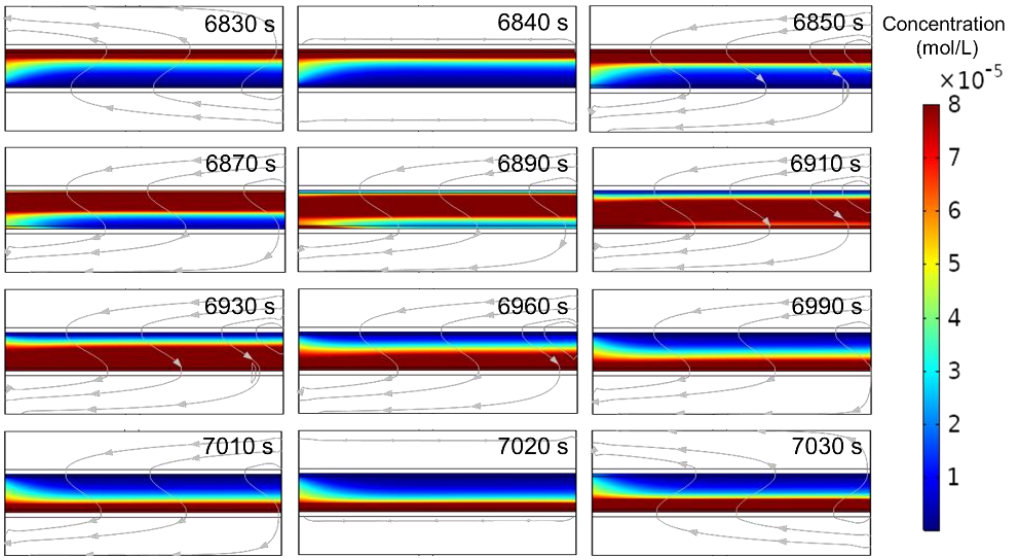

Fig. S7. 6 Representative BSA distribution in the middle channel of the module at quasi-stationary state. The module was operated at a switching interval of 180 s.

Representative BSA concentration profiles in y-direction at different membrane positions

The BSA concentration profiles in y-direction at different membrane positions (x = 5, 122.5, 240 mm) are plotted for a simulation with: $c_{F,BSA}$ = 5 g/L, Q_F = 0.25 ml/min, Q_{DF} = 1.8 ml/min and t_S = 420 s. The selected times represent the initial phase of before and after the first switching event as well as a situation when quasi-stationary state is reached. Nevertheless, also at quasi-stationary state the dynamic profiles change shortly before and after a switching event.

In the initial phase, the concentration profile at the beginning and the end of the flow channel (positions 5 and 240 mm) show a clear difference, while in quasi-stationary state BSA stretches along the x-direction almost homogenously. However, in y-direction the BSA profiles clearly show the effect of concentration polarization, accumulation BSA up to concentrations of around 160 g/L at the membrane surface.

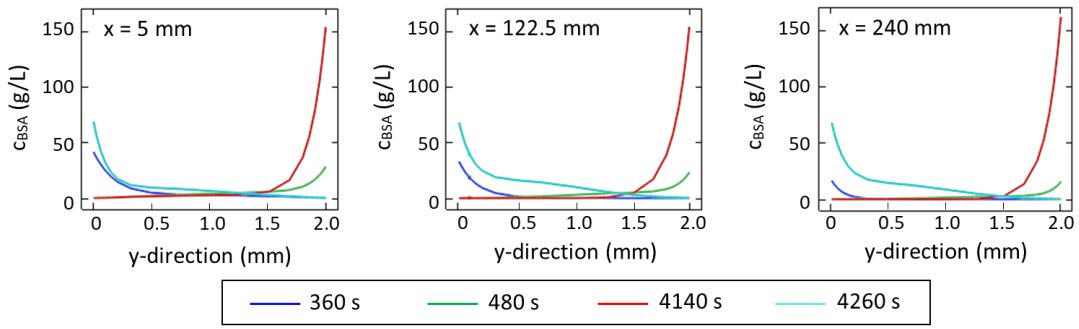

Fig. S7. 7 Concentration profiles of BSA above the membrane at different position (x = 5, 122.5, 240 mm) and different times for a simulation with: $c_{F,BSA}$ = 5 g/L, Q_F = 0.25 ml/min, Q_{DF} = 7.2 ml/min and t_S = 420s.

Time course of the pressure in the middle part of the module during a simulation with alternating flow direction of DF buffer

The pressure in the middle part increases during the period between two switching events. The pressure increase corresponds with the amount of accumulated BSA in the boundary layer above the membrane surface. When switching the flow direction of DF buffer, the pressure built-up drops abruptly and restarts the period of pressure increase at the intrinsic pressure drop of the membrane at the given flux.

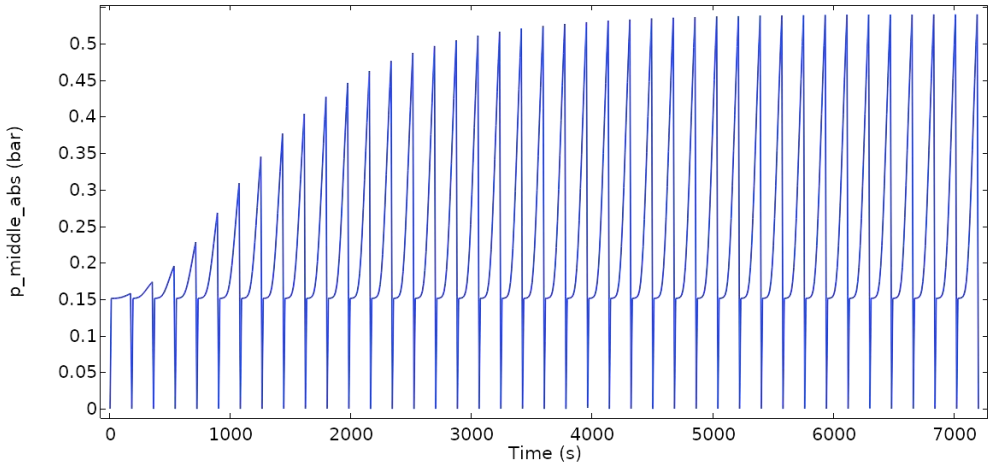

Fig. S7.8 Progression of the pressure in the middle part of the module for a simulation applying an alternating flow direction DF buffer. It was decided by the amount of the concentrated BSA at the membrane surface and the membrane area covered by the BSA, which is related to the hydrodynamic flow patterns.

Time course of the pressure in the upper module part for unidirectional DF buffer flow

In case of unidirectional DF buffer flow, the pressure in the upper module part reaches a plateau value in the course of a long-term simulation run without switching

events. All simulations shown are conducted at DV = 5, $c_{F,BSA}$ = 5 g/L, but varying feed flow rates Q_F. At higher Q_F the adjustment of the maximum pressure is achieved in a shorter time. For tangential flow filtration one may expect a reduced concentration polarization and consequently a reduced pressure built-up for higher Q_F values. However, in case of a constant number of diavolumes applied, the effect of the proportional increase of the required DF buffer flux prevails.

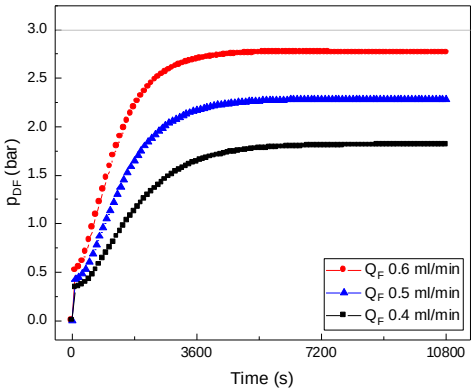

Fig. S7.9 Progression of pressure built-up in the DF buffer part with constant DV 5 at various flow rate of feed solution using unidirectional diafiltration.

Typical time course of the BSA concentration in the retentate when operating with switching DF buffer flow direction

The simulated BSA concentration in the retentate shows a wave-like fluctuation comparable to the one of salt shown in Fig. S7.5. However, a closer look reveals that due to BSA accumulation in the boundary layer, the adjustment of a quasi-stationary state requires longer times. In addition, the accumulated BSA causes stronger concentration fluctuations when the detached volume compartment including high BSA concentrations moves to the opposite membrane after a switching event.

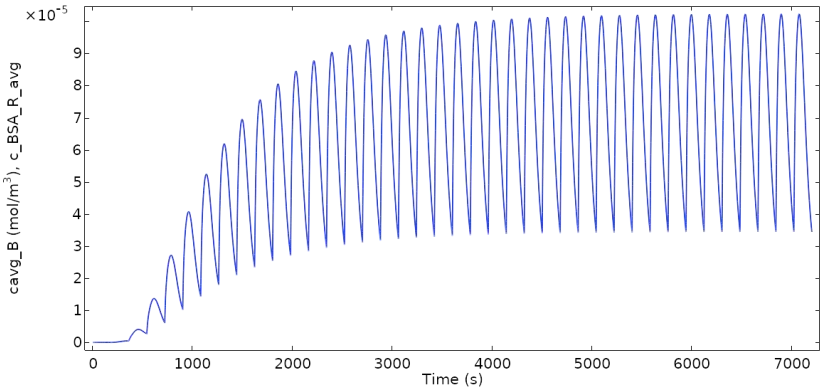

Fig. S7. 10 Periodic fluctuations of the concentration of BSA in the retentate for a simulated experiment with: $c_{F,BSA}$ = 7.5·10^{-5} mol/m^3 (5 g/L), $c_{F,salt}$ = 100 mM, Q_{DF} = 1.8 ml/min, Q_F = 0.25 ml/min and t_S = 180 s.

Semi-empirical correlation describing the maximum pressure drop in the boundary layer (p_{BSA})

The results of the maximum pressure drop p_{BSA} in the boundary layer is plotted in Fig. S7.11 for 23 experiments ranging in their operation conditions from $c_{F,BSA}$ = 0 - 5 g/L, DV = 7.2; 14.4, t_s = 120 - 420 s. In addition, the determined semi-empirical correlation is plotted. For the correlation we defined the effective mass flow rate of BSA, $\dot{N}_{BSA,eff}$, as the time weighted amount of BSA transported towards the membrane surface.

$$\dot{N}_{BSA,eff} = c_{F,BSA} \cdot Q_{DF} \cdot \frac{(Q_F \cdot t_S)^3}{2 + (Q_F \cdot t_S)^3} \quad \text{(S7.1)}$$

In this term, the first part ($c_{F,BSA} \cdot Q_{DF}$) determines the maximum value of $\dot{N}_{BSA,eff}$ and therefore also the maximum pressure drop p_{BSA} in case of unidirectional flow of the DF buffer ($t_s \rightarrow \infty$). The second term describes how much this maximum pressure drop is reduced if a switching interval of t_s is applied. Besides, the switching interval the second term depends on the feed flow rate Q_F which itself is inversely proportional to the liquid residence time in the middle part of the module. As can be seen in Fig. S7.11, the defined effective mass flow rate shows a very good correlation to p_{BSA} with a calculated R^2 of 0.977. Based on this correlation, the theoretical p_{BSA} is predictable for any assigned combination of operation parameters in the mentioned range. This means vice versa, starting with a given pressure drop p_{BSA} and fixing the operation parameters except for one, the value of the unknown parameter can be estimated.

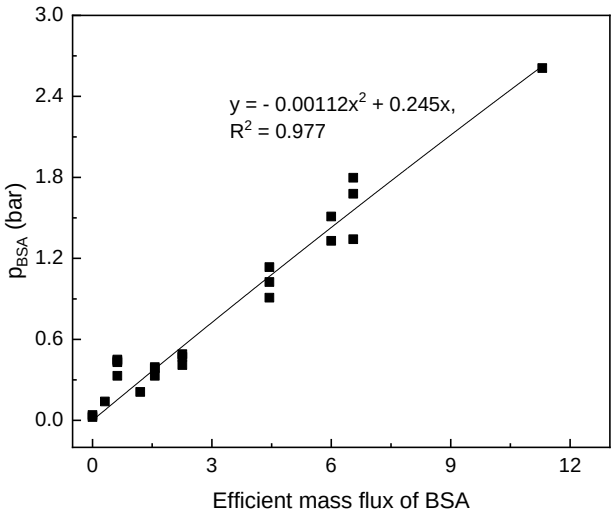

Fig. S7.11 Semi-empirical correlation between pressure between pressure drop in the boundary layer (p_{BSA}) and the effective mass flow rate of BSA.

8 Conclusions and Outlook

Single pass tangential flow filtration (SPTFF) is a promising technology to overcome currently existing hurdles in the design of continuous downstream processing schemes. It offers the possibility to increase the concentration of target biomolecules or to change the buffer composition during a single, continuous passage of the membrane module without the need for recirculation of the retentate. However, there exists the need to improve this technology by avoiding the multiple filtration and mixing units required so far for intermittent concentration and dilution steps. Accordingly, the main focus of this work was to develop and realize a truly continuous ultrafiltration/diafiltration (UF/DF) process requiring only a single membrane module for the concentration of protein solutions and the formulation of bioproducts.

In the first part of the study, a small prototype of a new type of SPTFF system consisting of two commercial UF membranes in a high-resolution 3D-printed module was designed for concentrating protein solutions. The feed-retentate channel of the module consists of a defined hollow-grid structure confined by two adjacent membranes. The fresh diafiltration buffer was pumped into the upper lateral part of the module and then penetrated the first membrane into the feed-retentate channel for buffer exchange. Simultaneously, permeate penetrates the second membrane, placed between the feed-retentate channel and the lower lateral part. At first, the relationship between the resulting water fluxes and the adjusted pressure values in the different compartments of the module was investigated in this novel system. Next, the correlation between the obtained permeate fluxes and the concentration of the model protein BSA in the feed solution was studied. Afterwards, the time for the system to reach a stationary status (such as stable concentration of BSA in the effluent and stable pressure in each compartment of the module) was determined. The proof-of-principle of simultaneous concentration and buffer exchange was given. Finally, via varying the ratio of flow rates between the feed and the retentate flows, different values of the concentration factor (CF) were obtained and the maximum CF with this system reached up to around 5-fold. When compared to the conventional UF process for biomolecule concentrating, the new module design has the advantage of that the protein solution has to pass only one pump, which is especially significant for shear and temperature sensitive proteins. Besides, the system provides the unique opportunity to continuously supply fresh diafiltration buffer through one membrane while permeate is withdrawn through the second membrane. This allows truly simultaneous ultra- and diafiltration, thus avoiding sudden changes of the conditions of the solution in which sensitive biomolecules are dissolved. Subsequently, the

membrane module was scaled-up and optimized for plain buffer exchange by continuous DF. In order to alleviate the concentration polarization (CP) phenomenon of retained BSA at the membrane surface, the direction of DF buffer and permeate perfusion through the membranes was alternated cyclically, thus realizing a process with an inherent backflush to sweep away the accumulated macromolecules. The results show that this operation mode strongly reduced the degree of CP, leading to a decreased pressure built-up in the system. As a result, a larger value of diavolumes (the flow rate ratio of fresh diafiltration buffer and feed solution) could be applied without exceeding the pressure limitation of the system. The influence of various parameters such as diavolumes, intervals to switch the flow direction of the permeate, the flow rate of the feed solution, the flow modes between feed solution and fresh DF buffer (co-current, counter-current) and scales of the module, on the buffer exchange performance were investigated in detail. By stepwise improvement, the buffer exchange efficiency was successfully increased from 87% and 95% to a final efficiency of 99.3% applying 7.2 diavolumes in the scaled-up module. This finding indicates that the 3D-printed single-unit membrane module provides diafiltration efficiencies beyond the ones of a conventional two-stage counter-current SPTFF setup.

In the last part of the study, a 2D finite element method (FEM) was developed in order to achieve a better understanding of the underlying transport processes of dissolved species within the novel membrane module. The model was validated by comparison with experimental results and used to screen the optimal parameter settings for high diafiltration efficiency. Due to the presence of a porous grid-structure in each part of the membrane module, the Brinkman equation was used to describe the hydrodynamics including the transient pressures and velocities during the switching events of the flow direction of the permeate. The modeling of the transport of dissolved species was achieved by common mass balance including convective flux tangential to and towards the membrane, back diffusion into the bulk solution and eddy dispersion caused by the flow through the coarse grid. After fitting once, an empirical equation based on experimental data was able to describe the relationship between the resulting pressures and the transient BSA concentration. The simulated results of the velocity and concentration profiles showed good consistency with the experimental data, validating the applicability of the developed model. By multiple simulation runs with various parameter settings in terms of different diavolumes, BSA concentrations in the feed solution, flow rates of the feed solution, unidirectional or alternating perfusion of DF buffer through the membrane, and the intervals between the switching events in alternating mode, the following insights could be gained:

(i) When focusing on the maximum buffer exchange efficiency, longer intervals between the switching of the flow direction of DF buffer result in a better diafiltration performance. The reason can be found in the fact that after a switching event, a part of the permeate containing high salt loads will be flushed back into the middle channel, increasing the residual salt concentration in the retentate. In consequence, unidirectional operation, namely no switching events at all, results in the best diafiltration efficiencies, despite the limitation that the flow rate of DF buffer has to be reduced in order not to exceed the maximum pressure of the setup.

(ii) When the applicable feed load per unit membrane area should be maximized, higher feed flow rates than the one acceptable for unidirectional DF buffer flow are required. In order to exceed this limit, switching events of DF buffer flow direction have to be conducted to prevent the built-up of high pressures in the system because of the formation of the concentration polarization. In this case, a decreased switching interval allows a higher feed flow rate, however, at the expense of a reduced buffer exchange efficiency.

(iii) When comparing the achieved buffer exchange efficiencies in dependence of the applied number of diavolumes, it shows that the developed single-unit membrane module exceeds the performance of a two-stage counter-current SPTFF system and approaches the performance of a three-stage counter-current SPTFF system.

To summarize, the system presented in this work significantly simplifies the complexity of the current single pass filtration units for continuous UF/DF. The developed FEM modeling provides a thorough understanding of the transport processes of species within the module, facilitating the screening process for optimal parameter settings to meet diverse demands. The BSA concentrations used in this study reached up to 5 g/L, which however, is still well below the common protein concentration of around 60 g/L applied during diafiltration in final formulation steps of the biopharmaceutical industry. Therefore, perspective work will focus on the experimental investigation of diafiltration efficiencies using higher concentrations of different proteins in the feed solution. In addition, the grid-structure of the middle and lateral parts of the membrane module has a strong influence on eddy diffusive effects. In future prototypes it might be beneficial to optimize the grid structures in the different parts of the module independently, because they also differ in their functions. For this, also the design of the 3D-printed grid structures should be based on a detailed, three-dimensional simulation of the fluid dynamics in the structure, instead of the trial and error approach applied currently. Finally, a further scale-up of the module by a stacked plate and frame design of multiple DF buffer, retentate and permeate channels

operating in parallel would be an interesting option to further improve the applicability of the system for continuous bioprocessing.

9 Comprehensive Reference List

[1] P. Gronemeyer, R. Ditz, J. Strube, Trends in upstream and downstream process development for antibody manufacturing, Bioengineering. 1 (2014) 188–212. https://doi.org/10.3390/bioengineering1040188.

[2] B. Kiss, U. Gottschalk, M. Pohlscheidt, New bioprocessing strategies: development and manufacturing of recombinant antibodies and proteins, 2018. https://doi.org/10.1007/978-3-319-97110-0.

[3] A.L. Zydney, New developments in membranes for bioprocessing – a review, J. Memb. Sci. 620 (2021) 118804. https://doi.org/10.1016/j.memsci.2020.118804.

[4] R.M. Nerem, Stem cell engineering, 2014. https://doi.org/10.1089/ten.tea.2013.0764.

[5] A.L. Zydney, Continuous downstream processing for high value biological products: a review, Biotechnol. Bioeng. (2016). https://doi.org/10.1002/bit.25695.

[6] A. Jungbauer, Continuous downstream processing of biopharmaceuticals, Trends Biotechnol. 31 (2013) 479–492. https://doi.org/10.1016/j.tibtech.2013.05.011.

[7] R.G. Harrison, P.W. Todd, S.R. Rudge, D.P. Petrides, Bioseparations Science and Engineering, 2015. https://doi.org/10.1093/oso/9780195391817.001.0001.

[8] R.C. Houp, Ultrafiltration and diafiltration, J. Valid. Tecnhology. (2009). https://doi.org/10.1353/jaas.0.0062.

[9] A. Jungbauer, Continuous downstream processing of biopharmaceuticals, Trends Biotechnol. 31 (2013) 479–492. https://doi.org/10.1016/j.tibtech.2013.05.011.

[10] F. Lipnizki, J. Boelsmand, R.F. Madsen, Concepts of industrial-scale diafiltration systems, Desalination. 144 (2002) 179–184. https://doi.org/10.1016/S0011-9164(02)00309-0.

[11] Michel Jaffrin, Membrane filtrtaion process, 2015.

[12] B. Anand Mahajan, Downstream Processing: An overview and process steps, MyPrivateTutor. (2018). https://www.myprivatetutor.ae/blog/downstream-an-overview-and-process-steps.

[13] R. Van Reis, A.L. Zydney, Membrane separations in biotechnology, Curr. Opin. Biotechnol. 12 (2001) 208–211. https://doi.org/10.1016/S0958-1669(00)00201-9.

[14] R. van Reis, A. Zydney, Bioprocess membrane technology, J. Memb. Sci. (2007). https://doi.org/10.1016/j.memsci.2007.02.045.

[15] H. Fröhlich, L. Villian, D. Melzner, J. Strube, Membrane technology in bioprocess science, Chemie-Ingenieur-Technik. 84 (2012) 905–917.

https://doi.org/10.1002/cite.201200025.

[16] R. van Reis, A.L. Zydney, Bioprocess membrane technology, J. Memb. Sci. 297 (2007) 16–50. https://doi.org/10.1016/j.memsci.2007.02.045.

[17] A.L. Zydney, Perspectives on integrated continuous bioprocessing - opportunities and challenges, Curr. Opin. Chem. Eng. 10 (2015) 8–13. https://doi.org/10.1016/j.coche.2015.07.005.

[18] M.M. Rohani, Effect of electrostatic interactions during protein ultrafiltration: effects of ligand chemistry and protein surface charge distribution, (2011) 1–216.

[19] M. Hadidi, Ultrafiltration of bacterial polysaccharides and protein-polysaccharide conjugates used in vaccines, (2016).

[20] C. Charcosset, Membrane processes in biotechnology: an overview, Biotechnol. Adv. 24 (2006) 482–492. https://doi.org/10.1016/j.biotechadv.2006.03.002.

[21] EMD Millipore, Single-pass tangential flow filtration, (2014) 1–4.

[22] L.J. Zeman, A.L. Zydney, Microfiltration and Ultrafiltration: Principles and Applications, Marcel Dekker Inc., New York, 1996.

[23] A. Simon, L. Vandanjon, G. Levesque, P. Bourseau, Concentration and desalination of fish gelatin by ultrafiltration and continuous diafiltration processes, Desalination. 144 (2002) 313–318. https://doi.org/10.1016/S0011-9164(02)00333-8.

[24] S. Chockchaisawasdee, V.I. Athanasopoulos, K. Niranjan, R.A. Rastall, Synthesis of galacto-oligosaccharide from lactose using β-galactosidase from kluyveromyces lactis: Studies on batch and continuous UF membrane-fitted bioreactors, Biotechnol. Bioeng. 89 (2005) 434–443. https://doi.org/10.1002/bit.20357.

[25] C. Casey, T. Gallos, Y. Alekseev, E. Ayturk, S. Pearl, Protein concentration with single-pass tangential flow filtration (SPTFF), J. Memb. Sci. 384 (2011) 82–88. https://doi.org/10.1016/j.memsci.2011.09.004.

[26] A. Arunkumar, N. Singh, M. Peck, M.C. Borys, Z.J. Li, Investigation of single-pass tangential flow filtration (SPTFF) as an inline concentration step for cell culture harvest, J. Memb. Sci. 524 (2017) 20–32. https://doi.org/10.1016/j.memsci.2016.11.007.

[27] J. Rucker-Pezzini, L. Arnold, K. Hill-Byrne, T. Sharp, M. Avazhanskiy, C. Forespring, Single pass diafiltration integrated into a fully continuous mAb purification process, Biotechnol. Bioeng. 115 (2018) 1949–1957. https://doi.org/10.1002/bit.26708.

[28] M.G. Jabra, C.J. Yehl, A.L. Zydney, Multistage continuous countercurrent diafiltration for formulation of monoclonal antibodies, Biotechnol. Prog. 35 (2019)

6–11. https://doi.org/10.1002/btpr.2810.

[29] A.M.K. Nambiar, Y. Li, A.L. Zydney, Countercurrent staged diafiltration for formulation of high value proteins, Biotechnol. Bioeng. 115 (2018) 139–144. https://doi.org/10.1002/bit.26441.

[30] S. Bhattacharjee, A.S. Kim, M. Elimelech, Concentration polarization of interacting solute particles in cross-flow membrane filtration, J. Colloid Interface Sci. 212 (1999) 81–99. https://doi.org/10.1006/jcis.1998.6045.

[31] L. Song, M. Elimelech, Theory of concentration polarization in crossflow filtration, J. Chem. Soc. Faraday Trans. 91 (1995) 3389–3398. https://doi.org/10.1039/FT9959103389.

[32] E. Binabaji, J. Ma, S. Rao, A.L. Zydney, Theoretical analysis of the ultrafiltration behavior of highly concentrated protein solutions, J. Memb. Sci. 494 (2015) 216–223. https://doi.org/10.1016/j.memsci.2015.07.068.

[33] G.B. van den Berg, C.A. Smolders, Flux decline in ultrafiltration processes, Desalination. 77 (1990) 101–133. https://doi.org/10.1016/0011-9164(90)85023-4.

[34] M.C. Porter, Concentration Polarization with Membrane Ultrafiltration, Ind. Eng. Chem. Prod. Res. Dev. 11 (1972) 234–248. https://doi.org/10.1021/i360043a002.

[35] S. Bhattacharya, S.T. Hwang, Concentration polarization, separation factor, and Peclet number in membrane processes, J. Memb. Sci. 132 (1997) 73–90. https://doi.org/10.1016/S0376-7388(97)00047-1.

[36] I. Gitlin, J.D. Carbeck, G.M. Whitesides, Why are proteins charged? Networks of charge-charge interactions in proteins measured by charge ladders and capillary electrophoresis, Angew. Chemie - Int. Ed. 45 (2006) 3022–3060. https://doi.org/10.1002/anie.200502530.

[37] N.S. Pujar, A.L. Zydney, Electrostatic and Electrokinetic Interactions during protein transport through narrow pore membranes, Ind. Eng. Chem. Res. 33 (1994) 2473–2482. https://doi.org/10.1021/ie00034a032.

[38] R. Van Reis, J.M. Brake, J. Charkoudian, D.B. Burns, A.L. Zydney, High-performance tangential flow filtration using charged membranes, J. Memb. Sci. (1999). https://doi.org/10.1016/S0376-7388(99)00048-4.

[39] A. Mehta, A.L. Zydney, Effect of membrane charge on flow and protein transport during ultrafiltration, Biotechnol. Prog. 22 (2006) 484–492. https://doi.org/10.1021/bp050324x.

[40] W.C. McGregor, Membrane Separations in Biotechnology, Marcel Dekker Inc., New York, 1986.

[41] L. Palacio, J.I. Calvo, P. Prádanos, A. Hernández, P. Väisänen, M. Nyström,

Contact angles and external protein adsorption onto UF membranes, J. Memb. Sci. 152 (1999) 189–201. https://doi.org/10.1016/S0376-7388(98)00203-8.

[42] W.R. Bowen, F. Jenner, Theoretical descriptions of membrane filtration of colloids and fine particles: an assessment and review, Adv. Colloid Interface Sci. 56 (1995) 141–200. https://doi.org/10.1016/0001-8686(94)00232-2.

[43] H. Lutz, Ultrafiltration for Bioprocessing, Sawston, 2015.

[44] M. Peter-Varbanets, C. Zurbrügg, C. Swartz, W. Pronk, Decentralized systems for potable water and the potential of membrane technology, Water Res. 43 (2009) 245–265. https://doi.org/10.1016/j.watres.2008.10.030.

[45] Millipore, Protein concentration and diafiltration by tangential flow filtration, Tech. Br. (2003) 1–23.

[46] R. Bian, K. Yamamoto, Y. Watanabe, Effect of shear rate on controlling the concentration polarization and membrane fouling, Desalination. 131 (2000) 225–236. https://doi.org/10.1016/S0011-9164(00)90021-3.

[47] E. Matthiasson, B. Sivik, Concentration polarization and fouling, Desalination. 35 (1980) 59–103. https://doi.org/10.1016/S0011-9164(00)88604-X.

[48] J.G. Wijmans, S. Nakao, C.A. Smolders, Flux limitation in ultrafiltration: Osmotic pressure model and gel layer model, J. Memb. Sci. 20 (1984) 115–124. https://doi.org/10.1016/S0376-7388(00)81327-7.

[49] K.A.S. V.L. Vilker, C.K. Colton, Concentration polarization in protein ultrafiltration. Part II: theoretical and experimental study of albumin ultrafiltered in an unstirred batch cell, AIChE. J. 27. (1981) 637–645.

[50] J.A. Howell, O. Velicangil, Theoretical considerations of membrane fouling and its treatment with immobilized enzymes for protein ultrafiltration, J. Appl. Polym. Sci. 27 (1982) 21–32. https://doi.org/10.1002/app.1982.070270103.

[51] S.S.L. Peppin, J.A.W. Elliott, Non-equilibrium thermodynamics of concentration polarization, Adv. Colloid Interface Sci. 92 (2001) 1–72. https://doi.org/10.1016/S0001-8686(00)00029-4.

[52] G. Belfort, R.H. Davis, A.L. Zydney, The behaviour of suspentions and macromolecular solutions in crossflow microfiltration, J. Memb. Sci. 96 (1994) 1–58.

[53] E.S. Tarleton, R.J. Wakeman, Understanding flux decline in crossflow microfiltration: Part I - Effects of particle and pore size, Chem. Eng. Res. Des. 71 (1993) 399–410.

[54] L. Song, Flux decline in crossflow microfiltration and ultrafiltration: mechanisms and modeling of membrane fouling, J. Memb. Sci. 139 (1998) 183–200. https://doi.org/10.1016/S0376-7388(99)00075-7.

[55] A.I.C. Morão, A.M. Brites Alves, M.C. Costa, J.P. Cardoso, Nanofiltration of a clarified fermentation broth, Chem. Eng. Sci. 61 (2006) 2418–2427. https://doi.org/10.1016/j.ces.2005.11.007.

[56] S. Nakatsuka, A.S. Michaels, Transport and separation of proteins by ultrafiltration through sorptive and non-sorptive membranes, J. Memb. Sci. 69 (1992) 189–211. https://doi.org/https://doi.org/10.1016/0376-7388(92)80039-M.

[57] S. Zhao, L. Zou, Relating solution physicochemical properties to internal concentration polarization in forward osmosis, J. Memb. Sci. 379 (2011) 459–467. https://doi.org/10.1016/j.memsci.2011.06.021.

[58] J. Hosch, E. Staude, Preparation and investigation of chemically modified porous polyamide ultrafiltration membranes, J. Memb. Sci. 121 (1996) 71–82. https://doi.org/10.1016/0376-7388(96)00166-4.

[59] M. Nyström, Fouling of unmodified and modified polysulfone ultrafiltration membranes by ovalbumin, J. Memb. Sci. 44 (1989) 183–196. https://doi.org/https://doi.org/10.1016/S0376-7388(00)83351-7.

[60] T. Luo, S. Abdu, M. Wessling, Selectivity of ion exchange membranes: a review, J. Memb. Sci. (2018). https://doi.org/10.1016/j.memsci.2018.03.051.

[61] S. Wardeh, H.P. Morvan, CFD simulations of flow and concentration polarization in spacer-filled channels for application to water desalination, Chem. Eng. Res. Des. 86 (2008) 1107–1116. https://doi.org/10.1016/j.cherd.2008.04.010.

[62] V. Aguirre-Montesdeoca, A.E.M. Janssen, A. Van der Padt, R.M. Boom, Modelling ultrafiltration performance by integrating local (critical) fluxes along the membrane length, J. Memb. Sci. 578 (2019) 111–125. https://doi.org/10.1016/j.memsci.2019.02.040.

[63] H. Lutz, Ultrafiltration for Bioprocessing, (2015) 244. https://doi.org/10.1016/B978-1-907568-46-6.00002-1.

[64] B. Kwon, J. Molek, A.L. Zydney, Ultrafiltration of PEGylated proteins: fouling and concentration polarization effects, J. Memb. Sci. 319 (2008) 206–213. https://doi.org/10.1016/j.memsci.2008.03.035.

[65] S.T. Kelly, A.L. Zydney, Protein fouling during microfiltration: comparative behavior of different model proteins, Biotechnol. Bioeng. 55 (1997) 91–100. https://doi.org/10.1002/(SICI)1097-0290(19970705)55:1<91::AID-BIT11>3.0.CO;2-6.

[66] M.K. Ko, J.J. Pellegrino, Determination of osmotic pressure and fouling resistance and their effects of performance of ultrafiltration membranes, J. Memb. Sci. 74 (1992) 141–157. https://doi.org/https://doi.org/10.1016/0376-7388(92)87079-D.

[67] E. Matthiasson, The role of macromolecular adsorption in fouling of ultrafiltration membranes, J. Memb. Sci. 16 (1983) 23–36. https://doi.org/https://doi.org/10.1016/S0376-7388(00)81297-1.

[68] A.G. Fane, C.J.D. Fell, A. Suki, The effect of ph and ionic environment on the ultrafiltration of protein solutions with retentive membranes, J. Memb. Sci. 16 (1983) 195–210. https://doi.org/https://doi.org/10.1016/S0376-7388(00)81310-1.

[69] S.P. Palecek, A.L. Zydney, Hydraulic permeability of protein deposits formed during microfiltration: effect of solution pH and ionic strength, J. Memb. Sci. 95 (1994) 71–81. https://doi.org/https://doi.org/10.1016/0376-7388(94)85030-5.

[70] K.L. Jones, C.R. O'Melia, Ultrafiltration of protein and humic substances: Effect of solution chemistry on fouling and flux decline, J. Memb. Sci. 193 (2001) 163–173. https://doi.org/10.1016/S0376-7388(01)00492-6.

[71] A. Robert van Reis, Membrane Separations in Biotechnology, New York, 1986.

[72] R.W. Baker, Membrane Technology and Applications, West Sussex, 2012.

[73] J.E. Flinn, Membrane science and technology. Boston, 1970.

[74] D. Bhattacharyya, S.L. Back, R.I. Kermode, M.C. Roco, Prediction of concentration polarization and flux behavior in reverse osmosis by numerical analysis, J. Memb. Sci. 48 (1990) 231–262. https://doi.org/10.1016/0376-7388(90)85007-8.

[75] K. Madireddi, R.B. Babcock, B. Levine, J.H. Kim, M.K. Stenstrom, An unsteady-state model to predict concentration polarization in commercial spiral wound membranes, J. Memb. Sci. 157 (1999) 13–34. https://doi.org/10.1016/S0376-7388(98)00340-8.

[76] R. Wu, K. Su, Z. Wang, T. Hao, S. Liu, A comprehensive investigation of filtration performance in submerged hollow fibre membrane modules with different fibre geometries, Sep. Purif. Technol. 221 (2019) 93–100. https://doi.org/10.1016/j.seppur.2019.03.082.

[77] A. Subramani, S. Kim, E.M.V. Hoek, Pressure, flow, and concentration profiles in open and spacer-filled membrane channels, J. Memb. Sci. 277 (2006) 7–17. https://doi.org/10.1016/j.memsci.2005.10.021.

[78] P. Bacchin, B. Espinasse, Y. Bessiere, D.F. Fletcher, P. Aimar, Numerical simulation of colloidal dispersion filtration: description of critical flux and comparison with experimental results, Desalination. 192 (2006) 74–81. https://doi.org/10.1016/j.desal.2005.05.028.

[79] B. Marcos, C. Moresoli, J. Skorepova, B. Vaughan, CFD modeling of a transient hollow fiber ultrafiltration system for protein concentration, J. Memb. Sci. 337 (2009) 136–144. https://doi.org/10.1016/j.memsci.2009.03.036.

[80] M.F. Gruber, C.J. Johnson, C.Y. Tang, M.H. Jensen, L. Yde, C. Hélix-Nielsen, Computational fluid dynamics simulations of flow and concentration polarization in forward osmosis membrane systems, J. Memb. Sci. 379 (2011) 488–495. https://doi.org/10.1016/j.memsci.2011.06.022.

[81] L. Huang, M.T. Morrissey, Finite element analysis as a tool for crossflow membrane filter simulation, J. Memb. Sci. 155 (1999) 19–30. https://doi.org/10.1016/S0376-7388(98)00300-7.

[82] D.E. Wiley, D.F. Fletcher, Techniques for computational fluid dynamics modelling of flow in membrane channels, J. Memb. Sci. 211 (2003) 127–137. https://doi.org/10.1016/S0376-7388(02)00412-X.

[83] C. Sharma, D. Malhotra, A.S. Rathore, Review of computational fluid dynamics Applications in Biotechnology Processes, (2011). https://doi.org/10.1002/btpr.689.

[84] M. Kahrizi, J. Lin, G. Ji, L. Kong, C. Song, L.F. Dumée, S. Sahebi, S. Zhao, Relating forward water and reverse salt fluxes to membrane porosity and tortuosity in forward osmosis: CFD modelling, Sep. Purif. Technol. 241 (2020) 116727. https://doi.org/10.1016/j.seppur.2020.116727.

[85] D.E. Wiley, D.F. Fletcher, Computational fluid dynamics modelling of flow and permeation for pressure-driven membrane processes, Desalination. 145 (2002) 183–186. https://doi.org/10.1016/S0011-9164(02)00406-X.

[86] S. Shirazi, C.J. Lin, D. Chen, Inorganic fouling of pressure-driven membrane processes - a critical review, Desalination. 250 (2010) 236–248. https://doi.org/10.1016/j.desal.2009.02.056.

[87] Michaels, A.S., New separation technique for the CPI. Chem. Eng. Prog., 64 (1968) 31-43.

[88] W.F. Blatt, A. Dravid, A.S. Michaels, L. Nelsen, Solute polarization and cake formation in membrane ultrafiltration: causes, consequences, and control techniques, Membr. Sci. Technol. (1970) 47–97. https://doi.org/10.1007/978-1-4684-1851-4_4.

[89] J.C. Chen, Q. Li, M. Elimelech, In situ monitoring techniques for concentration polarization and fouling phenomena in membrane filtration, Adv. Colloid Interface Sci. 107 (2004) 83–108. https://doi.org/10.1016/j.cis.2003.10.018.

[90] A.L. Ahmad, K.K. Lau, M.Z.A. Bakar, S.R.A. Shukor, Integrated CFD simulation of concentration polarization in narrow membrane channel, Comput. Chem. Eng. 29 (2005) 2087–2095. https://doi.org/10.1016/j.compchemeng.2005.06.001.

[91] M.A. Monfared, N. Kasiri, A. Salahi, T. Mohammadi, CFD simulation of baffles arrangement for gelatin-water ultrafiltration in rectangular channel, Desalination.

284 (2012) 288–296. https://doi.org/10.1016/j.desal.2011.09.014.

[92] L. Mi, S.T. Hwang, Correlation of concentration polarization and hydrodynamic parameters in hollow fiber modules, J. Memb. Sci. 159 (1999) 143–165. https://doi.org/10.1016/S0376-7388(99)00046-0.

[93] S.R. Wickramasinghe, M.J. Semmens, E.L. Cussler, Mass transfer in various hollow fiber geometries, J. Memb. Sci. 69 (1992) 235–250. https://doi.org/https://doi.org/10.1016/0376-7388(92)80042-I.

[94] A.G. Fane, Ultrafiltration: factors influencing flux and rejection. Progress in Filtration and Separation, Vol. 4, Elsevier, Amsterdam, 1986.

[95] M.W. Chudacek, A.G. Fane, The dynamics of polarisation in unstirred and stirred ultrafiltration, J. Memb. Sci. 21 (1984) 145–160. https://doi.org/10.1016/S0376-7388(00)81551-3.

[96] A. Macedo, E. Duarte, M. Pinho, The role of concentration polarization in ultrafiltration of ovine cheese whey, J. Memb. Sci. 381 (2011) 34–40. https://doi.org/10.1016/j.memsci.2011.07.012.

[97] G. De Luca, F. Bisignano, F. Paone, S. Curcio, Multi-scale modeling of protein fouling in ultra filtration process, J. Memb. Sci. 452 (2014) 400–414. https://doi.org/10.1016/j.memsci.2013.09.061.

[98] J.G. Wijmans, S. Nakao, J.W.A. Van Den Berg, F.R. Troelstra, C.A. Smolders, Hydrodynamic resistance of concentration polarization boundary layers in ultrafiltration, J. Memb. Sci. 22 (1985) 117–135. https://doi.org/10.1016/S0376-7388(00)80534-7.

[99] M. Khraisheh, N. Dawas, M.S. Nasser, M.J. Al-Marri, M.A. Hussien, S. Adham, G. McKay, Osmotic pressure estimation using the Pitzer equation for forward osmosis modelling, Environ. Technol. 41 (2019) 1–22. https://doi.org/10.1080/09593330.2019.1575476.

[100] G. Jonsson, Boundary layer phenomena during ultrafiltration of dextran and whey protein solutions, Desalination. 51 (1984) 61–77. https://doi.org/10.1016/0011-9164(84)85053-5.

[101] J. Fernández-Sempere, F. Ruiz-Beviá, P. García-Algado, R. Salcedo-Díaz, Visualization and modelling of the polarization layer and a reversible adsorption process in PEG-10000 dead-end ultrafiltration, J. Memb. Sci. 342 (2009) 279–290. https://doi.org/10.1016/j.memsci.2009.06.046.

[102] C.W. Hull, Apparatus for production of three-dmensonal objects by stereo thography, Patent. (1984) 16. https://patents.google.com/patent/US4575330.

[103] A.B. Badiru, V.V. Valencia, David. Liu. (2017). Additive Manufacturing Handbook: Product Development for the Defense Industry (1st ed.). CRC Press.

https://doi.org/10.1201/9781315119106.

[104] S. Tsuda, H. Jaffery, D. Doran, M. Hezwani, P.J. Robbins, M. Yoshida, L. Cronin, Customizable 3D printed “Plug and Play” millifluidic devices for programmable fluidics, Plos One. 10 (2015) 1–13. https://doi.org/10.1371/journal.pone.0141640.

[105] R. Amin, S. Knowlton, A. Hart, B. Yenilmez, F. Ghaderinezhad, 3D-printed microfluidic devices, (2016).

[106] A. Vanderploeg, S.E. Lee, M. Mamp, The application of 3D printing technology in the fashion industry, Int. J. Fash. Des. Technol. Educ. 10 (2017) 170–179. https://doi.org/10.1080/17543266.2016.1223355.

[107] C. Groth, J.W. Graham, W.R. Redmond, Three-dimensional printing technology, XLVIII (2014) 475 – 485.

[108] Leo Gregurić. PolyJet – 3D Printing Technologies Simply Explained , All 3DP. https://all3dp.com/2/polyjet-3d-printing-technologies-simply-explained/ (accessed March 20, 2021).

[109] Hamzah Meraj, 3D Printing Technologies, Slideshare https://www.slideshare.net/hamzaaaaaah/3dprinting-technologies?from_action=save (accessed March 20, 2021).

[110] Wohlers Associates Inc. (2013). Wohlers report. Fort Collins, CO: Wohlers.

[111] R. Bogue, 3D printing: The dawn of a new era in manufacturing?, Assem. Autom. 33 (2013) 307–311. https://doi.org/10.1108/AA-06-2013-055.

[112] R. Kwak, V.S. Pham, B. Kim, L. Chen, J. Han, Enhanced salt removal by unipolar ion conduction in ion concentration polarization desalination, Sci. Rep. 6 (2016) 1–11. https://doi.org/10.1038/srep25349.

[113] A. Tschöpe, M. Wyrwoll, M. Schneider, K. Mandel, M. Franzreb, A magnetically induced fluidized-bed reactor for intensification of electrochemical reactions, Chem. Eng. J. 385 (2020) 123845. https://doi.org/10.1016/j.cej.2019.123845.

[114] E. Mattio, F. Robert-Peillard, C. Branger, K. Puzio, A. Margaillan, C. Brach-Papa, J. Knoery, J.L. Boudenne, B. Coulomb, 3D-printed flow system for determination of lead in natural waters, Talanta. 168 (2017) 298–302. https://doi.org/10.1016/j.talanta.2017.03.059.

[115] C. Calderilla, F. Maya, V. Cerdà, L.O. Leal, 3D printed device including disk-based solid-phase extraction for the automated speciation of iron using the multisyringe flow injection analysis technique, Talanta. 175 (2017) 463–469. https://doi.org/10.1016/j.talanta.2017.07.028.

[116] T. Huber, D. Clucas, M. Vilmay, B. Pupkes, J. Stuart, S. Dimartino, C. Fee, 3D printing cellulose hydrogels using LASER induced thermal gelation, J. Manuf. Mater. Process. 2 (2018) 42. https://doi.org/10.3390/jmmp2030042.

[117] C.J. Fee, S. Dimartino, T. Huber, Separation Medium, 3 (2017). https://patents.google.com/patent/WO2017103863A1/pt.

[118] A. Shafiee, A. Atala, Printing technologies for medical applications, Trends Mol. Med. 22 (2016) 254–265. https://doi.org/10.1016/j.molmed.2016.01.003.

[119] M. Attaran, The rise of 3-D printing: The advantages of additive manufacturing over traditional manufacturing, Bus. Horiz. 60 (2017) 677–688. https://doi.org/10.1016/j.bushor.2017.05.011.

[120] C. Fee, S. Nawada, S. Dimartino, 3D printed porous media columns with fine control of column packing morphology, J. Chromatogr. A. 1333 (2014) 18–24. https://doi.org/10.1016/j.chroma.2014.01.043.

[121] M.G. Moleirinho, S. Feast, A.S. Moreira, R.J.S. Silva, P.M. Alves, M.J.T. Carrondo, T. Huber, C. Fee, C. Peixoto, 3D-printed ordered bed structures for chromatographic purification of enveloped and non-enveloped viral particles, Sep. Purif. Technol. 254 (2021) 117681. https://doi.org/10.1016/j.seppur.2020.117681.

10 Appendix

10.1 Analytical methods

Bovine serum albumin (BSA) was used as model protein in this study. The concentration of dissolved BSA in solution was detected at a wavelength of 280 nm and it was measured by UV spectroscopy. In the beginning a separate spectrometer was used for this purpose. Later, the UV measurement was done online using the UV detector included in the used FPLC system. Afterwards, the concentration was calculated based on a calibration curve with given BSA concentrations.

For the buffer exchange efficiencies, the buffer concentration was detected by the conductivity meter of the FPLC system. The conversion of conductivities into fractions of the original feed buffer remaining in the retentate after diafiltration was conducted by the help of calibration curves determined from standards of known concentrations. In all experiments the feed solution contained 30 mM NaH_2PO_4 and 100 mM NaCl. In the case of diafiltration experiments using a diafiltration buffer containing 30 mM NaH_2PO_4 and 5 mM NaCl, even a 100% exchange efficiency does not reduce the conductivity of the retentate down to values close to zero. This fact was considered by preparing the standards by dilution of the feed solution with increasing amounts of diafiltration buffer (Fig. S6.1A). In later diafiltration experiments pure water was used as diafiltration buffer. On the one hand this simplifies the preparation of calibration standards, on the other hand the calibration curve had to be divided into two sections (see Fig.S6.1B), because a single straight line is not a good fit of the required correlation if the conductivity stretches over several orders of magnitude.

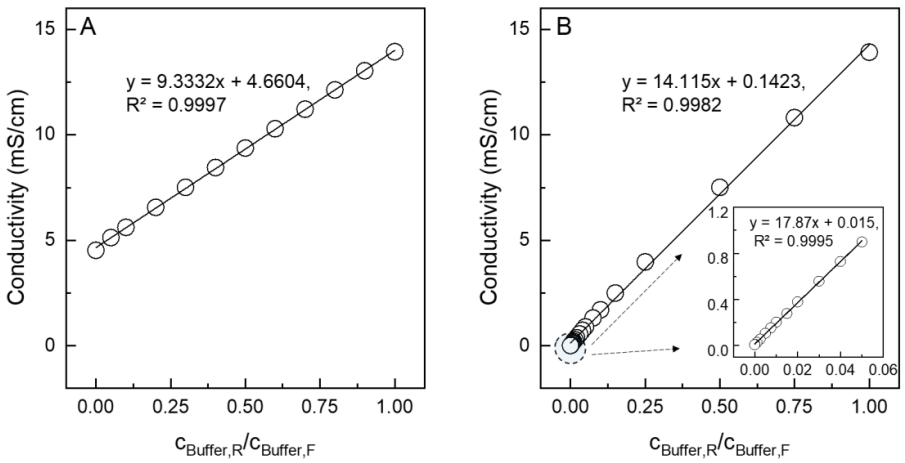

Fig. S6. 1 Calibration curves for the conversion of conductivities into fractions of feed buffer concentration remaining in the retentate. A. using 30 mM NaH_2PO_4 but only 5 mM NaCl as DF buffer. B. Using pure water as DF buffer.

10.2 2D-view of the designed membrane modules

A. Upper lateral part

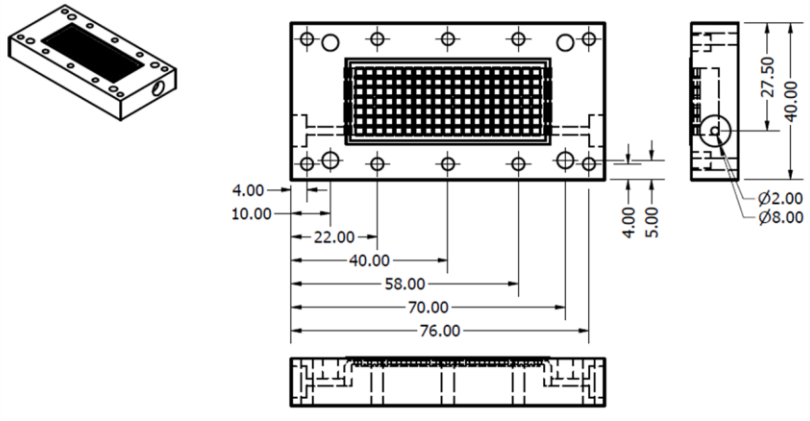

B. Middle part

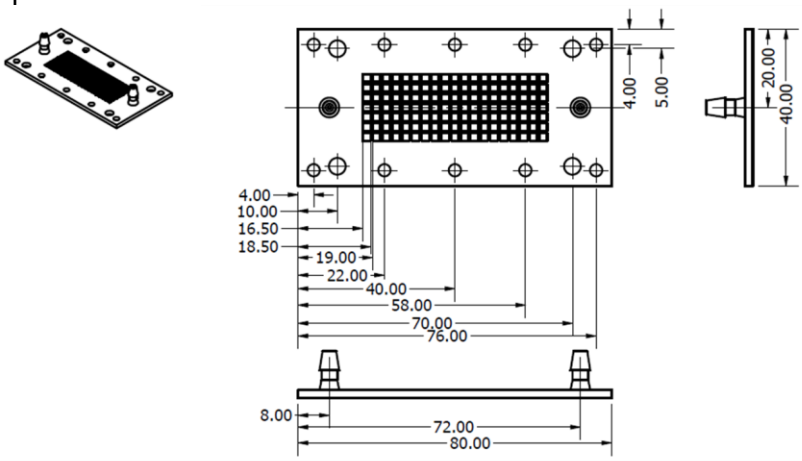

C. Lower lateral part

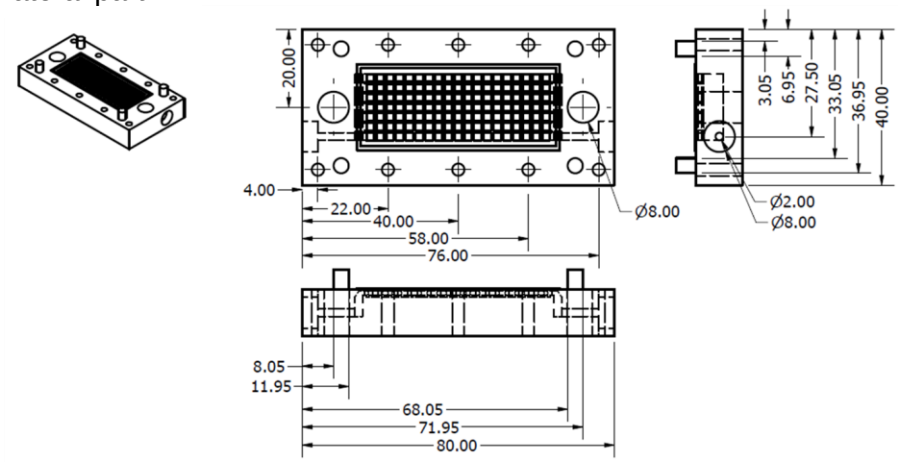

Fig. 10.1 Construction drawing with dimensioning of the small prototype membrane module.

A. Upper lateral part

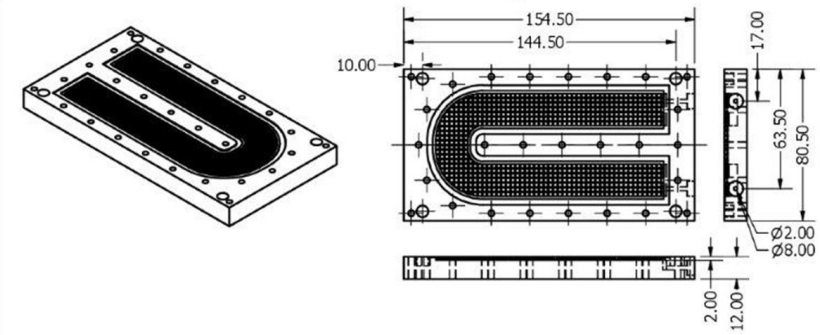

B. Middle part

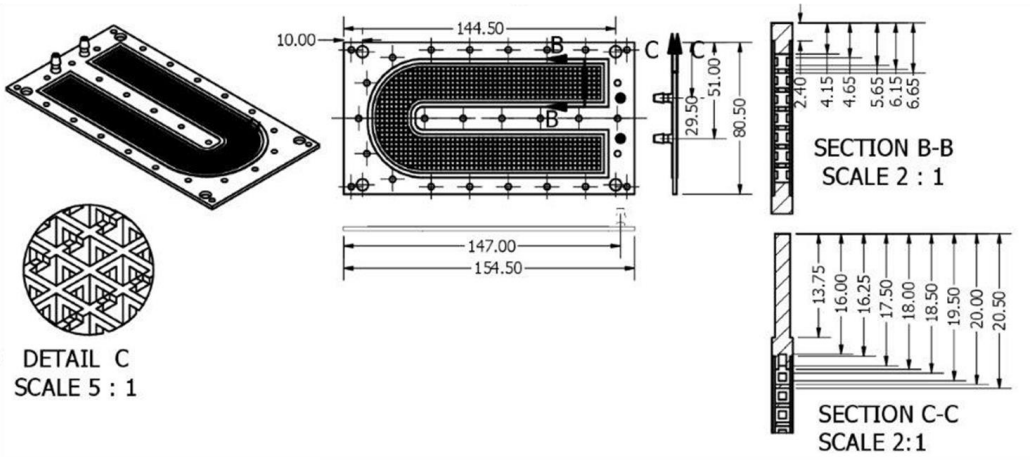

C. Lower lateral part

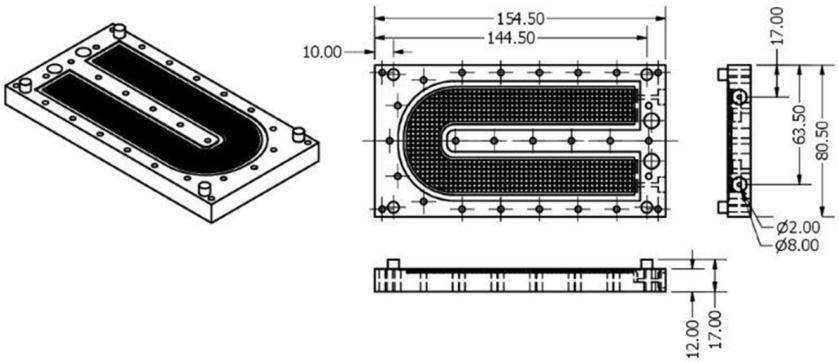

Fig. 10.2 Construction drawing with dimensioning of the upscaled membrane module.

11 Abbreviations and Nomenclatures

Abbreviations

Name	Meaning	Name	Meaning
CP	Concentration polarization	FEM	Finite element method
NFF	Normal flow filtration	FVM	Finite volume method
TFF	Tangential flow filtration	CAD	Computer-aided design
SPTFF	Single pass tangential flow filtration	CFD	Computational fluid dynamics
UF	Ultrafiltration	SLA	Stereo lithography
DF	Diafiltration	SLS	Selective laser sintering
MF	Microfiltration	FDM	Fused deposition modeling
NF	Nanofiltration	MJ	Material jetting
RO	Reverse osmosis	SPE	Solid phase extraction
FO	Forward osmosis	PES	Polyethersulfone
SPDF	Single pass diafiltration	RT	Residence time
mAbs	Monoclonal antibodies	CF	Concentration factor
IgG	Immunoglobulin G	DE	Diafiltration efficiency
MWCO	Molecular weight cutoff	DV	Diavolumes
kDa	kilo Daltons	DSP	Downstream processing
BSA	Bovine serum albumin	TMP	Transmembrane pressure
IEP	Isoelectric point	SD	Standard deviation

Symbols

Symbol	Unit	Description
u	m/s	Flow velocity transverse to the membrane
v	m/s	Flow velocity normal to the membrane
D	m²/s	Diffusion coefficient
R	1/m	Resistance
J	L/(m² h)	Flow flux
L_P	L/(m² h bar)	Volumetric permeability of membrane
c	g/L	Concentration of species
K	m²	Intrinsic permeability of membrane
μ	Pa·s	Dynamic viscosity
ν	m²/s	Kinematic viscosity
ρ	kg/m³	Mass density of solute
P	bar	Pressure
Q	mL/min	Flow rate
A	m²	Membrane effective area
δ	m	Membrane thickness
k	m/s	Mass transfer coefficient
Sh	-	Sherwood number
d	m	Diameter
Re	-	Reynold number
Sc	-	Schmidt number
L	m	Length of the feed flow channel
τ	Pa	Shear stress
γ	m/s/m	Shear rate
h	m	Channel height
N	-	Dimensionless filtration factor
k	J/K	Boltzman constant
T	K	Absolute temperature
ε	-	Porosity
τ	-	Tortuosity
π	bar	Osmotic pressure
m	kg	Mass
λ	S/m	Conductivity

Index

Name	Meaning	Name	Meaning
p, P	permeate	SD	Deposited solutes
w	Pure water	SR	Removed by stirring
W	Permeable wall	g	Global
B	Bulk solution	pol	Polarization
M	Membrane surface	∇	Gradient
$\vec{}$	Vector	Δ	Difference
ov	Overall	DF	Diafiltration buffer
L	Laminar flow	F	Feed
t	Turbulent flow	R	Retentate
h	Equivalent hydraulic	in	Inlet
G	Gel layer	out	Outlet
lim	Limiting	$\bar{}$	Average value
F	Filtration factor	i	Species of solute
Fc	Critical filtration factor	D, i	Dispersion effect
P	Particle	e, i	Diffusive effect
S	Polarized solutes	F, i	Diffusion effect